DETERMINING THE ELECTROMAGNETIC CONSTANTS OF GROUND AND ANALYSING HF PROPAGATION WITH THE AID OF A MODERN INTERFEROMETRIC DIRECTION FINDER

by

Petrus Johannes Coetzee

A thesis submitted in partial fulfilment of the requirements for the degree of Philosophiae Doctor (Engineering)

in the

Department of Electrical, Electronic and Computer Engineering
Faculty of Engineering, Built Environment and Information Technology

UNIVERSITY OF PRETORIA

September 2018

SUMMARY

DETERMINING THE ELECTROMAGNETIC CONSTANTS OF GROUND AND ANALYSING HF PROPAGATION WITH THE AID OF A MODERN INTERFEROMETRIC DIRECTION FINDER

by

Petrus Johannes Coetzee

Supervisor: Prof. W.P. du Plessis

Department: Electrical, Electronic and Computer Engineering

University: University of Pretoria

Degree: Philosophiae Doctor (Engineering)

Keywords: direction finding, ground electromagnetic constants, ground wave, High Frequency (HF), Interferometric, ionogram, ionosonde, ionosphere, NVIS, ray-tracing, single site location (SSL), skywave, soil moisture, time domain reflectometry, wave tilt

Although high frequency (HF, 3 to 30 MHz) radio propagation (both skywave and ground wave) has been studied for more than a century and is a mature science at this point in time, some answers remain elusive and must be further investigated. The advent of modern, cost effective computers and especially Digital Signal Processing (DSP) techniques and hardware as implemented in an interferometric HF direction finder (DF) have opened exciting new opportunities to study and gain new insights into classic propagation phenomena that are due to the electromagnetic properties of an imperfect earth. These include the propagation loss and the tilt of a ground wave signal. An interferometric DF can also now add a new dimension to the study of the propagation of skywave HF signals through the ionosphere.

Until recently it was challenging to analyse, in near real time, skywave ionospheric propagation modes between a transmitter and a receiver that monitors the signal. Received

signal strength used to be one of the few available indicators of propagation conditions. During the course of this study, techniques were developed that utilises the elevation angle as measured by an interferometric DF and the output of a ray-tracing algorithm to study and identify propagation effects that the HF signal was subjected to. It is now possible to identify phenomena such as multi-hop and multi-layer propagation. The ionospheric layer(s) that refracted the received signal as well as the Optimum Working Frequency (OWF) for the circuit can now also be identified. The most stable region of the ionosphere for propagation over a specified circuit can also be determined with this new approach, thus helping to improve the reliability of HF communications.

Accurate electromagnetic ground constants are required for applications such as the modelling of ground wave propagation of radio signals and determining the radiation characteristics of antennas above a real, imperfect earth. Accurate electromagnetic ground constants are thus paramount in any HF link planning or propagation study, but are not always available for a specific frequency and geographical location. A RF technique, Time Domain Reflectometry (TDR), implemented in modern, cost effective consumer equipment is used to determine the soil moisture content. With the aid of a previously published ground model, an easy to use method was developed to determine the electromagnetic ground parameters (conductivity and relative dielectric constant) at any radio frequency using the measured soil moisture content. This method offers significant advantages in terms of simplicity, speed and cost when compared with current techniques. It has been verified over the 2 to 30 MHz frequency range, but should be applicable up to 200 MHz, the upper frequency limit of the ground model used.

An innovative application of an interferometric DF is to determine the forward wave tilt of a ground wave signal in the proximity of the DF antenna array. This application offers significant advantages in terms of simplicity and speed when compared to current manual techniques to determine wave tilt. The soil moisture content can be determined from the wave tilt and in conjunction with the ground model described above, an easy to use method was developed to determine the electromagnetic ground parameters with greater accuracy than is possible from the ITU publications. Having accurate ground electromagnetic

constants in hand is very beneficial for the modelling of both ground wave and skywave propagation for the geographical location of the DF.

Single Site Location (SSL) direction finding is a technique used to determine the origin (position of the transmitter) of a long-distance HF signal with the aid of a single, interferometric DF, an ionospheric model and a ray-tracing system. The elevation angle of the intercepted signal is used to calculate a ground range by modelling the path that the signal travelled through the ionosphere. With the measured direction (azimuth angle) and the calculated ground range, it is possible to determine the origin of the HF transmission.

Simply being able to intercept (monitor) a signal and determining the wave angle (azimuth and elevation) with the aid of an interferometric DF does not guarantee the quality of the calculated SSL ground range. The reigning propagation conditions for the communications circuit must also be taken into consideration for optimum results. However, computing the performance of a SSL system is a complex problem with many variables to be considered. To overcome this difficulty, a quality factor, which only depends on the standard propagation metrics for HF communication links, was derived. Measured results are presented to demonstrate that this quality factor is a useful indicator of SSL performance.

OPSOMMING

DIE BEPALING VAN DIE ELEKTROMAGNETIESE KONSTANTES VAN GROND EN DIE ANALISE VAN HOË FREKWENSIE VOORTPLANTING MET BEHULP VAN 'N MODERNE INTERFEROMETRIESE RIGTINGPEILER

deur

Petrus Johannes Coetzee

Studieleier:	Prof. W.P. du Plessis
Departement:	Elektriese, Elektroniese en Rekenaaringenieurswese
Universiteit:	Universiteit van Pretoria
Graad:	Philosophiae Doctor (Ingenieurswese)

Sleutelwoorde:	Elektromagnetiese eienskappe van grond, enkelstasie ligging bepaling, golfhelling, grondgolf, grondvog, Hoë Frekwensie (HF), HF voortplanting, interferometriese rigtingpeiling, ionogram, ionosfeer, ionosonde, luggolf weerkaatsing, steilhoekstraling, straalopsporing, tyddomein weerkaatsing

Die voortplanting van hoë frekwensie (HF, 3 tot 30 MHz) radio seine (beide luggolf en grondgolf) word al vir meer as 'n eeu bestudeer en is teen hierdie tyd 'n volwasse wetenskap. Ten spyte hiervan is daar nog baie onbeantwoorde vrae wat verder ondersoek moet word. Die beskikbaarwording van moderne, kragtige rekenaars en veral digitale seinverwerkingstegnieke en hardeware soos in 'n moderne interferometriese rigtingpeiler (RP) vervat, het opwindende nuwe geleenthede geskep om van die klassieke verskynsels opnuut te bestudeer en verdere insigte te verkry. Dit sluit die padverlies en die helling van

HF grondgolfseine as gevolg van die invloed van ’n nie-ideale aarde in, sowel as die voortplanting van ’n luggolfsein deur die ionosfeer.

Tot onlangs was dit baie uitdagend om bykans intyds die ionosferiese pad wat ’n luggolf sein tussen ’n sender en ’n ontvangsstasie gevolg het, te bepaal. Die ontvangde seinsterkte was een van die min kenmerke wat ’n aanduiding van die voortplantingstoestande kon gee. Gedurende hierdie studie is nuwe tegnieke ontwikkel wat die invalshoek van ’n sein soos bepaal deur middel van ’n interferometriese rigting peiler en die uitset van ’n ionosferiese straalopsporingsalgoritme gebruik om ionosferiese voortplantingseffekte te identifiseer en te bestudeer. Dit is nou moontlik om effekte soos veelvuldige weerkaatsings en voortplanting via veelvuldige ionosferiese lae te identifiseer. Met hierdie nuwe benadering is dit ook nou moontlik om te bepaal deur watter ionosferiese lae die sein terug gebuig is sowel as die mees geskikte frekwensie vir die toepaslike kommunikasiekring. Die mees stabiele gebied van die ionosfeer kan nou ook bepaal word wat meer betroubare HF kommunikasie tot gevolg sal hê.

Akkurate elektromagnetiese grondkonstantes word vir toepassings soos die modellering van grondgolfvoortplanting van radioseine en die bepaling van die stralingseienskappe van antennas bo ’n werklike, nie-ideale aarde benodig. Akkurate elektromagnetiese grondkonstantes is dus baie belangrik in die beplanning van HF skakels of die bestudering van HF voortplanting, maar is nie dikwels geredelik beskikbaar vir ’n spesifieke frekwensie of ligging nie. ’n RF tegniek, tyddomeinweerkaatsing soos in moderne, koste-effektiewe toerusting vervat is, word gebruik om die voginhoud van grond te bepaal. In samewerking met ’n elektromagnetiese model van grond is ’n gebruikersvriendelike tegniek ontwikkel om die benodigde grondkonstantes (geleiding en relatiewe diëlektriese konstante) by enige radiofrekwensie in samewerking met die voginhoud van grond te bepaal. Hierdie nuwe tegniek is aansienlik eenvoudiger, vinniger en goedkoper as bestaande tegnieke. Dit is oor die 2 tot 30 MHz frekwensie bereik bevestig maar behoort tot 200 MHz, die boonste grens van die grondmodel, geldig te wees.

’n Innoverende toepassing van ’n interferometriese RP is om die helling van ’n grondgolf sein in die omgewing van die antennaskikking te meet. Dit het baie voordele wanneer dit

met bestaande meganiese tegnieke om golfhelling te bepaal vergelyk word. Die grondvoginhoud kan uit die golfhelling bepaal word en in samewerking met die elektromagnetiese model van grond soos in die vorige paragraaf beskryf, kan die elektromagnetiese veranderlikes baie maklik by enige frekwensie bepaal word. Die berekende waardes is meer akkuraat as dié van die ITU publikasies. Die beskikbaarheid van akkurate elektromagnetiese veranderlikes is baie handig vir die modellering van grondgolf en luggolf voortplanting in die omgewing van die RP.

Enkel Stasie Ligging (ESL) rigtingpeiling is ’n tegniek om die oorsprong (ligging van die sender) van ’n langafstand luggolf HF sein deur middel van ’n enkele, interferometriese rigtingpeiler te bepaal. Die invalshoek word gebruik om ’n afstand na die sender te bereken deur die pad wat die sein deur die ionosfeer gevolg het, te modelleer. In samewerking met die rigtinginligting kan die ligging van ’n sender bepaal word.

Die vermoë om ’n uitsending te kan monitor en die invalshoek (rigting en elevasie) deur middel van ’n interferometriese RP te bepaal waarborg egter nie die kwaliteit van die berekende ESL afstand nie. Die huidige ionosferiese toestande vir die kommunikasiekring moet ook in aanmerking geneem word om optimale resultate te verseker. Dit is egter ’n komplekse taak om die werkverrigting van ’n ESL stelsel te bereken aangesien die ionosferiese pad wat deur die sein gevolg is, deur baie faktore beïnvloed word. Om hierdie uitdaging te oorbrug is ’n kwaliteitsfaktor wat slegs van die standaard veranderlikes vir HF kommunikasieskakels afhanklik is, afgelei. Gemete resultate bevestig dat hierdie kwaliteitsfaktor ’n bruikbare aanduiding van die ESL werkverrigting bied.

ACKNOWLEDGEMENTS

- I wish to extend my sincere gratitude and high appreciation to my supervisor, Prof. Warren du Plessis for his guidance towards the success of this study.
- Thanks to my wife, Gillian, and sons Jean-Pierre and Jayden for their continuous support.
- My parents for all their never-ending enthusiasm for all my endeavours.
- To my colleague Dion Janse van Rensburg for the many fruitful passage discussions and sound boarding sessions.
- And most important of all: to the Creator of the heavens and the earth, electromagnetic waves and the ionosphere, how great Thou are!

LIST OF ABBREVIATIONS

AoA	Angle of Arrival
Armscor	Armaments Corporation of South Africa
ARTIST	Automatic Real Time Ionospheric Scaling Technique
ASAPS	Advanced Stand Alone Prediction System
CAT	Central African Time (GMT + 2 hours)
CCIR	Comité Consultatif International pour la Radio, Consultative Committee on International Radio
CW	Continuous Wave
dB	deciBell
dBm	deciBell referenced to 1 mWatt
DF	Direction Finder
DPU	Digital Processing Unit
EFOT	Estimated Frequence Optimum de Travail (80 to 85% of the MUF)
EMP	Electromagnetic Pulse
EUV	Extreme Ultraviolet
FFT	Fast Fourier Transform
FOT	Frequence Optimum de Travail

GMT	Greenwich Mean Time
GPS	Global Positioning System
GWPS	Ground Wave Prediction System
HF	High Frequency (3 to 30 MHz)
IARU	International Amateur Radio Union
IC	Integrated Circuit
IF	Intermediate Frequency
ICEPAC	Ionospheric Communications Enhanced Profile Analysis and Circuit Prediction Program
IEEE	Institute of Electrical and Electronics Engineers
IONCAP	Ionospheric Communications Analysis and Prediction Program
IRI	International Reference Ionosphere
ITS	The Institute for Telecommunication Sciences
ITU-R (Rec.)	International Telecommunication Union-Radiocommunication Sector (Recommendation)
LCD	Liquid Crystal Display
LoB	Line-of-Bearing
LOS	Line-Of-Sight (communications)
MUF	Maximum Useable Frequency
MW	Medium Wave (300 kHz to 3 MHz)

MQP	Multiple, quasi-parabolic (segments)
NEC	Numerical Electromagnetics Code
NEMP	Nuclear Electromagnetic Pulse
NCDXF	Northern California DX Foundation
NVIS	Near Vertical Incidence Skywave (propagation)
O-wave	Ordinary-wave of a signal that travelled through the ionosphere
OWF	Optimum Working Frequency
PC	Personal Computer
PIM	Parameterized Ionospheric Model
RF	Radio Frequency
RMS	Root Mean Square
RX	Receiver
SNR	Signal-to-Noise Ratio
SSN	Smoothed Sunspot Number
SSL	Single Site Location
TEC	Total Electron Content
TDR	Time Domain Reflectometry
UTC	Coordinated Universal Time
VHF	Very High Frequency (30 to 300 MHz)
VLF	Very Low Frequency (3 to 30 kHz)

VNA	Vector Network Analyser
VOACAP	Voice of America Coverage Program
X-wave	Extraordinary-wave of a signal that travelled through the ionosphere

LIST OF SYMBOLS

α	Attenuation Constant
β	Phase Constant
σ	Ground Conductivity
ε_r	Relative Dielectric Constant
δ	Skin Depth
$\emptyset$	Elevation Angle
θ	Ray Incidence Angle
μ	Magnetic Permeability
ω	Angular Frequency
Υ	Electromagnetic Wave Propagation
C	Capacitance
f	Frequency
f_b	Gyro-frequency

f_c	Critical frequency
f_oE	Critical or plasma frequency of the E layer (for the Ordinary-wave)
f_oF_1	Critical or plasma frequency of the F1 layer (for the Ordinary-wave)
f_oF_2	Critical or plasma frequency of the F2 layer (for the Ordinary-wave)
f_xF_2	Critical or plasma frequency of the F2 layer (for the Extraordinary-wave)
h_mF_2	Height of the F2 layer at the critical frequency
j	$= \sqrt{-1}$
$N(h)$	Electron density as a function of height
N_m	Amount of free electrons per cubic meter
R	Resistance

TABLE OF CONTENTS

CHAPTER 1 INTRODUCTION

1.1 PROBLEM STATEMENT

1.1.1 Context of the problem

Although the coverage offered by modern communication systems (cellular telephones, Wi-Fi, satellite, etc.) expands on nearly a daily basis, there are still instances where traditional High Frequency radio (HF, 3 to 30 MHz) ground wave and skywave communications are viable and cost effective alternatives. Examples include the aftermath of natural disasters such as earthquakes, tsunamis, tornadoes, floods, mudslides, etc. or man-made tragedies such as terrorist attacks. Under these circumstances, networks may become overloaded or the infrastructure severely damaged, reducing the capabilities of the network (Witvliet, 2015, pp. 2–3). This can especially be problematic in lesser-developed countries where back-up networks may be less common or capable (Coetzee, 2004; McNamara, 1991, pp. 2–3). Furthermore, short-range skywave communications are for security reasons preferable to using the local cellular network in many tactical military deployments. During peacekeeping missions in a foreign country, unlawful elements may have access to cellular networks, thus potentially compromising any operations.

A good example of where HF systems can be useful is when a group needs to operate deep in a remote ravine where the geography may negatively influence the commonly used line-of-sight communication channels such as Very High Frequency (VHF) radio or cellular signals and an alternative communications mode needs to be utilised. Distances involved are typically short in terms of how the crow flies, but the terrain may be very challenging. Under these circumstances, Near Vertical Incidence Skywave (NVIS) communications as depicted

in Figure 1.1 are very effective (Goodman, 1992, p. 218). The high take-off angle for NVIS communications is quite the opposite of long distance HF communications where low radiation angles are typically required (Goodman, 1992, p. 222; Witvliet *et al*., 2015).

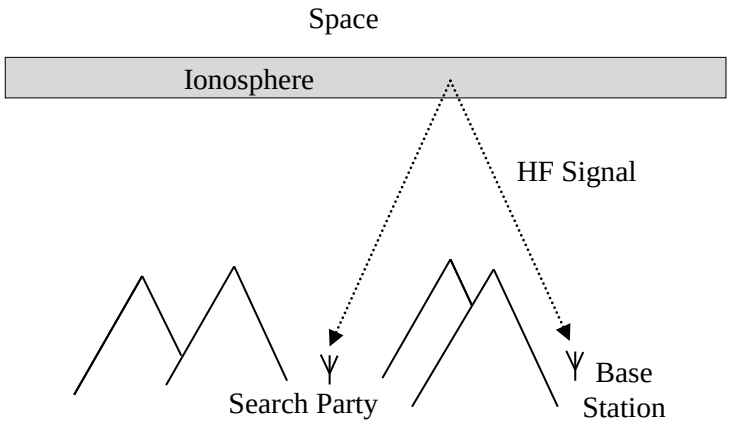

Figure 1.1. An example of short-range NVIS communications in mountainous areas.

A HF signal can propagate via various mechanisms between a transmitting and a receiving station. The space wave consists of all the signals that may reach a receiver under line-of-sight conditions. This is also referred to as the direct signal (Goodman, 1992, pp. 182, 183). The space wave and surface wave are collectively referred to as ground wave propagation (DeMinco, 1999). (Ground wave propagation is discussed in Chapter 3.) Propagation via ionospheric refraction and reflection is referred to as skywave propagation and is discussed in Chapter 5.

The ground wave component of the HF wave can provide unique capability for communications and is important in a variety of military applications as well (Goodman, 1992, p. 184). It is strongly affected by the environment and must be accurately modelled to predict tactical communications performance including interference from jamming sources, and to predict communications in difficult geographical environments such as built-up, forested and mountainous terrain (Hill, 1982). Ground wave propagation is also utilised for commercial broadcast beyond line-of-sight (LOS) (Davila, 1993).

Central to successful HF communications is the ability to accurately determine the electromagnetic properties of the ground for the operational frequency. The electromagnetic properties of ground define the path loss of ground wave communications as well as the performance (radiation angle and gain) of an antenna located close to the surface of the earth (in terms of wavelength) that is used for skywave propagation via the ionosphere (IEEE Std 356, 2011, p. 1; Goodman, 1992, p. 192).

For successful skywave communications, a sound knowledge of ionospheric propagation is essential. Fortunately, there are many modern computer programs available that can predict optimum frequencies and guide antenna choices. Examples include the Voice of America Coverage Program (VOACAP), adopted from the Ionospheric Communications Analysis and Prediction Program (IONCAP) (Teters *et al*., 1983) and the Ionospheric Communications Enhanced Profile Analysis and Circuit Prediction Program (ICEPAC), also a descendant of IONCAP (Tascione *et al*., 1987). DX Atlas and HamCap make use of the VOACAP engine to predict propagation conditions on a global scale. These two programs can download real-time space weather conditions from the Internet via the IonoProbe utility. Another option is Proplab-Pro, which was developed by Solar Terrestrial Dispatch (Alberta, USA). Proplab-Pro Version 3 uses the 2007 version of the International Reference Ionosphere (IRI) (Bilitza, 2001). It makes use of advanced two-dimensional and three-dimensional ray-tracing algorithms. The Advanced Stand Alone Prediction System (ASAPS) is based on an ionospheric model developed by Space Weather Services within the Australian Bureau of Meteorology and the International Telecommunication Union Radiocommunication Sector (ITU-R)/Comité Consultatif International pour la Radio, Consultative Committee on International Radio (CCIR) models (ITU-R Rec.P533-10; ITU-R Rec.P372-10 and CCIR Report 322). A global network of near real-time ionospheric sounders (known as ionosondes) ensures that the data used by some of these prediction programs are accurate and current, contributing to the usefulness of the results (Frissell *et al*., 2014).

HF transmissions need to be monitored for regulatory purposes to ensure that broadcasters comply with their licence requirements (ITU-R Handbook on Spectrum Monitoring, 2011, p. 189), for law enforcement purposes (smuggling, piracy and trafficking) and especially during times of conflict (Giesbrecht *et al*., 2004). It is also of paramount importance to confirm the origins of HF transmissions. A direction finder is part of the equipment base that can be used to monitor HF transmissions and determine the line-of-bearing of a signal. The line-of-bearing (LoB) can be determined by various techniques. Direction finders typically utilises amplitude comparison techniques such as Adcock or Watson-Watt, or phase comparison techniques as implemented in interferometric direction finders. The most advanced direction finders operate on the interferometric principle. They are typically used by government agencies and the military to determine the elevation and azimuth angles of a HF skywave signal (ITU-R Handbook on Spectrum Monitoring, 2011, pp. 262, 277) in electronic warfare (EW) and law enforcement applications (McNamara, 1991, p. 149; Coetzee, 2004).

The availability of elevation information allows Single Site Location (also known as Single Station Location) direction finding (simply referred to as SSL) to be performed. SSL is a technique to determine the origin (geographical location) of a long-distance HF signal with the aid of a single interferometric direction finder (ITU-R Handbook on Spectrum Monitoring, 2011, p. 293). The capability is often offered by the manufacturers of interferometric direction finders. The elevation angle of the intercepted signal is used to calculate a ground range by modelling the path that the signal travelled through the ionosphere. The best results are obtained with the aid of ray-tracing (sometimes referred to as ray-retracing) techniques. With the measured direction (azimuth angle) and the calculated ground range, it is possible to determine the origin of the HF transmission with useful accuracy under suitable operating conditions (ITU-R Handbook on Spectrum Monitoring, 2011, p. 293). Position is usually determined by triangulating the azimuth results of multiple direction finders (ITU-R Handbook on Spectrum Monitoring, 2011, p. 278), so the requirement for only a single direction finder is a significant benefit of SSL.

Longer distance skywave propagation (beyond line-of-sight) via the ionosphere is one of the main attractions of HF. The classic approach to analysing HF propagation is by monitoring beacons or known transmissions on various frequencies. The extent of the propagation on the beacon frequency between the two locations is determined by the quality of the received signal. An example of a global beacon network operating on multiple frequencies is the Northern California DX Foundation (NCDXF)/International Amateur Radio Union (IARU) International Beacon Project (http://www.ncdxf.org/beacon). The received signal strength and SNR are used as quality of service indicators i.e., to what extent is there propagation between the beacon transmitter and the receiving station. The results can be compared to frequency predictions such as generated by VOACAP, which are typically enhanced by ionospheric measurements performed by ionosondes (Frissell *et al*., 2014).

Using antennas with different characteristics such as possessing low or high radiation angles, clockwise or anti-clockwise circular polarization or directional properties yield further information regarding the propagation mechanism (Witvliet *et al*., 2015). These techniques however provide little information regarding the exact elevation angle of the received signal, the ionospheric layer(s) via which the signal propagated, the presence of multi-path propagation and if present, the type of multi-path propagation, etc.

1.1.2 Research gap

HF propagation is a multi-facetted science where there are still some unanswered questions pertaining to both ground wave and skywave propagation. In many instances, answers can only be obtained by new approaches and by making use of new technologies. In this respect, some answers can be provided with the aid of an interferometric DF, an instrument that was in the past not often used for HF propagation research purposes.

The propagation of a HF signal over ground is mainly influenced by the conductivity and dielectric constant of the soil at the frequency of operation. Modern computer programs require realistic values for the ground characteristics in order to be able to accurately compute the path loss and area coverage of the ground wave signal. Various sources and

techniques are available to determine the required constants. These include probe impedance (self-impedance) methods (Makki *et al*., 2008), wave tilt methods (King, 1976), mutual impedance methods (Kissick *et al*., 1978; Beziuk *et al*., 2007) and laboratory impedance measurements with the aid of a Vector Network Analyser (VNA) (Santos *et al*., 2009; Lytle, 1973). These approaches are generally cumbersome, may require specialised instrumentation and may not be applicable to the frequency of interest.

The ITU published graphs for relative permittivity (ε_r) and conductivity (σ) in the Radiocommunication Sector Recommendations (ITU-R Rec.P527-3, 1992, p. 2; ITU-R Rec.P527-4, 2017, pp. 1,19; ITU-R Rec.P832-4, 2015). However, the validity and usefulness of these ITU graphs are questionable. The Institute of Electrical and Electronics Engineers (IEEE) made the following statement regarding the published data (IEEE Std 356, 2011, p. 2):

> *"The International Telecommunications Union (ITU) has published world surface conductivity maps for a number of frequency bands, although these are no longer being updated. The curves of conductivity and relative permittivity in ITU-R Rec.P527-3 exhibit no dispersion in the band 3 MHz to 30 MHz, whereas measured values show significant dispersion in the band for which surface soils typically can show characteristics from lossy conductors to lossy dielectrics (King et al., 1981). The real and imaginary parts of the complex relative permittivity form a Hilbert transform pair. As a result, the conductivity and relative permittivity are not independent variables. Their mutual coupling is described by the Kramers–Kronig relations (King et al., 1981). Therefore, the ITU values for the HF band are inconsistent with the results of complex variable theory and are in error."* Copyright © 2011 IEEE, with permission.

This statement relating to a professional ITU standard (ITU-R Rec.P527-3, 1992, p. 2) is extraordinary and illustrates the problem with conventional values for soils at radio frequencies. The source of this misconception seems to be a report by Pearce, Hulse and Walker (1973) in which they incorrectly concluded that the relative dielectric constant is

basically constant from 50 MHz to more than 500 MHz. ITU-R Rec.P527-4 was published in June 2017, but unfortunately no updates were made to the graphs and information regarding the 3 to 30 MHz frequency range. (ITU-R Rec.P527-4, 2017, pp. 1, 19). The message is clear: The published ε_r and σ graphs and tables, even by international bodies like the ITU, are not reliable or accurate enough and a better solution is required.

HF signals can also propagate via the ionosphere (ITU-R Handbook on Spectrum Monitoring, 2011, p. 279). Successful HF skywave propagation depends on the correct choice of antenna (influenced by the electromagnetic properties of the ground in the vicinity of the antenna (IEEE Std 356, 2011, p. 4) and operating frequency. The requirement for accurate electromagnetic ground parameters once again comes to the fore.

The SSL technique of direction finding has many practical and financial (cost) benefits. However, the SSL technique suffers from a serious drawback in that the accuracy of the results tends to vary from day-to-day and even hour-to-hour, making it very difficult to determine which results can be trusted and which must be discarded (Baker and Burden, 1992; McNamara, 1991, p. 175). Some measure of the quality of the SSL calculation will go a long way to restoring confidence in the results.

Mewes used an interferometric DF to gather data for the development of a frequency prediction program (Mewes, 1997), but no information is presented on using an interferometric DF to determine more details regarding the reigning propagation conditions. No mention is made of how to determine if propagation was via a single path or multiple paths, a single hop or multiple hops or via which layer(s) of the ionosphere.

Being able to not only classify propagation in terms of received signal strength but also in terms of via which layer(s) the signal propagated, single hop or multiple hops, stable or unstable propagation and received elevation angle will greatly enhance the knowledge and understanding of the propagation mechanism between two locations. There is however very little published literature on how this can be accomplished.

1.2 RESEARCH OBJECTIVES AND QUESTIONS

As outlined in Section 1.1, there are still some unanswered questions when it comes to HF propagation in its various forms.

Various sources and techniques are available to determine the electromagnetic constants of soil (IEEE Std 356, 2011, p. 6; ITU-R Report P.879-1, 1986) required to accurately model an antenna in close proximity to the earth and that are also needed to model ground wave propagation. These techniques seem to be more focused on the classic broadcast frequencies (Medium Wave and Low Wave) below the frequency range of interest, the HF band.

If the values and graphs of ε_r and σ published by the ITU (ITU-R Rec.P527-4, 2017, pp. 1,19; ITU-R Rec.P.832-4, 2015) are in error and the electromagnetic constants of ground are frequency dependent, then is there a method to accurately and easily determine these parameters? Can an interferometric DF contribute to this?

Determining the wave angle with the aid of an interferometric DF does not guarantee the quality of the SSL ground range estimate. The reigning propagation conditions for the communications circuit must also be taken into consideration for optimum results. However, computing the performance of a SSL system is a complex problem, which requires accurate modelling of the ionospheric conditions and complex ray-tracing techniques. How can this difficulty be overcome to allow operators of interferometric direction finders to easily estimate the quality of their results?

For HF skywave communications, simply being able to intercept (monitor) a signal provides limited information regarding the propagation mechanisms that were involved. How can a modern interferometric direction finder provide more information regarding the propagation conditions? Is additional information required to identify the ionospheric effects on the received signal?

1.3 APPROACH

From the literature study a universal RC network soil model (Longmire *et al.*, 1975) was identified that could form the basis to determine ε_r and σ as a function of frequency. The challenge was to provide the required inputs to the RC network soil model to enable the electromagnetic parameters to be calculated. A modern, cost effective measurement system using radio frequency (RF) principles was identified to provide the required inputs to the RC network soil model, resulting in the soil moisture content technique (Coetzee, 2014) to calculate the required ground electromagnetic constants over the HF frequency range for a specific geographical location.

The calculated constants were used as inputs to a Numerical Electromagnetics Code (NEC)-based computer program (Burke *et al.*, 2004) to determine the input impedance of a dipole antenna in close vicinity to the ground. The results were compared to previously published values to confirm the validity of the soil moisture content technique to determine ε_r and σ at a specific frequency.

The path loss of a ground wave signal is determined by the electromagnetic properties of the soil. Path loss can be calculated by GRWAVE, a computer program published by the ITU (ITU-R, SG3, 2018). GRWAVE requires, among other inputs, accurate values for ε_r and σ at the frequency of interest to produce reliable results. The soil moisture content technique was used to determine the required constants and the path loss between two positions was calculated over the 2 to 30 MHz frequency range using GRWAVE. The path loss was then measured and the results compared.

The imperfect (lossy) characteristics of ground cause a ground wave signal to tilt in the direction of propagation. The soil moisture content technique was used to calculate the electromagnetic properties of soil over the HF band for various soil moisture percentages. These values were then used to calculate the expected wave tilt over frequency and the calculated values were compared to previously published values to confirm the validity of

the calculations. An interferometric direction finder was deployed at Paardefontein, South Africa and the forward wave tilt for a ground wave signal over the HF band was measured from four directions. The results were compared with the expected values for the measured soil moisture percentage, confirming that an interferometric direction finder and a ground wave signal can be utilised to provide a good indication of ε_r and σ in the proximity of the antenna array.

Ionospheric HF skywave propagation between two points is defined by various metrics such as the Maximum Useable Frequency (MUF), the Frequence Optimum de Travail (FOT) and the Lowest Useable Frequency (LUF) for the circuit. The variability of range accuracy of a SSL result was investigated in terms of these parameters to determine whether it was possible to relate the SSL accuracy to these classic parameters. Measurements were performed using a modern interferometric direction finder to confirm the results.

An interferometric direction finder was also used to monitor various beacon transmissions. The elevation angle versus distance results of ray-tracing through data provided by an ionospheric model was used in conjunction with the elevation angle results of the DF to analyse the propagation of the beacon signals. It was possible to identify the ionospheric layers via which the signal propagated, multi-path propagation in its various forms as well as the highest evaluation angle that will be refracted by a specific layer of the ionosphere.

1.4 RESEARCH GOALS

The use of RF techniques to measure geophysical properties (for the exploration for oil and minerals as well as to determine the water content of the soil) has matured over the last few decades (Robinson *et al.*, 2003). One of the research goals of this thesis was to utilise the existing geophysical knowledge to develop a new method that can quickly and cost effectively determine the electromagnetic properties of soil for HF applications.

Research goal number two was to use an interferometric DF to determine the electromagnetic properties of the ground in the proximity of the antenna field.

In terms of the propagation of skywave signals, the goal was to use elevation angle results produced by an interferometric DF to gain new insights into HF propagation.

1.5 RESEARCH CONTRIBUTION

A technique was developed to determine the electromagnetic constants of ground. The soil moisture percentage is measured using RF techniques in the form of TDR, and in conjunction with Longmire's universal RC network ground model, it is now possible to easily and with useful accuracy determine ε_r and σ at any frequency up to 200 MHz.

The research has also indicated that the wave tilt of a HF ground wave signal as measured by an interferometric direction finder can be utilised to provide a useful indication of the electromagnetic constants of the ground in the vicinity of the antenna field.

A quality factor indicator for the SSL results using widely available propagation metrics was developed, considerably enhancing the real world usefulness of the interferometric DF and the SSL technique.

The interferometric direction finder can also be utilised to analyse the propagation of a HF skywave signal. Reigning ionospheric conditions such as propagation via an unstable or a stable part of the ionosphere (corresponding to the FOT), multi-hop propagation or multi-layer propagation and propagation via the E, F1 or F2 layer(s) of the ionosphere can be clearly identified in conjunction with the results from ray-tracing through an ionospheric model.

The following journal papers were published during the course of the Ph.D. study:

1. Coetzee, P. J. (2014). A technique to determine the electromagnetic properties of soil using moisture content, *South African Journal of Science* **110**(5/6): 85–88.

2. Coetzee, P. J. and Du Plessis, W. P. (2016). Definition of a quality factor for single site location estimates, *Radio Science* **51**(6): 555–562.

3. Coetzee, P. J. and Du Plessis, W. P. (2017). Interferometric measurement of soil electrical properties using ground wave tilt, submitted to the *IEEE Geoscience and Remote Sensing Letters* (GRSL).

4. Coetzee, P. J. and Du Plessis, W. P. (2018). Performance limiters of Near Vertical Incidence Skywave Propagation, submitted to the *IEEE Antennas and Propagation Magazine*.

1.6 OVERVIEW OF STUDY

HF propagation is an extremely diverse field with many common and quite a few exotic modes of propagation possible. These modes of propagation have been the subject of many studies and experiments. In this thesis, the emphasis is on how a HF interferometric DF can be utilised in determining the main factors influencing both ground wave and skywave propagation of HF signals.

Ground wave and skywave are two vastly different topics although both are common to HF propagation. Background information for the various topics are provided at the beginning of Chapters 2, 3, 5 and 6 to differentiate between known knowledge and the new contributions.

This thesis consists of seven chapters.

Chapter 1 provides the background for this thesis. The lack of reliable electromagnetic constants for ground at the frequency of interest is stated as a major research gap. In addition, for determining the position of a HF skywave transmission with the aid of SSL it was

determined that the ability to assign a quality factor to the measured results would greatly enhance the usefulness of SSL for military and law enforcement applications.

Chapter 2 discusses the soil moisture technique that was developed to determine the electromagnetic properties of soil at the frequency of interest in conjunction with TDR and the previously published universal RC network soil model. The calculated properties of soil are compared to those obtained using the technique based on the impedance of a low dipole antenna.

In **Chapter 3,** realistic electromagnetic parameters for ground are calculated. These values are used as inputs to the ITU's GRWAVE ground wave propagation prediction program and the prediction is compared to measured results. This was done to validate the soil moisture technique to determine the electromagnetic properties of soil at the frequency of interest.

Chapter 4 describes the wave tilt of a HF ground wave signal due to the electromagnetic properties of soil. The expected wave tilt is calculated as a function of the soil moisture percentage. An interferometric direction finder is used to measure the wave tilt over the HF frequency range and the results are compared with the calculated values. This was done to confirm that an interferometric direction finder can provide a useful indication of the electromagnetic properties of the soil in the vicinity of the DF array.

Chapter 5 presents the principles of HF ionospheric propagation.

Chapter 6 discusses using a single HF interferometric direction finder to determine the origin of a signal propagating via oblique ionospheric propagation, also referred to as skywave propagation. The conditions under which most reliable results can be obtained is analysed and a quality factor for the results is introduced. This is verified by a measurement campaign.

Chapter 7 presents the conclusions.

CHAPTER 2 DETERMINING THE ELECTROMAGNETIC PARAMETERS OF SOIL

2.1 INTRODUCTION

Accurate electromagnetic ground constants are required for many applications including the modelling of ground wave propagation of radio signals, calculating clutter and reflection in radar applications, calculating the soil penetration of an electromagnetic wave and to model antennas above a real, imperfect earth (IEEE Std 356, 2011, p. 1). Electromagnetic ground constants are also widely used in geological surveys and agricultural applications (Topp *et al.*, 1980).

Various sources and techniques are available to determine the required electromagnetic constants (Lytle, 1973), but they are in general cumbersome, may require specialized instrumentation and may not be applicable to the frequency of interest (IEEE Std 356, 2011, p. 6; ITU-R Report P.879-1, 1986). According to the IEEE the main techniques are

- direct current resistivity methods,
- surface impedance methods using VLF signals,
- propagation studies in which the receiver is sometimes located underground (also limited to VLF),
- wave tilt method,
- self-impedance methods,

- mutual impedance methods, and
- TDR.

The drawback of all these techniques, with the possible exception of TDR and wave tilt, is that they cannot easily provide the required soil parameters at a specific frequency. To overcome these difficulties a new procedure for determining the electromagnetic parameters of ground at any frequency is presented.

2.2 GROUND PARAMETERS PUBLISHED BY THE ITU

The International Telecommunications Union (ITU) published various graphs for relative permittivity, and conductivity in ITU-R Rec.P832-4 (2015).

These graphs are for frequencies of 30 kHz and 1 MHz (the VLF and Medium Wave (MW) ranges) and thus not applicable to the frequency range of interest namely the HF band (3 to 30 MHz). According to the IEEE the validity and usefulness of this ITU publication is questionable (IEEE Std 356, 2011, p. 2) over the HF frequency range. To overcome these difficulties, a new procedure for determining the electromagnetic properties of soil at the frequency of interest is presented.

2.3 BACKGROUND

Geophysical prospecting has been a major driving force in the understanding and presentation of earth electrical parameters. The most basic approach is to determine the ground conductivity of earth *in-situ* by measurements of the DC resistivity using the four-probe method. Two electrodes are used to inject current and the potential distribution is measured in the vicinity of the current electrodes with the aid of another pair of probes. In practical applications not DC but low frequency alternating currents and voltages are used (IEEE Std 356, 2011, p. 10).

The fact that the earth also influences both the propagation of ground wave radio signals as well as the behaviour of antennas in proximity to the ground (IEEE Std 356, 2011, p. 1) has led to efforts to model not only the DC behaviour of the earth, but also the RF characteristics.

The most basic electromagnetic model of the earth is that of a lossy dielectric having a frequency independent ε_r of about 10, a fixed σ on the order of 0.001 to 0.1 S/m and a relative magnetic permeability of 1. Originally, the main utilization of ground wave propagation occurred at VLF and LF for military and navigation applications as well as at Low Wave and Medium Wave for commercial broadcasts. This is borne out by the 30 kHz and 1 MHz earth conductivity maps published by the ITU (ITU-R Rec.P832-4 (2015)).

In the 1960's concerns regarding the effects of a nuclear electromagnetic pulse (NEMP) on electrical and electronic systems led to renewed research on the modelling of the electromagnetic behaviour of soil. The frequency components of a NEMP extent to more than 100 MHz and several researchers focused on better understanding of the earth in this higher frequency range (Scott, 1971; King, 1969; Tesche, 2002). This resulted in electromagnetic models of the earth that are very applicable to the HF frequency range.

Currently the focus on electromagnetic modelling of the earth is for lightning research purposes (Alipio *et al., 2014).*

2.4 UNIVERSAL RC NETWORK SOIL MODEL

During the 1970s, Conrad L. Longmire and H. Jerry Longley, working for the Mission Research Corporation, developed a universal RC network soil impedance model (Longmire and Longley, 1973) for the Defence Nuclear Agency. During October 1975, Longmire and Ken S. Smith expanded this model making it valid from 1 Hz to 10 GHz (Longmire and Smith, 1975). This research was conducted to quantify the effect of an Electromagnetic Pulse

(EMP) generated by a high altitude nuclear explosion coupling into structures and underground-buried cables through the soil.

EMP is a very fast nanosecond time domain pulse with a frequency spectrum beyond 100 MHz. Longmire modelled soil as a Resistor–Capacitor (RC)–transmission line with the variation of conductivity and the dielectric constant with frequency as a function of water content. Thus, if one knows the water content of the soil, one can predict with good accuracy what the value of σ and ε_r will be at a specific frequency. Longmire and Smith based their research on work done by Scott (1971).

Scott has presented results of measurements of the electrical conductivity and dielectric constant, over the frequency range of 100 Hz to 1 MHz, for many samples of soil and rock. It was noted that the results for the many samples could be correlated quite well in terms of just one parameter: the water content. By averaging his data, he produced a set of curves $\varepsilon_r(f)$ and $\sigma(f)$ as functions of frequency (f) for various values of water content. Thus, if one knows the σ or the ε_r at one frequency, one can estimate both as functions of frequency using Scott's 'universal' curves. If the water content of a soil is known, it is possible to predict what the soils' σ and ε_r will be at a specific frequency with generally useful accuracy.

Longmire observed that all of Scott's curves for $\varepsilon_r(f)$ would very nearly coincide with each other if displaced to the right or left, that is that there is just one curve for $\varepsilon_r(f/f_0)$, where f_0 scales with water content (Longmire *et al*., 1975). Longmire's contribution was thus to show how to use the frequency-dependent parameters to formulate a time-domain treatment of electromagnetic problems. The time-domain method solved Maxwell's equations in dispersive soils, based on the assumption that each volume element of the soil could be represented by an RC network. The real and imaginary parts of this model are related to the σ and the ε_r respectively. A consequence of the RC network model is that the variation of σ and ε_r with frequency are not independent. It is also clear that the ε_r increases with frequency and σ decreases with frequency. In terms of the RC network, this means that as the water content is varied, only the R values change, while the C values remain fixed.

Wilkenfeld measured the conductivity and dielectric constant of several samples of grout and concrete over the frequency range of 1 MHz to 200 MHz. From the data published by Scott and Wilkenfeld, Longmire and Smith developed a "universal soil impedance (actually, admittance) model" that operates from 1 Hz to 10 GHz and includes both Scott's and Wilkenfeld's data. The 10% moisture curves are taken as references and are scaled to the left or right for different moisture percentages.

Despite the availability of more modern frequency dependant soil models (Visacro *et al.*, 2012; Pedrosa *et al.*, 2010; Portela *et al.*, 1999), it was determined that Longmire and Smith's universal RC network soil impedance model delivers the best performance over the HF frequency range (Mokhtari *et al.*, 2016; Cavka *et al.*, 2014).

The surface wave component of an electromagnetic wave propagates along and is guided by the earth's surface. This is similar to the way that an electromagnetic wave is guided along a transmission line. Charges are induced in the earth by the surface wave. These charges travel with the surface wave and create a current in the earth (Terman, 1955). The earth carrying this current can be represented by a leaky capacitor (a resistance R shunted by a capacitive reactance C). The characteristics of the earth as a conductor can therefore be represented by an equivalent parallel RC circuit, where the earth's conductivity can be simulated with a resistor and the earth's dielectric constant by a capacitor. At Medium Wave frequencies the soil characteristics are dominated by the resistance but at higher frequencies the soil is both resistive and capacitive (DeMinco, 1999).

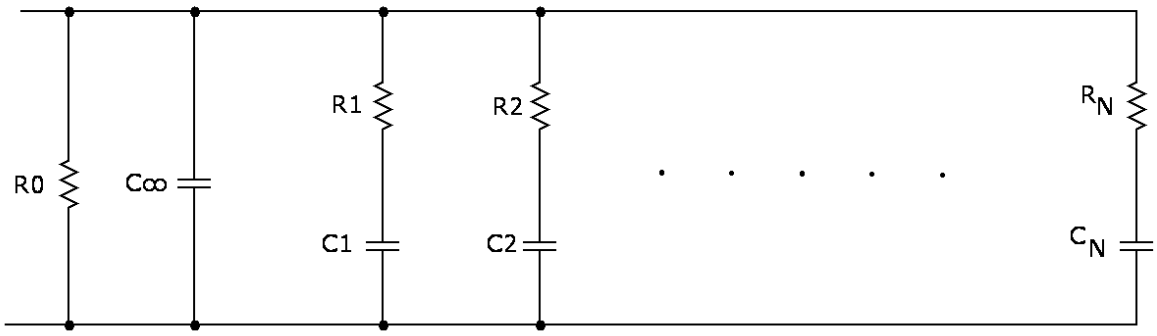

Figure 2.1. Universal RC network of the characteristics of the earth as a conductor.

In Figure 2.1, *R0* is the resistance at zero frequency (DC) and $C\infty$ is the capacitance at infinite frequency (Debye, 1929). The other branches provide transient responses with various time constants (Longmire *et al*., 1973).

2.5 DETERMINING THE MOISTURE CONTENT OF SOIL

Longmire and Longley's contribution also includes an indication on how the time-domain electrical parameters can be measured directly by pulse (RF) techniques.

TDR uses a narrow pulse of electromagnetic energy at one end of a parallel transmission line located in a lossy material. The characteristics of the reflected waveform are influenced by the dielectric properties of the medium. In the 1980s, Clarke Topp, a soil physicist working for Agriculture Canada, working from the time domain direction and, without knowledge of Longmire's work, used TDR to measure soil conductivity and dielectric constant and from there determine moisture content (Topp *et al*., 1980, 2003). Soil physicists have since extensively researched and documented TDR methods to obtain soil moisture content (Roth *et al.*, 1990; Oswald *et al.*, 2004; Robinson *et al.*, 2005; Nichol *et al*., 2002).

TDR is a complex electronic technology originally used primarily for testing high-speed communication cables. The early development of TDR for the unusual application of measuring water content in soils began somewhat by chance and continued almost in spite

of the goals set by the supporting organisations. TDR was originally used on coaxial transmission lines filled with soils in the laboratory. However, coaxial transmission lines are not practical for measurements in the field and techniques were developed to use parallel transmission lines consisting of two parallel rods placed in the soil. Originally, TDR cable testers were used for measurements in the field and the TDR waveform displayed on the oscilloscope screen was later manually analysed with pencil and ruler. Clearly, there was a need for a TDR instrument that could measure soil water content directly instead of recording travel time as cable lengths.

With the advent of powerful microprocessors, it became possible to do the entire required full waveform signal processing on a single Integrated Circuit (IC) and directly display the soil moisture content. These modern microprocessors are very compact and power efficient, making battery powered portable equipment possible.

A commercial application of the TDR technique used to measure soil moisture content is the Spectrum Technologies Field Scout TDR 300 (Spectrum Technologies, IL, USA). This instrument was designed to quickly and accurately make a large number of measurements, and together with an optional Global Positioning System (GPS), geo-locate the data and then afterwards download it to a notebook or a PC. A typical application for this TDR instrument is soil water content measurements on golf courses.

Figure 2.2. Example of the Fieldscout TDR 300 soil moisture meter (Spectrum Technologies, IL, USA).

2.6 CONFIRMING THE CALCULATED ELECTROMAGNETIC PARAMETERS OF SOIL

In free space a half wave dipole antenna has an impedance of very nearly 72 + j0 Ω. The input impedance changes as the antenna is brought closer to the surface of an imperfect earth. An antenna can thus be used as a "geological probe". Nicol published graphs to determine the electromagnetic parameters of soil from measuring the input impedance of a thin, halve-wave dipole at heights of 0.05 λ and 0.02 λ (Nicol, 1980).

EZNEC, an antenna modelling program (Lewallen, 2013) based on NEC-2 (Burke *et al*., 2004) can be used to calculate the input impedance of a thin dipole antenna close to the ground according to the defined ground constants. Using Longmire and Smiths' graphs to determine the soil constants for 10% soil moisture at a frequency of 5 MHz yield ε_r = 24.61 and σ = 0.0046. The wavelength at 5 MHz is nearly 60 m; a dipole antenna with a length 30

m was chosen for the calculations. If the height is taken as 0.02 λ (1.2 m) EZNEC calculates the input impedance at 5 MHz as 79.72 + j69.71 Ω.

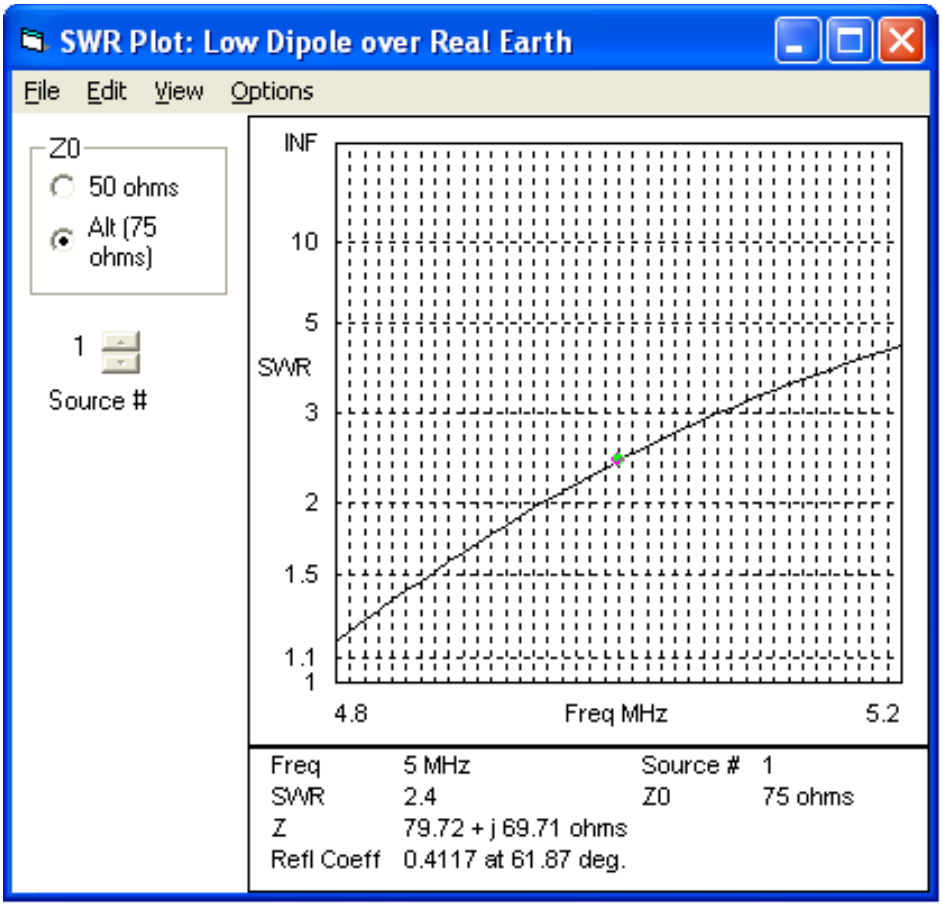

Figure 2.3. Input impedance of a dipole antenna with a length of 30 m, 0.02 λ above an imperfect earth (σ = 0.0046, ε_r = 24.61) according to EZNEC.

According to Nicol the input impedance of a dipole antenna under the same conditions (height and electromagnetic properties) is approximately 80 + j70 Ω (Nicol, 1980). As seen in Figure 2.3. these values correlate rather well with the 79.72 + j69.71 Ω calculated by EZNEC!

If the exercise is repeated for a height of 0.05 λ:

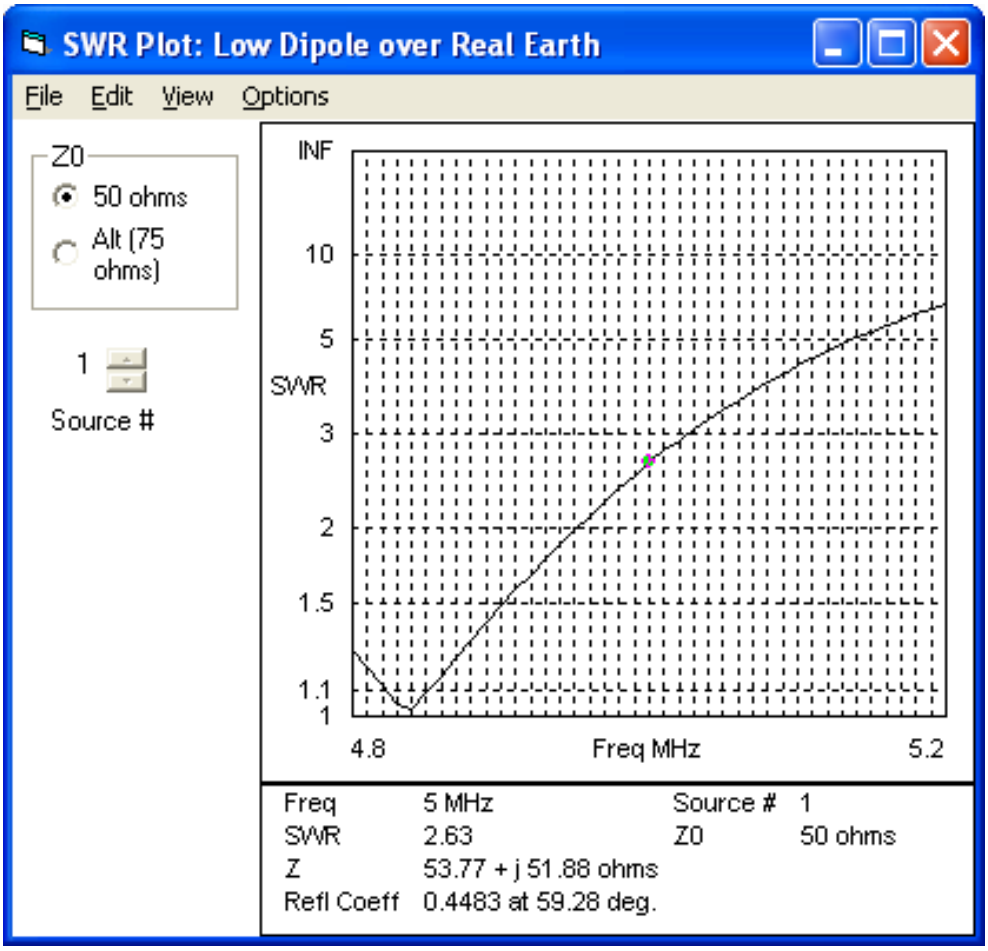

Figure 2.4. Input impedance of a dipole antenna with a length of 30 m, 0.05 λ above an imperfect earth (σ = 0.0046, ε_r = 24.61) according to EZNEC.

According to Nicol the input impedance of the dipole antenna is approximately 58 + j43 Ω. EZNEC calculates it as 53.77 + j51.88 Ω as shown in Figure 2.4. The correlation between Nicol's and EZNEC's results is acceptable (with-in 15%) although it is difficult to accurately read the values from Nicol's published graphs. A difference of less than 10% or less than 5%, which can be classified as a "good" agreement or an "excellent" between the two approaches would have been preferred.

The soil moisture technique in conjunction with Longmire's universal RC network soil model is considerably easier to use than Nicol's approach.

2.7 SUMMARY

It is now possible to easily and accurately determine soil moisture content using RF techniques (TDR) and to use the moisture percentage in conjunction with Longmire's universal RC network soil impedance model to determine the conductivity and dielectric constant for the frequency of interest. This technique promises enhanced accuracy for the modelling of ground wave propagation, transmitter area coverage, ground penetration of a RF signal, radiation patterns and input impedances of HF antennas as well as ground reflections at reflective antenna test ranges such as the National Antenna Test Range at Paardefontein, South Africa (Armscor, 2013).

CHAPTER 3 VALIDATING THE SOIL MOISTURE TECHNIQUE BY MEANS OF HF GROUND WAVE PROPAGATION

3.1 INTRODUCTION

A HF signal can propagate via various mechanisms between a transmitting and a receiving station. The space wave consists of all the signals that may reach a receiver under line-of-sight conditions. It also includes any earth-reflected signal. This is also referred to as the direct signal (Goodman, 1992, pp. 182, 183). The space wave and surface wave of Figure 3.1 are collectively referred to as ground wave propagation (DeMinco, 1999). Propagation via ionospheric refraction and reflection is referred to as skywave propagation and is discussed in Chapter 5.

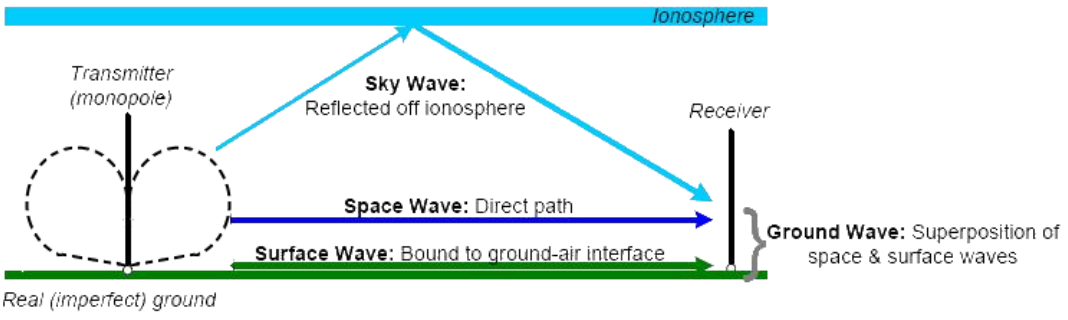

Figure 3.1. Simplified propagating wave components.

The basic principles of ground wave propagation are summarised as background to the measurements to confirm the validity of the soil moisture technique to determine the electromagnetic parameters of the ground.

3.2 GROUND WAVE PROPAGATION

"Ground wave" describes the total field (the line-of-sight, ground surface reflection, and surface (Norton) waves) observed at a point in space due to a radiation source located a finite distance above the earth. Any component reflected from the ionosphere or upper atmospheric layer (e.g. tropospheric scatter) is excluded, but the ground wave does include effects resulting from knife-edge and earth-spherical diffraction. The line-of-sight (or direct) wave and the ground reflected wave are together known as the space wave. Propagation of the ground wave depends on the relative geometry of the transmitter and receiver location and antenna heights, the polarization of the antennas, the electromagnetic properties of the ground as well the operational frequency. (DeMinco, 1999; Davila, 1993).

The radio wave propagates primarily as a surface wave when both the transmitter and receiver are near the earth in terms of wavelengths, due to the direct and ground-reflected waves in the space wave cancelling each other. As a result, the surface wave is the only wave that is left. This cancellation is a result of the zero elevation angle and that the two waves (direct and reflected) are equal in amplitude and opposite in phase. This is the condition that exists for the MW band as well as the lower HF frequencies.

The surface wave is predominantly vertically polarized, since the ground conductivity effectively shorts out most of the horizontal electric field component. What is left of the horizontal component is attenuated at a rate many times that for the vertical component of the field. When one or both antennas are elevated above the ground to a significant height with respect to a wavelength, the space wave predominates.

3.3 BACKGROUND

In an effort to explain the landmark achievement of Marconi in wirelessly bridging the Atlantic ocean, Zenneck postulated the existence of a surface-type wave in 1907. This wave would follow the earth's curvature over a considerable distance. The study of ground wave propagation started with Sommerfeld in 1909. His work supported Zenneck's theory, but was mathematically very complex. Some researchers debated the validity of Sommerfeld's work until Norton provided a solution in 1935. Wagner focused on the decomposition of the ground wave into surface and space wave components (Wagner, 1977).

A number of models and computer programs have been developed to calculate the basic transmission loss for ground and surface wave propagation for point-to-point communication circuits. WAGNER was developed to calculate ground wave loss over realistic, smoothly varying, inhomogeneous, irregular terrain (Ott, 1971a). It is based on an elementary function closely related to the Sommerfeld flat-earth attenuation function. Interesting to note is that the program was named after Wagner's integral equation for the calculation of the attenuation of a radio wave.

The Institute for Telecommunication Sciences (ITS) developed a program called WAGSLAB, a generalization of WAGNER that may be used over rough terrain (Ott, 1971b; Ott *et al.*, 1979). WAGSLAB allows for the effect of lossy, anisotropic slabs over irregular terrain.

A modern, commercially available, Windows compatible option is the Ground Wave Prediction System (GWPS) computer program that is used for predicting the propagation of radio waves in the MW and HF bands over the surface of the earth. The program can be used to generate area prediction charts of field strength, SNR and frequency range for the user selectable transmitter location. It is available from the Space Weather Services of the Bureau of Meteorology of the Australian Government.

3.4 GRWAVE

Path loss can be calculated by GRWAVE, a computer program published by the ITU ((ITU-R, SG3, 2018). GRWAVE is based on the theory of Rotheram (1981). The program was modified for execution on a PC by Dr John Cavanagh of the Naval Surface Warfare Centre in July of 1988. Later, CCIR adopted the program to compute ground wave transmission loss (CCIR, 1990). The program can also be used to determine field strength transmission loss from the designated transmitter to the designated receiver.

3.4.1 The GRWAVE computer model

The GRWAVE model considers a smooth (no terrain obstacles), homogeneous (a single set of ground constants), spherical earth bounded by a troposphere with exponential height variation. GRWAVE uses three different methods to calculate field strength depending on wavelength λ, path length d and antenna height h relative to the earth's radius a. At longer distances ($d > \lambda^{1/3}a^{2/3}$ and $h < \lambda^{2/3}a^{1/3}$), the residue series is used, at shorter distances ($h > \lambda^{1/3}a^{2/3}$ and $h < \lambda^{2/3}a^{1/3}$), the model employs the extended form of the Sommerfeld flat-earth theory (Sommerfeld, 1909). Geometric optics are used to calculate field strength at distances not covered by either residue series or the Sommerfeld theory ($h > \lambda^{2/3}a^{1/3}$ and d within the radio horizon) (Davila, 1993).

An examination of the code shows that the program uses five subroutines: geometric optics (GWGO), a flat earth attenuation function using Kings' Equation (King, 1969) with curvature correction from Hill and Wait (GWFEC); Hill and Wait's series (Hill and Wait, 1980) for small Q (GWSQ); a residue series module (GWRSS); and numerical integration (GWINT). Unfortunately, the documentation for this program was never completed (Davila, 1993).

3.4.2 GRWAVE input parameters

GRWAVE requires frequency, polarization, power, ground dielectric constant and conductivity, lower and higher antenna heights, and distance as inputs.

GRWAVE uses a number of variables to control the calculations and the operation of the computer code. Each variable has an initial default value that can be changed by the operator.

3.5 USING GRWAVE TO VALIDATE THE CALCULATED SOIL PARAMETERS

The received power level of a ground wave, HF signal between Pretoria, South Africa (located at 25°44'41.4" S and 28°16'16.2" E) and the South African National Antenna Test Range (NATR) at Paardefontein (located at 25°33'14.3" S and 28°22'31.00" E), was measured and compared to the value calculated by the GRWAVE computer model using electromagnetic parameters determined by the soil moisture technique described in Chapter 2.

A 100 W HF transmitter in conjunction with a wideband, monopole antenna with known characteristics operating against a ground screen was used at the Pretoria site. A Continuous Wave (CW) signal was transmitted on the selected frequency under command of the receive site.

A calibrated receiving antenna (Rohde & Schwarz HFH2-Z1, Munich, Germany) and a test receiver (Rohde & Schwarz ESH 3, Munich, Germany) were used to measure the received field strength (in dBµV/m) at Paardefontein. The measured field strength was converted to received power (dBm) and compared to the value calculated by GRWAVE for the specified operating conditions.

Figure 3.2. Example of an antenna used for field strength measurements.

Figure 3.3. Rohde & Schwarz ESH 3 test receiver.

A Spectrum Technologies Field Scout TDR 300 soil moisture meter (Spectrum Technologies, IL, USA) was used to determine the moisture percentage at various points between the South African sites located at Pretoria and Paardefontein. The average moisture content was 17.3% and from this result, the conductivity and relative dielectric constant were calculated for the applicable test frequency.

The tests were conducted over a great circle distance of 23.56 km. The measured and the GRWAVE calculated received power levels are compared in Figure 3.4.

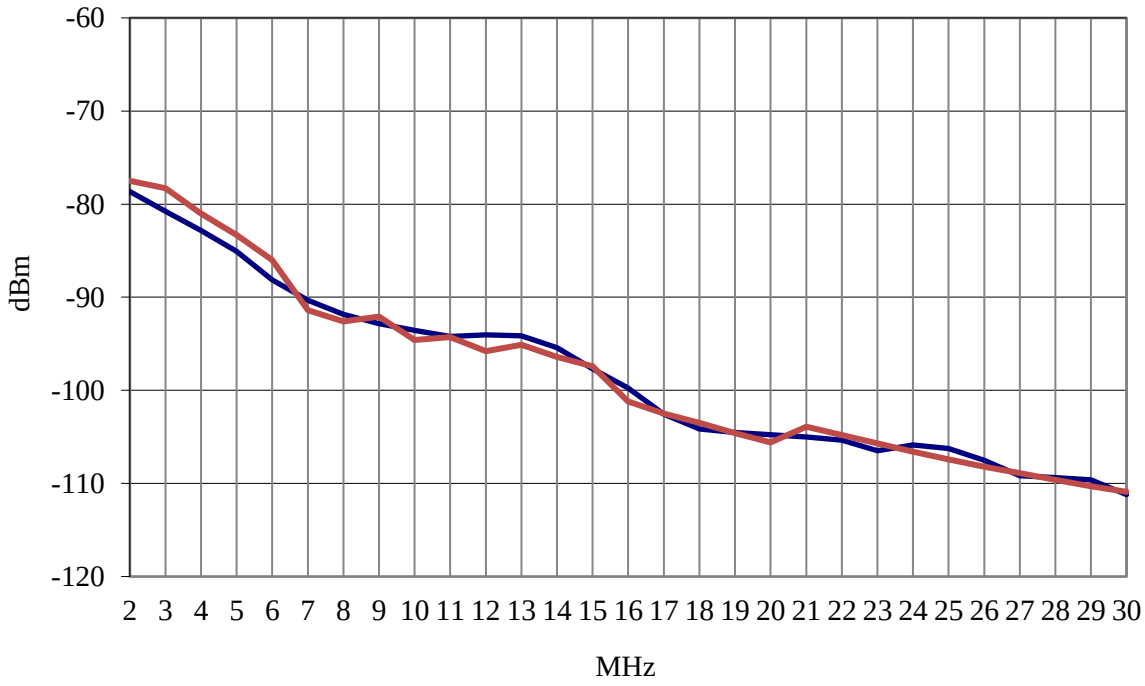

Figure 3.4. Measured (red) and calculated (blue) received power for a HF ground wave signal between Pretoria and Paardefontein.

3.6 SUMMARY

As seen in Figure 3.4 the measured and calculated results correlate very well. The fact that Paardefontein is located in open countryside with no major mountains between Paardefontein and the test transmitter's location in Pretoria contributed positively to the result. The ground wave propagation mechanism would be significantly affected by hilly

terrain, thus having a negative impact on the results. This is due to the contribution of the direct path or “space wave” component being reduced by the obstacles presented by the hilly terrain.

The universal soil impedance model and moisture percentage technique offers significant advantages in terms of simplicity, speed and cost in determining the electromagnetic properties of soil at any frequency of interest when compared with current techniques. In Figure 3.4, it is clear that the calculated electromagnetic constants provide excellent results for the prediction of ground wave propagation when used in conjunction with GRWAVE.

CHAPTER 4 DEDUCING THE ELECTROMAGNETIC PROPERTIES OF SOIL USING AN INTERFEROMETRIC DF AND GROUND WAVE TILT

4.1 INTRODUCTION

The non-ideal electromagnetic properties of soil cause a HF ground wave signal to tilt in the direction of propagation. The amount of tilt is determined by the electromagnetic properties of the ground (Wait *et al.*, 1996).

Wide-aperture interferometric HF Direction Finders (DF) are typically used to determine the elevation and azimuth angles of an HF skywave signal in Electronic Warfare (EW) and law-enforcement applications. The possibility to measure the wave tilt of a ground wave signal with the same type of interferometric DF is investigated in this chapter. The measured wave tilt can be used to estimate the soil moisture content. With the soil moisture content known, the electromagnetic constants of the ground in close proximity to the wave tilt measurement antenna can be determined with useful accuracy using the soil moisture technique and a previously published ground model (Coetzee, 2014). The calculated ground electromagnetic properties can be further utilised as inputs to ground wave propagation path loss calculations, ground wave transmitter area coverage calculations, as well as to calculate the optimum

antenna heights for the best take-off angle for HF skywave communications over specified circuits.

4.2 WAVE TILT

The surface impedance of soil gives rise to a small radial component of the electric field vector when a vertically polarised plane wave propagates over flat ground. The electric-field vector describes an ellipse in the plane containing the direction of propagation. The major axis of the ellipse is tilted forward in the direction of wave travel due to the power losses in the non-ideal ground (Eaton, 1976). The same applies for the magnetic field vector of a horizontally polarized wave (IEEE Std 356, 2011, p. 17).

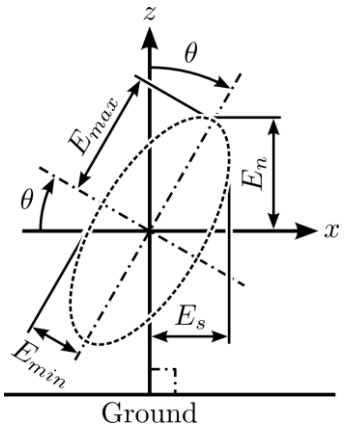

Figure 4.1. Electric vector due to wave tilt with propagation in the x direction.

The electromagnetic ground constants determine the forward tilt relative to the surface and axial ratio (r) of the ellipse.

The classic technique to measure the wave tilt of a ground wave signal is by using a small rotatable dipole to function as a goniometer by mounting it on a non-conductive tri-pod at a low height above the ground. The dipole is set up so that its plane of rotation is in the direction of the source. The dipole is tilted until the received signal level is at a minimum, at which point the angle of the dipole determines the angle of the wave tilt. A signal maximum will be obtained if the dipole is further rotated through 90° (Eliassen, 1957). It is

also possible to use a tuned-loop antenna to construct a goniometer that serves the same purpose (Underhill, 2012). This manual technique is clearly time consuming and prone to measurement errors (ITU-R Report P.879-1, 1986, p.70). A more automated process is highly desirable, especially for on-the-move or rapid deployment applications.

An interferometric DF is typically used to determine the elevation and azimuth angles of a HF skywave signal in electronic warfare and law enforcement applications (McNamara, 1991, p. 149; Coetzee, 2004). The wave tilt of a ground wave signal (elevation angle) can be automatically measured by the same interferometric DF, making it imminently suited to fulfil the above mentioned requirements.

The wave tilt measured over the HF frequency band can be used to estimate the soil moisture content. With the soil moisture content known the electromagnetic constants of the ground in close proximity to the DF antenna field can be determined with useful accuracy using the soil moisture technique and the previously published universal RC network soil impedance model.

4.3 WAVE TILT THEORY

The wave tilt theory is well known and has been extensively treated by various authors (Eaton, 1976; Eliassen, 1957; Wait, 1998). The applicable theory is summarized below.

From Figure 4.1 the elliptical electrical field is the results of the parallel (E_s) and the normal (E_n) components to the surface of the ground. The ratio of the absolute components of the parallel to the normal electric fields is given by:

$$\left|\frac{E_s}{E_n}\right| = \sqrt{\left(\frac{r^2+tan^2\theta}{1+r^2tan^2\theta}\right)} \ , \tag{4.1}$$

where r is the ratio of the minor axis to major axis (E_{min}/E_{max}) and θ is the forward tilt angle.

Furthermore,

$$\frac{E_s}{E_n} = \left|\frac{E_s}{E_n}\right| e^{j\varphi}, \tag{4.2}$$

where φ is the relative phase angles between the components. If φ is equal to zero the result is a straight line and if φ is equal to 90° the result is a circle. Note that φ does not affect the forward tilt angle.

It can further be shown that

$$\left|\frac{E_s}{E_n}\right| = \frac{1}{120\pi} \times \sqrt{\frac{\omega\mu}{\sqrt{\sigma^2+\omega^2\varepsilon^2}}}, \tag{4.3}$$

and

$$tan(2\varphi) = \frac{\sigma}{\omega\varepsilon}, \tag{4.4}$$

where σ is the absolute conductivity in S/m, ε is the absolute dielectric constant in F/m. ω is the angular frequency in rad/s and μ is the permeability of free space expressed in H/m.

The absolute dielectric constant is related to the relative dielectric constant, ε_r by:

$$\varepsilon = \varepsilon_r \varepsilon_0, \tag{4.5}$$

where

$$\varepsilon_0 = 8.854 \times 10^{-12} \text{ F/m}, \tag{4.6}$$

and the permeability of earth is one, giving

$$\mu = 4\pi \times 10^{-7} \text{ H/m}. \tag{4.7}$$

The relative dielectric constant can also be calculated from:

$$\varepsilon_r = \left|\frac{E_n}{E_s}\right|^2 \times cos(2\varphi), \tag{4.8}$$

and the conductivity over frequency is given by:

$$\frac{\sigma}{f} = \left|\frac{E_n}{E_s}\right|^2 \frac{sin 2\varphi}{18}, \tag{4.9}$$

with the result being in mS/m when the frequency, *f*, is expressed in MHz.

4.3.1 Expected wave tilt values

Previously published wave tilt and axial ratio measurement results (Adams *et al.*, 1984) indicate that wave tilt values of less than 20° and axial ratios of less than 10% can typically be expected over the HF frequency range.

Using the above equations and re-arranging the terms reveal that the forward wave tilt can be calculated from

$$\theta = \frac{1}{2} sin^{-1}\left(\left|\frac{E_s}{E_n}\right| \sqrt{\frac{2\,cos(2\varphi)+2}{\left|\frac{E_s}{E_n}\right|^4 + 2\,cos(2\varphi)\left|\frac{E_s}{E_n}\right|+1}}\right). \tag{4.10}$$

According to the IEEE, the real and imaginary parts of the complex relative permittivity of ground form a Hilbert transform pair. As a result, the conductivity and relative permittivity (of soil) are not independent variables. Their mutual coupling is described by the Kramers–

Kronig relations (IEEE Std 356, 2011, p. 2). This implies that the values of the electromagnetic constants (σ and ε_r) of ground are casual and frequency dependent (Tesche, 2002).

Curves for the electromagnetic constants were calculated from Longmire and Smith's model over the 1 to 30 MHz frequency range (refer to Chapter 2). Representative soil moisture contents were used for the dielectric constant curves shown in Figure 4.2 below.

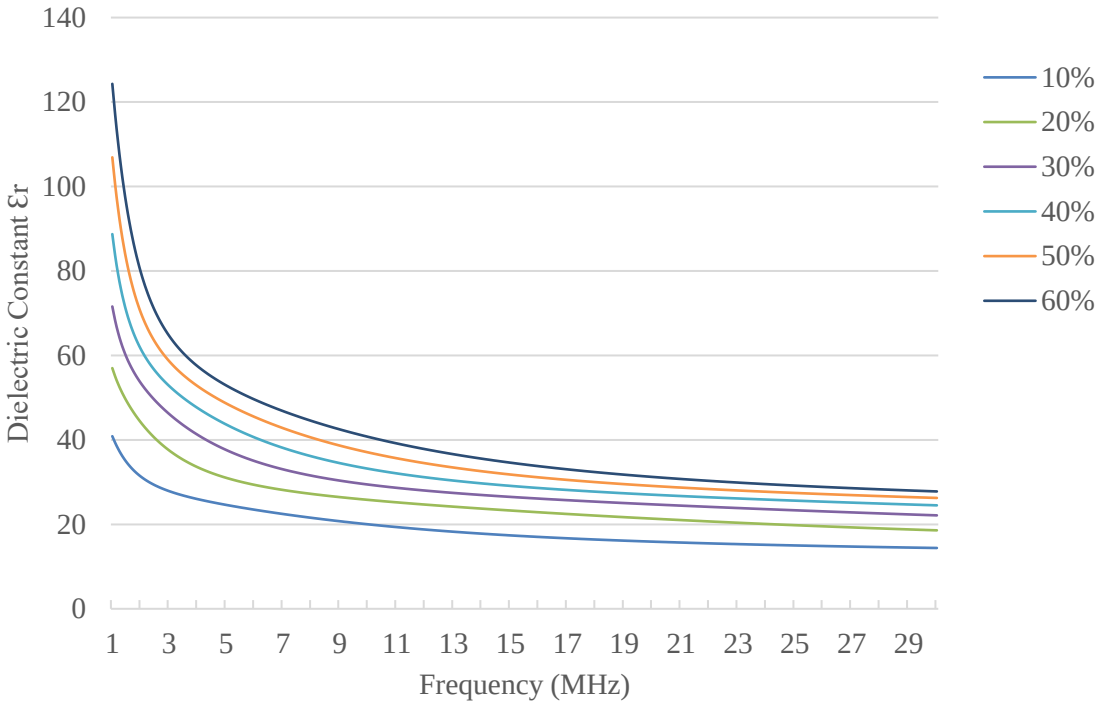

Figure 4.2. Calculated dielectric constant curves over the 1 to 30 MHz frequency range for various soil moisture percentages.

According to Longmire the conductivity of soil is a function of both the soil moisture content as well as the type of soil. The soil type causes a fixed offset of the conductivity and is determined by measuring the conductivity at DC (zero frequency). The calculated conductivity curves over the 1 to 30 MHz frequency range for representative soil moisture contents are displayed in Figure 4.3 below. The zero frequency conductivity at the measurement site was measured on average as 1.5 mS/m. The measurement was done with

a Spectrum Technologies Field Scout 24" Direct Soil Electric Conductivity Probe (Aurora, IL, United States of America).

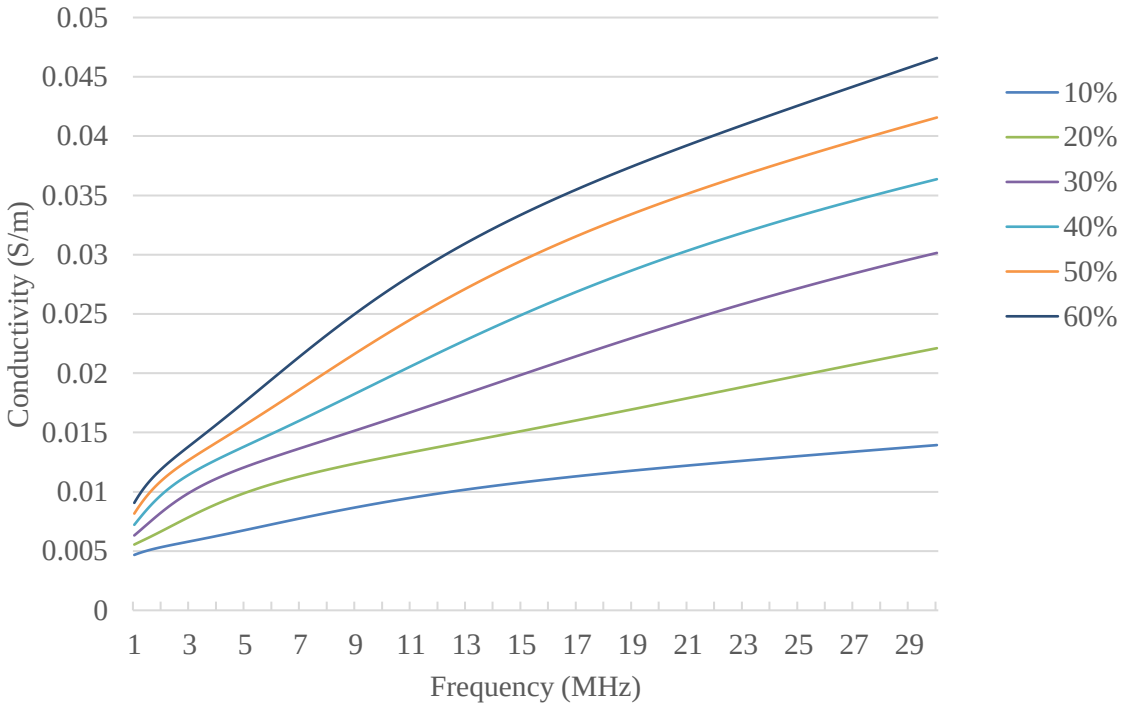

Figure 4.3. Calculated conductivity curves over the 1 to 30 MHz frequency range for various soil moisture percentages.

Taking the values for the dielectric constant and conductivity from Figures 4.2 and 4.3 and using (4.1) to (4.9) make it possible to calculate the absolute value of the electrical field components and the relative phase angle, φ, as a function of the soil moisture content. The expected forward wave tilt as a function of the soil moisture content over the HF frequency range is then calculated from (4.10). The calculated forward wave tilt as functions of the soil moisture contents are shown in Figure 4.4 below.

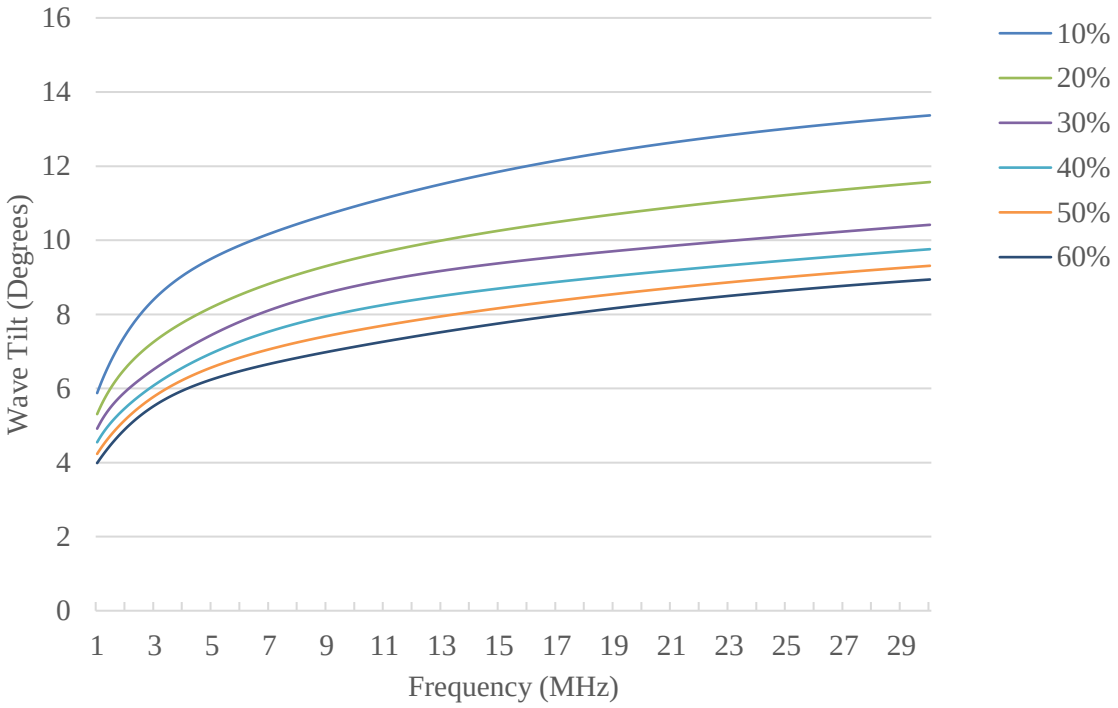

Figure 4.4. Calculated wave tilt over the 1 to 30 MHz frequency range for various soil moisture percentages.

The calculated wave tilt values of Figure 4.4 compare favourably with the measurements made at four widely spaced spot frequencies of 5.25, 7.25, 11.5 and 28 MHz by Adams *et al.* (1984) using the tilted dipole technique.

4.4 INTERFEROMETRIC DIRECTION FINDING PRINCIPLES

The line-of-bearing (LoB) of a signal can be determined by various methods. Direction finders typically utilise amplitude comparison techniques such as Adcock or Watson-Watt, or phase comparison techniques as implemented in interferometric direction finders. Watson-Watt direction finders can only provide azimuth information while interferometric direction finders are capable of providing elevation angle as well, adding another dimension to the DF result.

Interferometric direction finders operate on the wide aperture principle with the antenna systems being large in comparison to the wavelength of the signal being received. Wide aperture systems are much less sensitive to wavefront distortion than narrow aperture systems. In narrow aperture DF systems use is typically made of crossed loop or Adcock antennas with the aperture being small compared to the wavelength of the signal, resulting in high sensitivity to any wavefront distortion. The interferometric direction finder calculates the direction of arrival of the incoming wave from the phase measurements made on a number of spaced antennas. The interferometric DF antenna array can take many forms such as circular, Y, X or an L shape. The L-shaped array is used by the interferometric direction finder that was utilised in this thesis. The reference antenna is at the corner of the L with a north-south and an east-west leg. The inner pairs of antennas are separated by shorter distances than the outer pairs. In a 70 m, seven element L-array the inner antenna pairs are spaced 10 m, the next pair 25 m, and the outer pair spaced 40 m. The phase results of the closer antennas are used to resolve any phase ambiguities (phase wrapping) while the wider spaced antennas are used for more accurate measuring of the phase differences compared to the reference antenna. There is no requirement to know the absolute phases, only the phase differences that are used to calculate the received azimuth and elevation angles. Unlike beamforming direction finders, interferometers accept all the signals incident on the array (McNamara, 1991, pp. 149–150; ITU-R Handbook on Spectrum Monitoring, 2011, pp. 270–271).

A phase difference Φ exists between two antennas (receivers) spatially separated by a distance d when an incoming electromagnetic wave travels past them. The phase difference depends on the frequency of the incoming signal, the spacing (d) of the antennas as well as the arrival angle (θ) as illustrated in Figure 4.5.

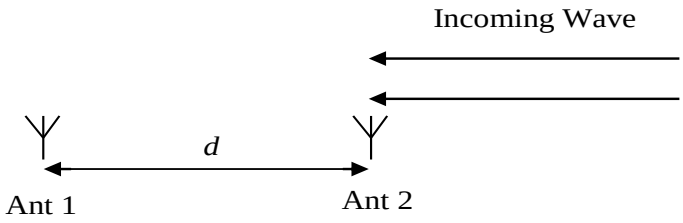

Figure 4.5. Basic interferometric principle.

In Figure 4.5 the wavelength λ (metre) is given by:

$$\lambda = \frac{299\,792\,458}{f}, \tag{4.11}$$

where f is the frequency in Hz.

The phase difference is given by

$$\phi = \frac{2\pi d}{\lambda}. \tag{4.12}$$

Figure 4.6 illustrates a wave arriving at the spaced antennas at an elevation angle θ

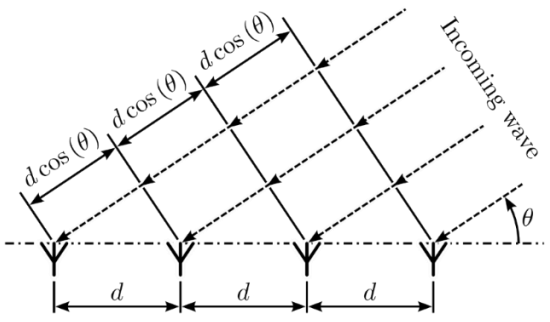

Figure 4.6. Spatial phase difference.

The phase difference between the equally spaced antennas of Figure 4.6 is given by

$$\phi = \frac{2\pi d \cos\theta}{\lambda}. \tag{4.13}$$

It is possible to calculate the azimuth as well as the elevation angles, collectively known as the wave angle, of an incoming electromagnetic signal by measuring the phase difference between a reference antenna and two orthogonally placed antennas as illustrated in Figure 4.7.

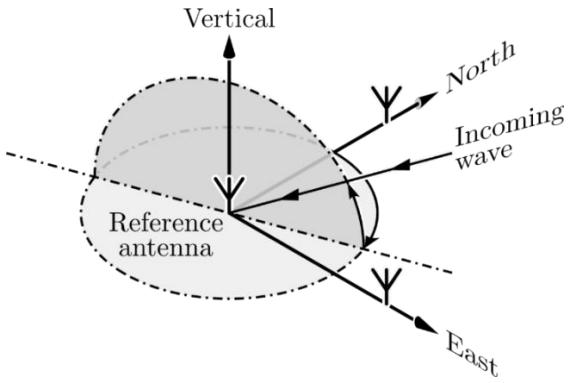

Figure 4.7. Three-dimensional interferometric principle.

The wave angle of the incoming signal can be calculated from the phase differences measured between the reference antenna and the north antenna as well as between the reference antenna and the east antenna (McNamara, 1991, p. 150). Identical, phase-coherent receiver channels (at least two channels if an antenna switch is utilised) are required to measure the phase differences illustrated in Figure 4.7. The antennas must also have identical responses and the feed lines connecting the antennas to the receivers must have identical electrical lengths (delays) to ensure that the measured results are a true reflection of the incoming wave front.

From the above it is clear that an interferometric direction finder is well suited to automatically measure the forward (vertical) wave tilt of a ground wave signal. It is however normally not suited to measure the horizontal tilt. This is not a problem as Figure 4.4 has

shown that the forward wave tilt is sufficient to determine the electromagnetic constants of the ground depending on the operating frequency, the conductivity at DC and the moisture content of the soil.

4.5 THE GEW TECHNOLOGIES MRD5000 WIDEBAND HF INTERFEROMETRIC DIRECTION FINDER

The GEW Technologies (www.gew.co.za) MRD5000 wideband HF interferometric DF covers the 500 kHz to 30 MHz frequency range. The receiver analogue bandwidths of 0.35/1/2 or 10 MHz are automatically selected depending on the staring bandwidth selected by the user. The different bandwidths ensure optimum dynamic range in challenging signal environments. The MRD5000 makes use of nine, coherent RF channels to enable single capturing for optimum DF quality results. (Switching is required if a seven or nine element antenna array is used with a three-channel DF, compromising the quality of the DF results.) The noise figure of the receiver is better than 14 dB, resulting in a receiver sensitivity of better than -116 dBm for a 10 dB Signal-to-Noise-Ratio (SNR) in a 2.5 kHz resolution bandwidth. The minimum signal duration for a DF result is less than 1 ms. This translates in a very high probability of detection of all current burst and frequency hopping transmissions in the selected bandwidth. The DF accuracy (azimuth and elevation) root-mean-square (RMS) error is better than 0.5° when the received SNR is higher than 20 dB. The resolution of the DF result (azimuth and elevation angles) is 0.1°

The MRD5000 operates on the wideband (digital) principle where an eight-hundred-point complex Fast Fourier Transform (FFT) is performed on the captured analogue bandwidth. The available resolution/bandwidth pairs vary from 62.5 Hz/50 kHz to 12.5 kHz/10 MHz. A DF result is calculated from the phase information from the complex FFT for each of the eight-hundred FFT bins, resulting in a DF scan rate of 1 GHz/s at a 2 MHz bandwidth and a 2.5 kHz resolution. The eight-hundred DF results are displayed as both a spectrum (amplitude versus frequency) and a waterfall (sonogram) on the user interface. Colour is

used to indicate the direction of the received signal, making it easy for an operator to identify signals originating from the target direction. The eight-hundred DF results are in contrast to the single DF result of the older generation, classic, narrowband analogue DF's.

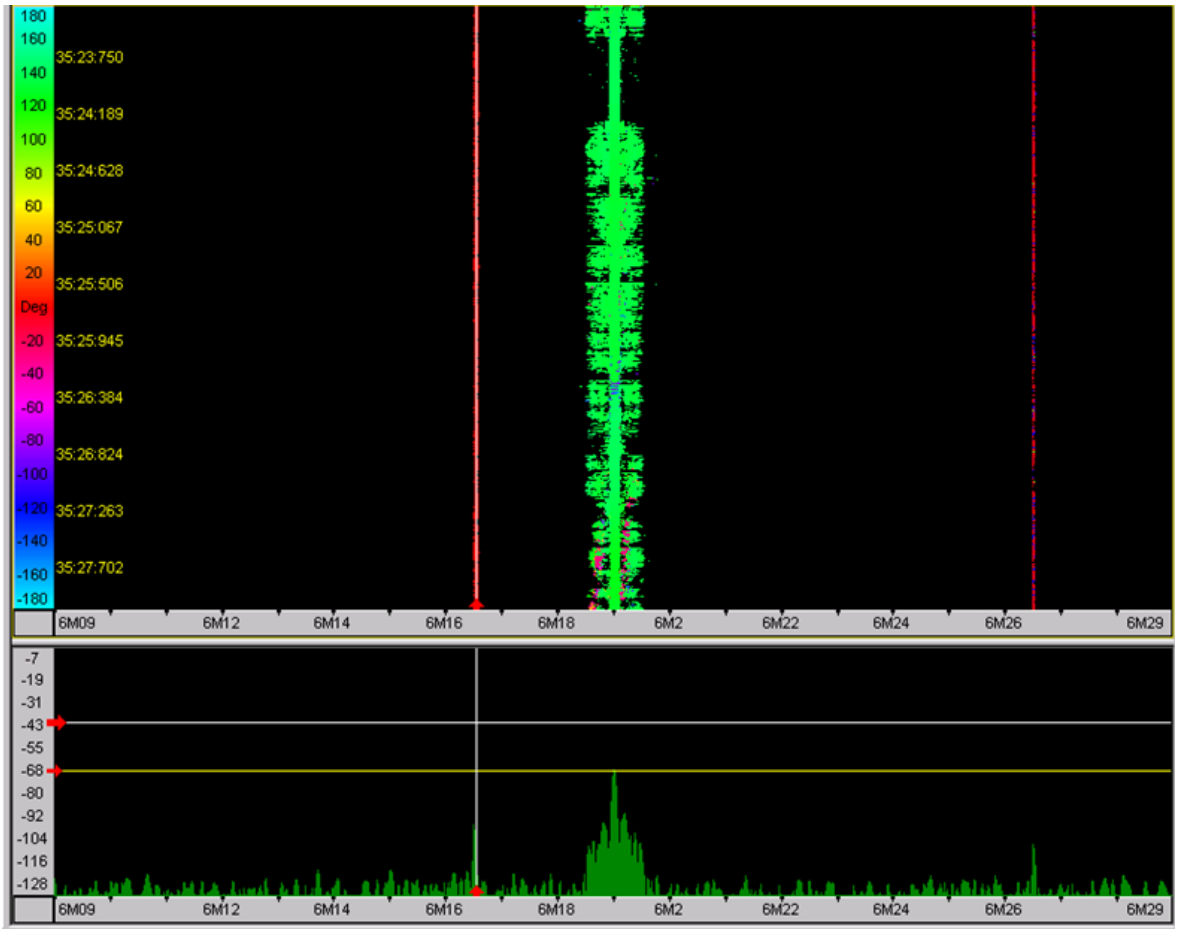

Figure 4.8. Spectrum and waterfall DF display of the user interface of the GEW MRD5000 wideband interferometric DF. Colour is used to indicate the angle-of-arrival.

The high speed of the MRD5000 allows up to five operators, each with his own user interface displaying a spectrum and a waterfall, to connect to the DF.

Figure 4.9. A photo illustrating the hardware of the GEW MRD5000 wideband interferometric DF.

The three units shown in Figure 4.9 make up the MRD5000 DF hardware. At the top is the GAS5000A antenna interface. This unit selects the antenna mode (circular or linear) and also provides nine, phase linear calibration signals to calibrate the coaxial cables, receiver paths as well as the digital paths of the DF.

The centre unit in Figure 4.9 is the MRD5000W multichannel DF receiver. A high speed, high purity frequency synthesizer provides nine phase linear oscillator signals to the nine receivers. The nine intermediate frequency (IF) outputs are routed with coaxial cables to the nine, analogue-to-digital-converter inputs of the bottom Digital Processing Unit (DPU). The DPU also contains the system controller as well as all the Digital Signal Processors.

An L-shaped, nine element, 125 x 125 m antenna array is utilised. Each antenna is a combination of an active, vertical monopole element (linear polarization) and two orthogonal, active crossed loops antennas. The outputs of the crossed loops are combined with a 90° phase shift to provide a circularly polarised signal. Clockwise or anti-clockwise polarization can be selected to monitor either the ordinary or the extraordinary-wave component. The GAS5000A selects the required input (linear or circular polarization) that is routed to the DF.

The DF antennas are spaced at 8, 20, 50 and 125 m.

Figure 4.10. A photo illustrating the deployed antenna array utilised by the GEW MRD5000 wideband interferometric DF.

The vertical elements of the DF antennas are typically used to determine the direction of ground wave signals or long distance, skywave signals that arrive at low elevation angles. The crossed loops are utilised for high elevation angle, NVIS skywave signals.

4.6 WAVE TILT MEASUREMENTS WITH AN INTERFEROMETRIC DIRECTION FINDER

The MRD5000 interferometric DF supplied by GEW Technologies (Pretoria, South Africa) was deployed at the South African National Antenna Test Range (NATR) at Paardefontein, located at 25°33'14.3" S and 28°22'31.00" E. The average soil moisture content during these measurements was determined to be 12% using TDR techniques (Coetzee, 2014). Test transmitters were deployed in all four quadrants and the wave tilt of ground wave signals

were measured over the 3 to 30 MHz frequency range. The results are presented in Figures 4.11 to 4.14 below.

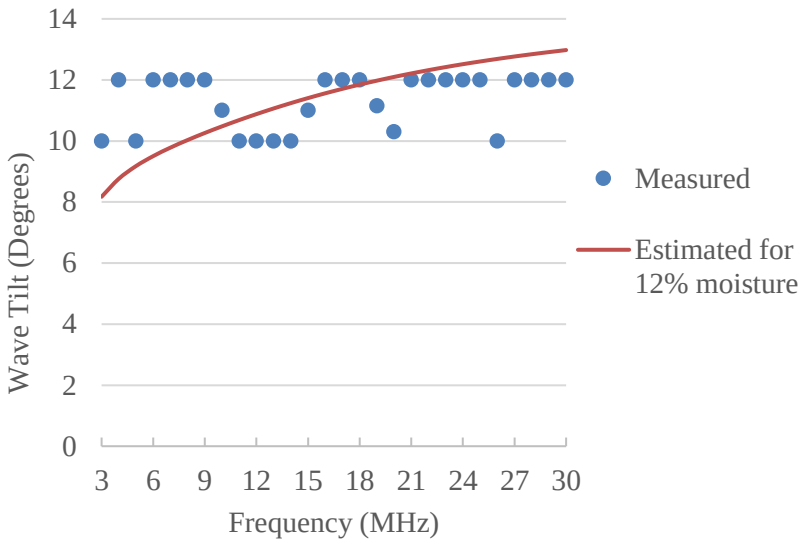

Figure 4.11. Estimated wave tilt for 12% soil moisture content and measured wave tilt from a direction of 66°.

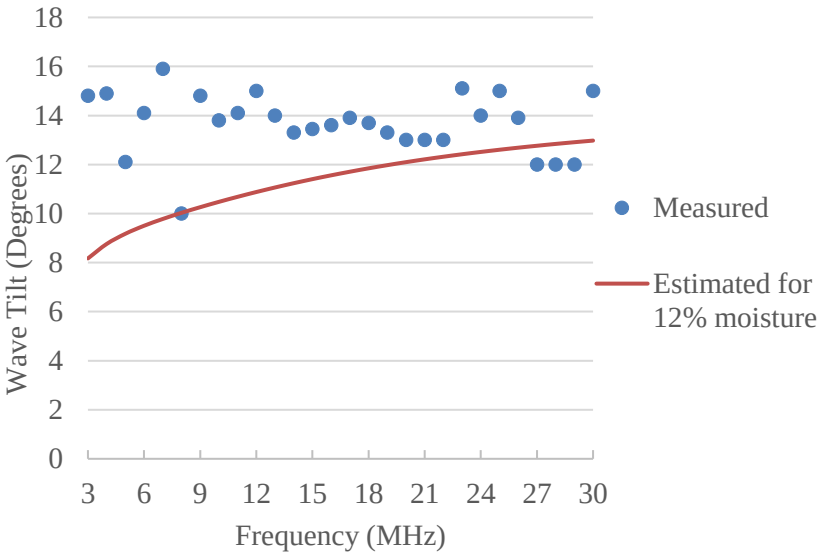

Figure 4.12. Estimated wave tilt for 12% soil moisture content and measured wave tilt from a direction of 108°.

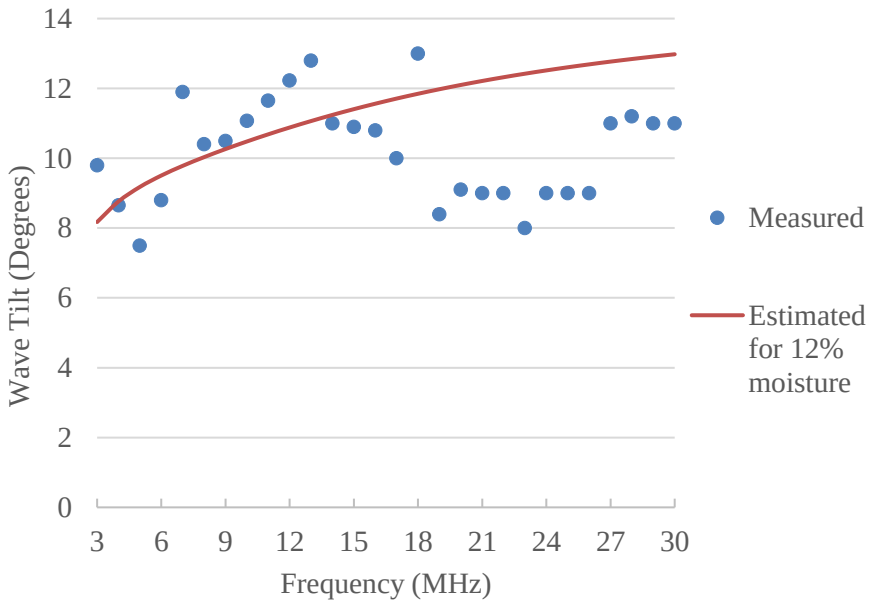

Figure 4.13. Estimated wave tilt for 12% soil moisture content and measured wave tilt from a direction of 275°.

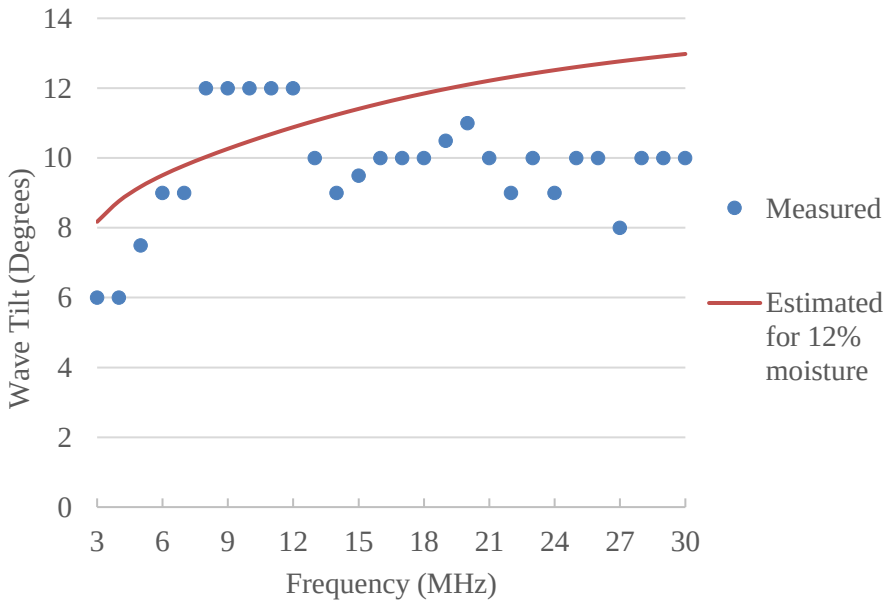

Figure 4.14. Estimated wave tilt for 12% soil moisture content and measured wave tilt from a direction of 342°.

The results indicate that above 5 MHz the measured wave tilt results correlate better with the calculated expected values of Figure 4.4 than what they do at frequencies below 5 MHz. This low-frequency cut-off can primarily be attributed to the size of the interferometric antenna array (125×125 m), and a larger array will produce better results on the lower frequencies with their associated longer wavelengths.

A difference in results from the various quadrants can be noted. Figures 4.13 and 4.14 show similar trends with the calculated results being approximated at lower frequencies but smaller wave tilt being measured at higher frequencies. Figure 4.11 has a slightly higher average wave tilt than Figures 4.13 and 4.14, but with less frequency variation. Finally, Figure 4.12 is unique in having a larger wave tilt across the entire band. These differences are due to the imperfect environment as underground electrical wires, water pipes and ducts are known to be present, influencing the results. The fact that these disturbances can be detected by measuring the wave tilt with an interferometric DF is a positive indication of the effectiveness and sensitivity of the technique.

The electromagnetic ground constants that correspond to the measured wave tilt results of Figures 4.11 to 4.14 were calculated and are presented in Figures 4.15 and 4.16. Note that for all the calculations the relative magnetic permeability, $\mu_{r,}$ was taken as 1 as there are no known deposits of magnetic materials in the Paardefontein area.

When the estimated relative permittivity graph of Figure 4.15 is compared with the theoretical values of Figure 4.2, it can be seen that the relative permittivity tend to stabilize between 15 and 20, especially towards the higher end of the HF frequency range. It can also be noted that the results from 108º, the direction with the underground services, are lower than those of the other directions.

The estimated conductivity results of Figure 4.16 increase with increased frequency. The same trend is displayed by the theoretical results of Figure 4.3. The results from 108º, the direction with the underground services, are lower than those of the other directions.

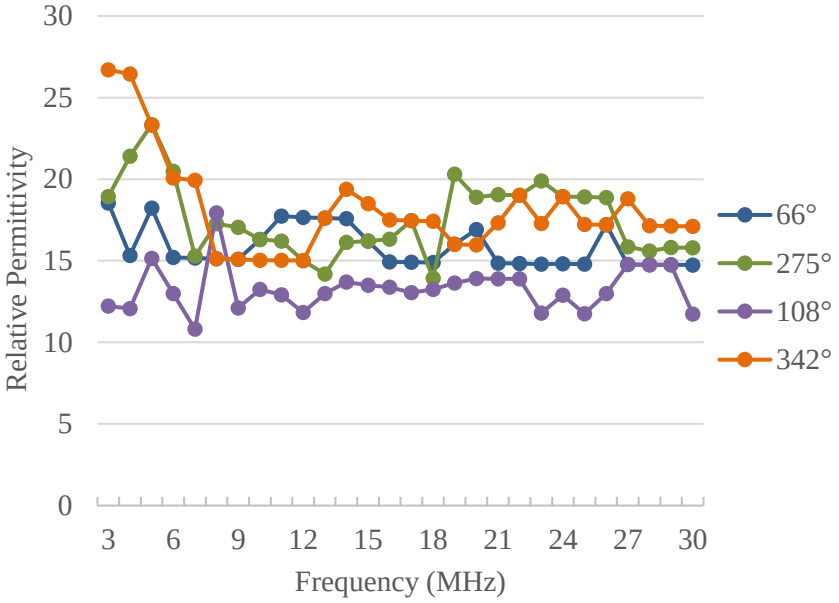

Figure 4.15. Estimated relative permittivity of soil for the measured wave tilts of Figures 4.11 to 4.14.

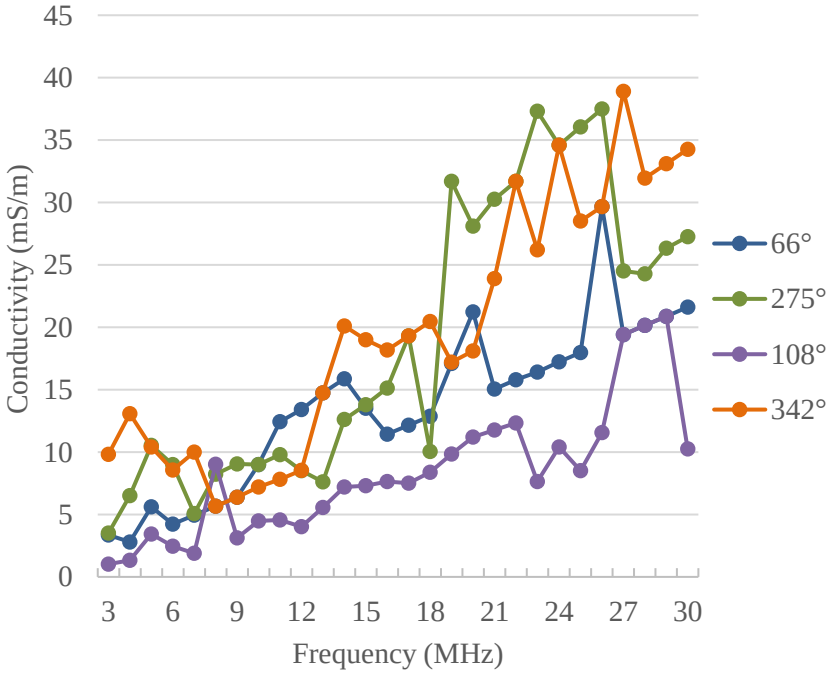

Figure 4.16. Estimated soil conductivity for the measured wave tilts of Figures 4.11 to 4.14.

The soil moisture content that will produce the wave tilt results of Figures 4.11 to 4.14 were calculated and are presented in Figure 4.17.

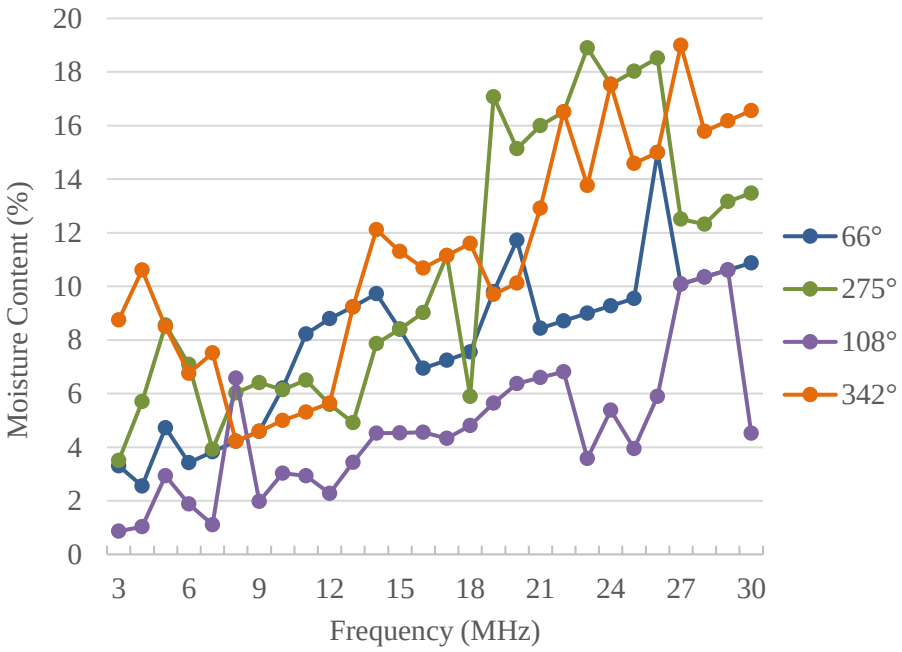

Figure 4.17. Estimated soil moisture content for the measured wave tilts for the four directions of Figures 4.11 to 4.14.

The Spectrum Technologies Field Scout TDR 300 soil moisture meter (Spectrum Technologies, IL, USA) determined the average moisture content to be 12% in the vicinity of the DF antenna field. The average of the estimated soil moisture content over the 3 to 30 MHz frequency range of Figure 4.17 is 8.6%. The average for frequencies above 5 MHz is 9%. As discussed in Section 4.6 above this low-frequency cut-off can primarily be attributed to the size of the interferometric antenna array (125×125 m), and a larger array will produce better results on the lower frequencies with their associated longer wavelengths. If the results from 108º, the direction with the underground services are excluded, the average soil moisture content increases to 10.3%. This value is within 14.2% of the average moisture content measured by the TDR 300.

4.7 POSSIBLE FUTURE WAVE TILT WORK

Blomquist noted that the wave tilt angle increased from typically 12° for the surrounding area to ≈14° when the measurement dipole was placed on top of a tarmac road as shown in Figure 4.15 below (Blomquist, 1975). The measurements were performed at a frequency of approximately 44 MHz. It is thus possible to detect the presence of the tarmac road by monitoring the wave tilt angle. This observation opens new applications of wave tilt of HF ground wave signals.

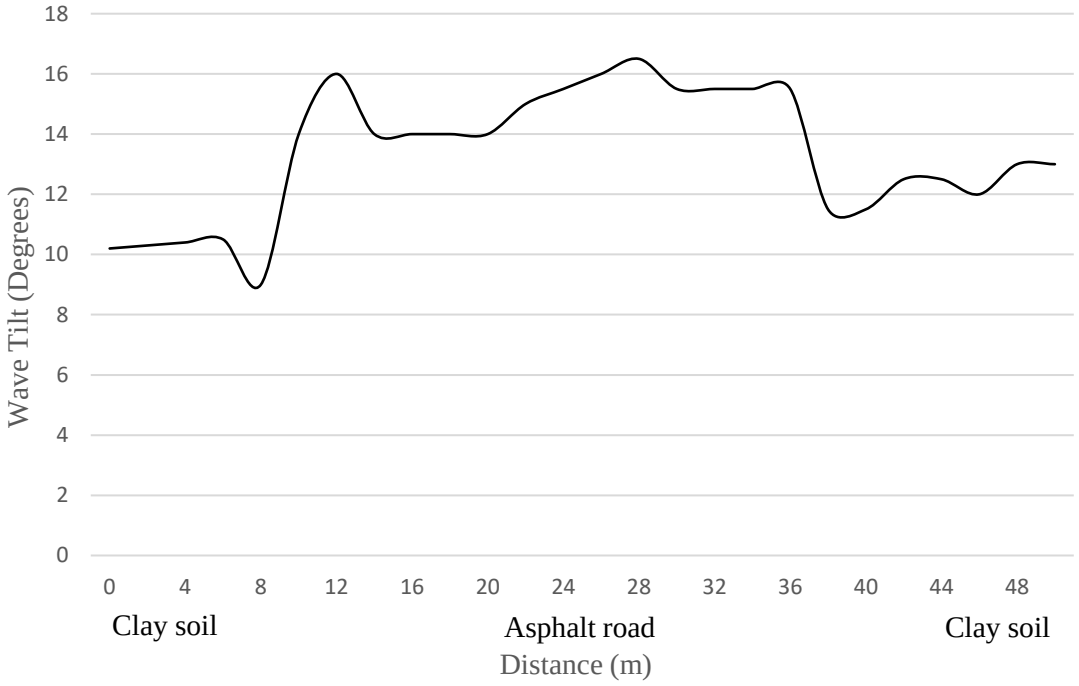

Figure 4.18. Measurements of the angle of tilt $\boldsymbol{\theta}$ at a boundary between sections of clay soil and an asphalt road [Taken from Blomquist, 1975, with permission].

From Maxwell's equations the complex propagation constant for an electromagnetic wave propagating through any material is defined by (IEEE Std 356, 2011, p. 6)

$$\Upsilon = \alpha + j\beta = j\omega\sqrt{\mu(\varepsilon + \frac{\sigma}{j\omega})}\,, \tag{4.14}$$

where α is the attenuation constant,

β is the phase constant,

ω is the angular frequency,

μ is the magnetic permeability of the medium,

ε is the permittivity of the medium,

σ is the conductivity of the medium,

and $j = \sqrt{-1}$.

For electromagnetic wave propagation through lossy media (partially conducting medium consisting of an imperfect dielectric or an imperfect conductor) the following applies

$$\Upsilon^2 = j\omega\mu(\sigma + j\omega\varepsilon)\ , \tag{4.15}$$

α and β are obtained from (4.14) and (4.15) by noting that

$$-\mathrm{Re}\Upsilon^2 = \beta^2 - \alpha^2 = \omega^2\mu\varepsilon, \tag{4.16}$$

and

$$|\Upsilon^2| = \beta^2 + \alpha^2 = \omega\mu\sqrt{\sigma^2 + \omega^2\varepsilon^2}. \tag{4.17}$$

From (4.16) and (4.17) follows

$$\alpha = \omega\sqrt{\frac{\mu\varepsilon}{2}\left[\sqrt{1 + \left[\frac{\sigma}{\omega\varepsilon}\right]^2} - 1\right]}. \tag{4.18}$$

The ground penetration or skin depth of radio energy is defined as the depth at which the amplitude of the field strength of electromagnetic radiation falls to $\frac{1}{e}$ (about 37%) of its

original value at (or more properly, just beneath) the surface. The skin depth, δ is defined as the reciprocal of the attenuation constant and can be written as

$$\delta = \frac{1}{\alpha}, \tag{4.19}$$

resulting in (Ulaby, 2007, p. 304; Baker-Jarvis *et al*., 2012)

$$\delta = \frac{\sqrt{2}}{\omega\sqrt{\mu\varepsilon}} \times \frac{1}{\sqrt{\left(\sqrt{1+\left(\frac{\sigma}{\omega\varepsilon}\right)^2}-1\right)}}. \tag{4.20}$$

With the electromagnetic constants of Figures 4.2 and 4.3 and using (4.20), it is possible to calculate the skin depth (ground penetration) as a function of soil moisture content over the HF frequency range for realistic dielectric constant and conductivity combinations as shown in Figure 4.16 below.

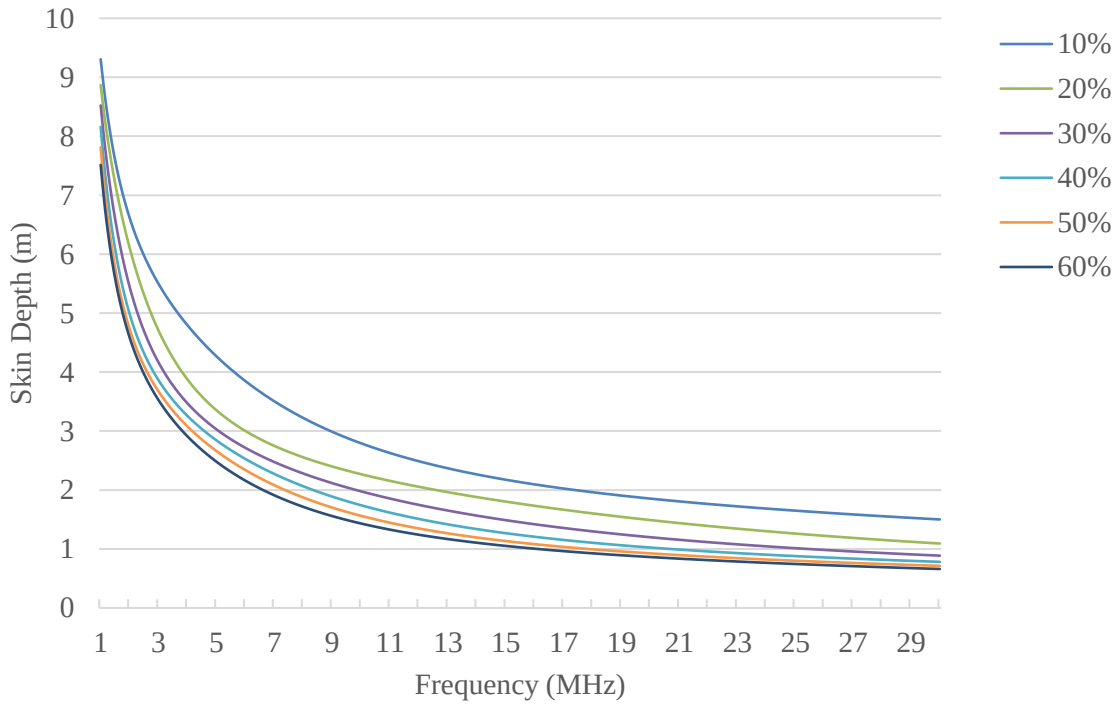

Figure 4.19. Skin depth as a function of soil moisture content over the 1 to 30 MHz frequency range.

The implication of the above is that as the forward wave tilt is a function of the electromagnetic constants of the ground, a significantly large subterranean disturbance or anomaly should have a detectable influence on the forward wave tilt angle of a HF signal.

At the higher end of the HF spectrum, the physical dimensions of an interferometric antenna array become small enough to allow mobile installations and applications. A co-operative HF transmitter operating on a suitably high HF or even low VHF frequency can serve as the ground wave signal source. By driving around with a mobile interferometric DF installation, it should thus be possible to detect underground cavities or tunnels, especially in areas where the ground is fairly homogeneous such as in dessert areas by monitoring the wave tilt angle deviation from the environmental average.

4.8 DISCUSSION AND SUMMARY

An interferometric DF offers significant advantages in terms of simplicity and speed in determining the wave tilt of an HF ground wave signal when compared to current manual techniques. Using this wave tilt value to determine the soil moisture content and then the electromagnetic constants of the ground from there is however not without pitfalls.

From Figure 4.4 it can be seen that the forward wave tilt is relatively insensitive to the soil moisture content. Increasing the soil moisture from 10 to 20% changes the wave tilt angle by less than a degree over the HF frequency range. If the soil moisture is increased from 50 to 60%, the effect on the wave tilt is even less. With the accuracy of most interferometric DF's specified as $\leq 1°$ RMS error, it becomes difficult to accurately determine the moisture content with such a measurement uncertainty regarding the wave tilt angle.

It was found that the deducing of the electromagnetic ground constants over the 3 to 30 MHz frequency range from the wave tilt results and using applicable soil moisture percentages as depicted in Figures 4.2 and 4.3 must only be used for indicative purposes. This is because a

small difference in the measured wave tilt results in a high percentage change in the calculated soil moisture content.

With an indication of the electromagnetic ground constants for the applicable frequency determined with the aid of an interferometric DF and Longmire's universal RC soil model, it is possible to model, at the frequency of interest and in the vicinity of the DF antenna array, ground wave propagation, transmitter area coverage, ground penetration, radiation patterns and input impedances of HF antennas with greater accuracy than is possible with the ground constant graphs published by the ITU.

CHAPTER 5 PRINCIPLES OF HF IONOSPHERIC PROPAGATION

5.1 INTRODUCTION

An overview of the ionosphere, characterisation thereof and the mechanism of the propagation of radio waves through the ionosphere are presented in this chapter. The terms most frequently used to describe ionospheric propagation and also used in this thesis (for example ionosondes and ionograms, MUF, skip zone, FOT, etc.) are defined.

5.2 BACKGROUND

Gauss was the first person who postulated the existence of ionized regions in the upper atmosphere in 1839 (Goodman, 1992, p. 3) after studying small variations of the earth's magnetic field.

In 1901 Marconi succeeded in transmitted the first long distance, trans-Atlantic signals from England to North America This achievement of Marconi was difficult to explain since it was known from the work of Hertz that radio waves travel nearly, but not quite, in straight lines unless they were deflected by an obstruction (McNamara, 1991, p. 1).

In 1902 three men (O. Heaviside, A. K. Kennelly and K. Nagaoka) independently postulated the existence of a permanent conducting layer high in the upper atmosphere which could guide radio waves for great distances. For many years, the ionosphere was referred to as the Kennelly-Heaviside layer in their honour (Goodman, 1992, p. 6).

J. E. Taylor and J. A. Fleming had respectively suggested in 1903 and 1906 that the conducting layer was produced by the ionizing action of ultraviolet light from the sun on the upper ionosphere. This implied the link between solar activity and radio propagation, which was confirmed as soon as commercial radio links were set up across the Atlantic.

In 1912 the radio engineer W. H. Eccles suggested that the number of ions, or electrically charged atoms, increased with the height of the atmosphere above the earth (McNamara, 1991, p. 1).

Interference between the ground wave and the wave reflected from the ionized layer let G. W. Pierce and Lee De Forest to calculate in 1912 a reflection height of 99 km for the skywave component, a very good estimate for what is now known as the E layer of the ionosphere.

In 1912 the U.S, Congress imposed the Radio Act of 1912 on radio amateurs, limiting their operations to the "useless" frequencies above 1.5 MHz. This led to the discovery of HF radio propagation via the ionosphere in 1923.

In 1924, E. V. Appleton and M. Barnett provided the final experimental proof of the existence of a reflecting layer in the upper atmosphere with their "frequency change" experiments (Goodman, 1992, p. 7). The transmitters' frequency was slowly varied while the signal strength of the received signal was monitored. The received signal consisting of the direct signal (ground wave) and the reflected (skywave) signal would be at a maximum if the difference in path lengths were multiples of wavelengths and at a minimum at an odd number of half wavelengths. Since the distance between the transmitter and receiver was known, it was a matter of simple triangulation to calculate the height of the reflecting layer. They deducted that the reflection had been from a height of 100 km.

Appleton also discovered that the E layer could be penetrated by waves above a certain frequency and that these penetrating waves could also be reflected back but from a much higher layer (Kirby *et al.*, 1934). This layer, 250 to 350 km above the earth, had a high electron density and reflected back shorter wavelengths. He deduced that this was the layer that reflected shortwave radio signals so that they could travel around the world. This layer was called the Appleton-Barnett layer. To prevent confusion Appleton called it the F layer because it was discovered after the E layer (Davies, 1990, p. 1).

The first direct measurements of the height of the reflecting layer were made in 1925 by G. Breit and M. A. Tuve. They used a pulse sounding technique, a forerunner of modern radar (McNamara, 1991, p. 2; Kirby *et al.*, 1934).

The Australian, R. A. Watson-Watt proposed the name ionosphere in 1926 (McNamara, 1991, p. 2), but it took a couple of years before being properly established in the literature seeing that his letter was only published in 1969 in the journal, Nature.

Appleton realised the potential implications of his experiments and proceeded to fully concentrate on the upper atmosphere. He was joined by many others, such as S. Chapman in his study of the ionosphere. In 1931 Chapman published a paper dealing with the Kennelly-Heaviside layer that provided a fundamental basis for our understanding of the ionosphere. Even today the Chapman hypothesis for ionized layer formation is a useful model, especially for the lower layers of the ionosphere. In 1932 Appleton published a complete theory of radio wave propagation in a magnetoionic media, such as the Kennelly-Heaviside layer (Goodman, 1992, p. 8; Davies, 1990, p. 70). Appleton was awarded a Nobel Prize in 1947 for his confirmation of the existence of the ionosphere in 1927.

At the outbreak of the Second World War, the overall structure and variations of the ionosphere were well described, but in general poorly understood. The decades following the Second World War saw an enormous increase of our understanding of the ionosphere and its place in the whole complex solar terrestrial environment. The advent of scientific

rockets and satellites, (Alouette 1 in 1962, Alouette 2 in 1965, the two ISIS satellites in 1969 and 1971, AEROS-A in 1972 and AEROS-B in 1975) also contributed greatly to the huge advances in the understanding of the ionosphere's effect on the propagation of radio waves (Davies, 1990, pp. 112, 261).

In 1963, the first operational geosynchronous satellite, Syncom 2, was launched. The radio beacons on-board this satellite, and its successors, enabled the measurement of total electron content (TEC) variation between geostationary orbit and a receiver on the earth. Today the TEC determined with the aid of dual channel GPS receivers contribute greatly to the characterization of the ionosphere in near real-time (Davies, 1990, p. 305).

5.3 THE IONOSPHERE

The ionosphere is the region of the earth's upper atmosphere (between an altitude of about 50 km to 1 000 km) that is ionised (forming an electrically conducting layer) due to Extreme Ultraviolet (EUV) radiation from the sun (Viggiano, 2004). It is the ionosphere which reflects HF radio waves, making long distance communications beyond line-of-sight possible (McNamara, 1991, p. 17; Goodman, 1992, pp. 19, 94).

The ionosphere is formed when EUV light from the sun strips electrons from the neutral atoms of the earth's atmosphere. When a bundle of EUV light (called a photon) hits a neutral atom, its energy is transferred as kinetic energy to an electron in the neutral atom that can then escape from the atom and move freely around, if the excess kinetic energy exceeds the binding energy of the electron (Goodman, 1992, p. 99). The neutral atom becomes positively charged and is known as a positive ion. This process is called photo-ionization (Goodman, 1992, p. 99). That part of the atmosphere in which the ions are formed is called the ionosphere. It is actually the free electrons that reflect radio waves as the ions are more than twenty thousand times heavier than the electrons and are just too massive to respond to the rapid oscillations of a radio wave (McNamara, 1991, p. 17).

The structure of the ionosphere at any particular location is quite complex. The intensity of the EUV radiation from the sun is stronger at some wavelengths depending on what type of atom is emitting the radiation (for example hydrogen). The neutral atmosphere is also complex, composed of a wide range of atoms and molecules such as oxygen, nitrogen and nitric oxide (Davies, 1990, p. 57).

The situation is further complicated due to the density of the atoms decreasing as the altitude increases, while the intensity of the EUV light which does the photo-ionizing decreases towards lower altitudes due to absorption through the upper layers of the atmosphere. The net result of these opposing effects, as illustrated by the electron density as a function of height profile in Figure 5.1, is to produce a layer of electrons with a maximum electron density at some particular altitude and lower electron densities above and below this altitude.

The sample electron density as a function of height profile in Figure 5.1 is modelled with the aid of the IRI over Southern Africa at noon during the summer. The ionosphere may contain up to four different layers (or regions) at different altitudes (Goodman, 1992, p. 101). The D layer covers the altitude range of about 50 to 90 km. The E layer covers the altitude range of about 90 to 110 km. In Figure 5.1, the F1 layer ranges from about 110 to 210 km and the F2 layer covers the altitude range above 210 km to the peak electron density at around 300 km.

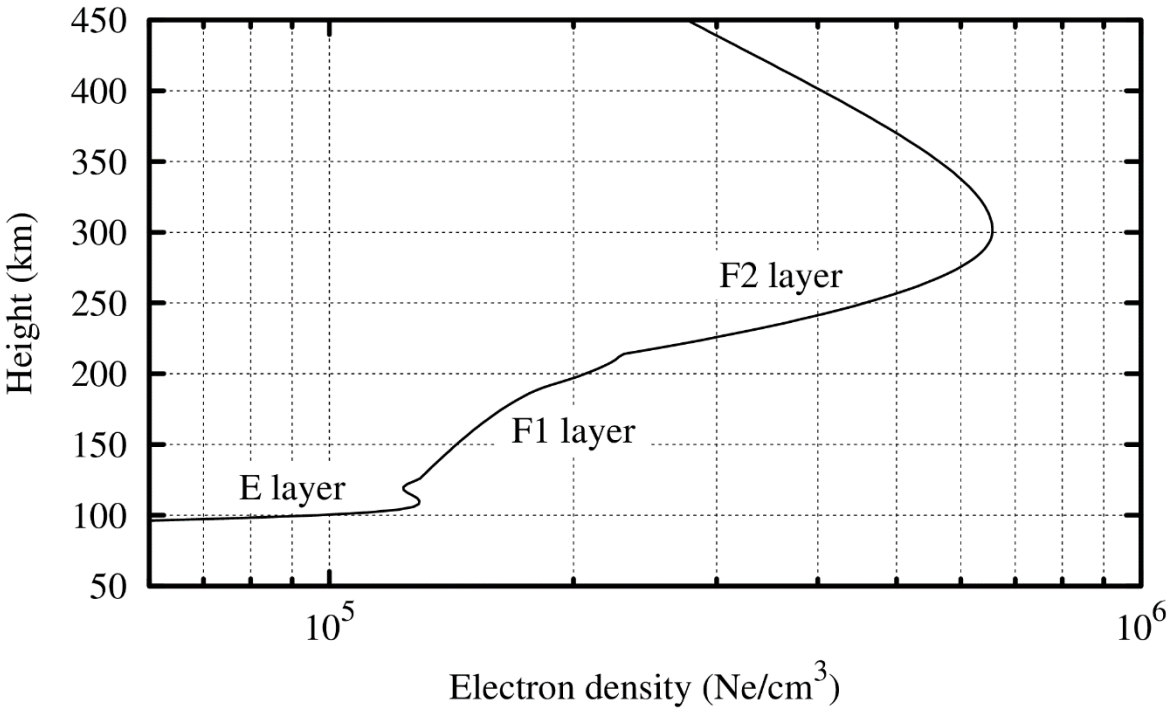

Figure 5.1. Sample daytime electron density profile as a function of height of the ionosphere as modelled by the IRI (2012).

The ionosphere is highly variable exhibiting changes linked to solar activity, diurnal and seasonal variability, geographical location (polar caps, auroral zones, equatorial regions), (Davies, 1990, p. 1) that are observed in the electron density as a function of height profiles, *N(h)*, and mostly affects HF propagation (Goodman, 1992, p. 94). Figure 5.2 shows a sample night-time *N(h)* profile. The shape of this profile is significantly different to the daytime profile shown in Figure 5.1.

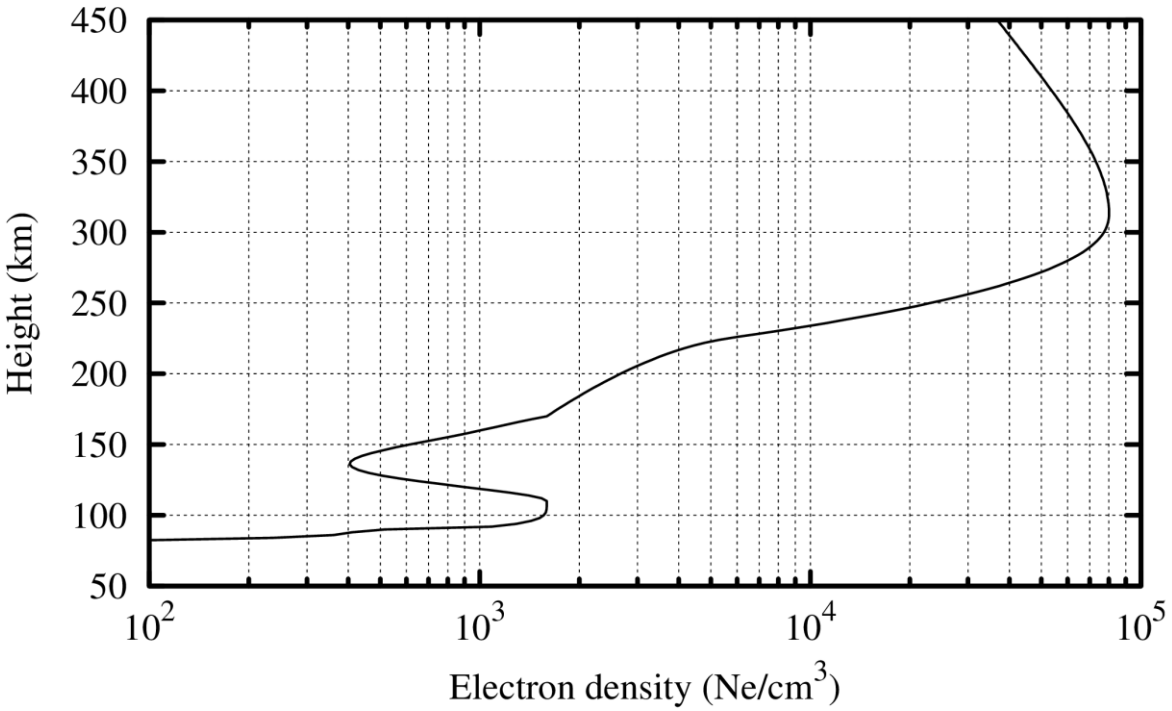

Figure 5.2. Sample night-time electron density profile as a function of height of the ionosphere as modelled by the IRI (2012).

Recombination of the free electrons and the positively charged ions occurs continuously. At night-time recombination can occur unhindered due to the absence of EUV radiation and, therefore, the density of the electrons drops steadily as the night wears on. Recombination is not completely accomplished throughout the whole ionosphere and some free electrons survive until dawn. They are then rapidly replenished by the rising sun. The density of the neutral atmosphere decreases rapidly with height with the result that there are fewer neutral atoms available. The most efficient recombination occurs in a two-stage process: in the first stage the positive ion interacts with a neutral molecule replacing one of the atoms in the molecule. In the second stage free electrons combine with the now positively charged molecule resulting in two neutral atoms (McNamara, 1991, p. 18; Davies, 1990, p. 63). The incomplete recombination ensures that the ionosphere can still be used for HF communications during the night-time. In fact, the higher and thinner ionosphere means that certain long distance communications are sometimes only possible at night.

As seen in Figure 5.2, the D and E layer regions disappear almost completely at night and the F1 layer combines with the F2 layer to form just an F layer. The F layer survives in a depleted (thinner) manner throughout the night, which, at night, makes the F layer the most important layer in terms of HF communications.

Pertaining to the ionosphere, the terms *layer* and *region* are often used interchangeably. Referring to Figure 5.1, the term *region* is most appropriate since it does not create the impression that sharp discontinuities exists in the electron density as a function of height profile at well-defined upper and lower boundaries. This led to the notion of an F1 and F2 layer comprising the F region.

There is however strong evidence for a distinct E layer since a valley is often observed between the E and F regions as can be seen in Figure 5.3.

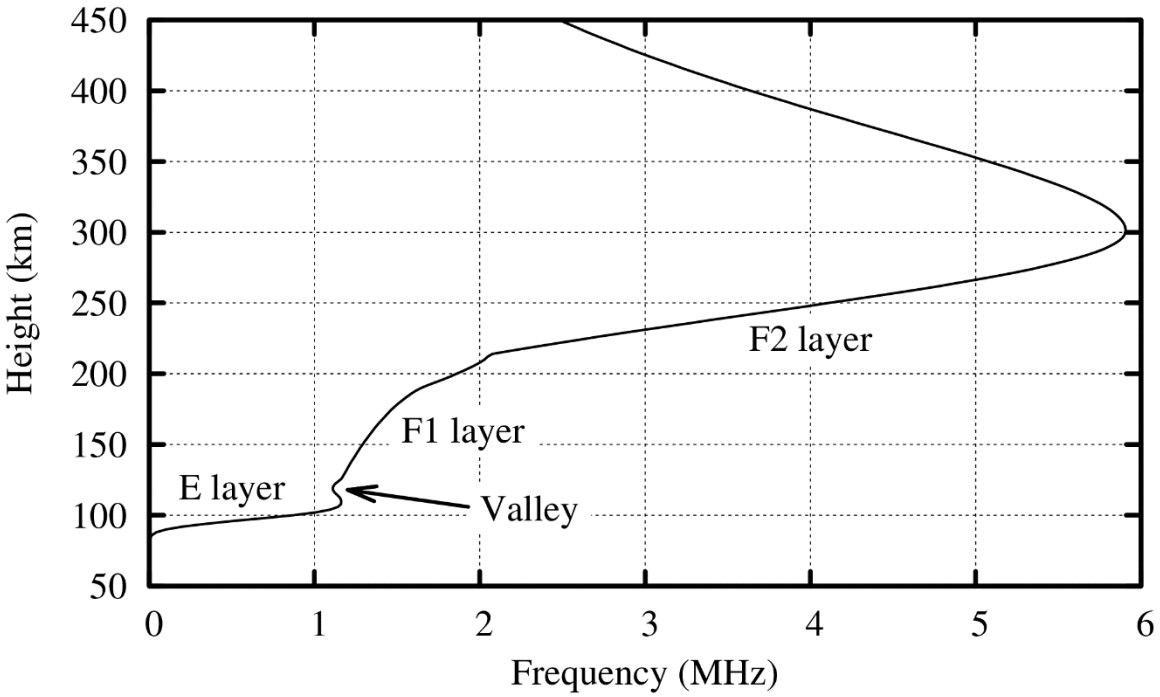

Figure 5.3. The valley between the E layer and the F region as modelled by the IRI (2012).

For the D region, there is no consistent tendency for a maximum to be produced within the 70 to 90 km height domain. Consequently, the term D *region* should be preferred over the

term D *layer* (Goodman, 1992, pp. 100, 101). The D region is sometimes responsible for most of the absorption encountered by HF signals which makes use of the skywave mode. In many instances, D region absorption is a primary factor in the determination of the lowest frequency that will be supported by the ionosphere for skywave communications over a given circuit (Goodman, 1992, p. 107).

The relationship between the ionosphere and radio waves is determined by the nature of the ionosphere. The plasma or critical frequency of a layer is the maximum frequency where reflection is possible via that layer. The critical frequency of a layer, f_c, is related to the maximum electron density in that layer, N_m, by

$$f_c \approx 9 \times 10^{-6} \times {N_m}^{0.5}\,, \tag{5.1}$$

where f_c is the critical frequency in MHz and N_m is the amount of free electrons per cubic meter (McNamara, 1991, p. 20). (5.1) can also be written in the more popular form of

$$N_m = 1.24 \times 10^{10} \times {f_c}^2\,, \tag{5.2}$$

(Goodman, 1992, p. 114; Davies, 1990, p. 94).

When a plane polarized radio wave enters the ionosphere, it splits into two characteristic waves that propagate independently through the ionosphere. These waves are known as the ordinary (f_o) and extraordinary-waves (f_x) and are elliptically polarized. The electric field of the ray can rotate either in a clockwise direction for the ordinary-wave or in an anti-clockwise direction for the extraordinary-wave, depending on the orientation of the raypath relative to the direction of the earth's magnetic field (McNamara, 1991, p. 40). There is a critical frequency for each of the layers namely f_oE, f_oF_1 and f_oF_2 for the ordinary-wave and f_xE, f_xF_1 and f_xF_2 for the extraordinary-wave (Appleton *et al.*, 1933).

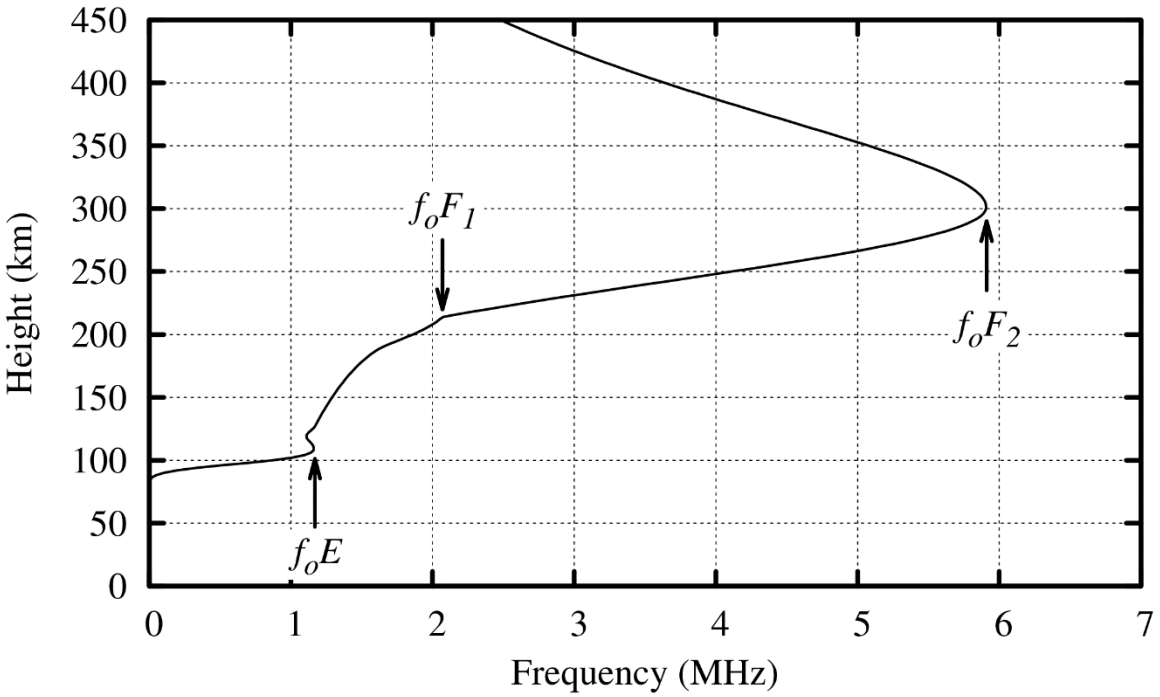

Figure 5.4. The ionosphere in terms of ordinary-wave critical frequencies as modelled by the IRI (2012).

The critical frequency of a layer as depicted in Figure 5.4 is equal to the maximum frequency that can be reflected from it at vertical incidence.

5.4 CHARACTERISING THE IONOSPHERE

The ionosphere has been extensively studied using measurements from satellites, rockets, incoherent scatter radars and ionosondes. For this study, it is necessary to define the behaviour of the ionosphere in terms of the propagation of radio waves and therefore the focus is on the characterisation of the ionosphere with the aid of radio probes, specifically ionosondes (Goodman, 1992, pp. 100–101; McNamara, 1991, p. 20).

An ionosonde is an instrument that transmits a burst of HF radio energy vertically upwards towards the ionosphere. The time taken for the echo to return to earth is measured and the (virtual) height of the ionospheric reflection point is calculated. The delay of the echo is frequency dependent and the output of the ionosonde is typically a graph of virtual height

versus frequency. The virtual height is what the height of reflection would have been had the radio wave continued to travel at the speed of light all the way to the point of reflection. This graph is known as an (vertical incidence) ionogram. An ionosonde can be thought of as a long distance radar operating in the HF frequency range, transmitting and receiving vertically away from the earth (McNamara, 1991, p. 52).

There are currently four operational ionosondes in South Africa located at Grahamstown (33.3°S, 26.5°E), Louisvale (28.5°S, 21.2°E), Madimbo (22.4°S, 30.9°E) and the latest one at Hermanus (34.5°S, 19.2°E). They are Digisondes manufactured by the University of Lowell, Massachusetts and make use of the "Automatic Real Time Ionospheric Scaling Technique" (ARTIST) software to scale the results (McKinnell *et al.*, 2011).

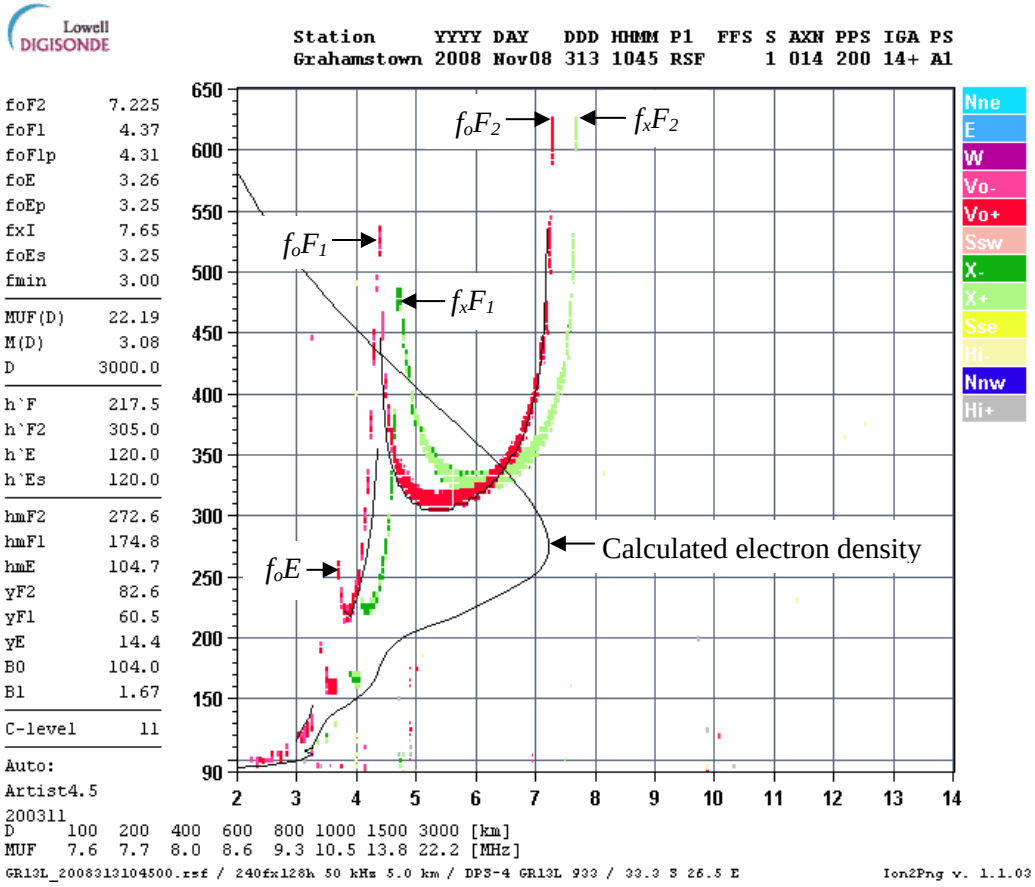

Figure 5.5. (Vertical incidence) Ionogram as generated by the Grahamstown, South Africa ionosonde at 10h45 UTC on 8 November 2008.

Vertical incidence ionograms as shown in Figure 5.5 have been used to study and quantify the ionosphere for more than 60 years or more than five solar cycles. Ionograms can also be obtained when the transmitter and receiver are separated by long distances. These ionograms are referred to as oblique ionograms.

The ionogram of Figure 5.5 was generated by stepping the transmitter and receiver from 2 MHz (lowest frequency) up to 15 MHz in 50 kHz steps. A pulse is transmitted on each frequency and the time delay for the reception of the echo is measured. If the frequency is below the critical frequency of the D region, there will be no returning signal due to absorption by the D region. Once the operational frequency of the ionosonde exceeds f_cD, reflections from the E layer are received. This is at a frequency of approximately 2.1 MHz in the ionogram of Figure 5.5. As the operating frequency of the ionosonde is increased, the time delay for the echo of a signal travelling vertically increases until the operating frequency is equal to the critical frequency of the E layer (as defined in (5.1)). At this point the layer will just be penetrated with virtually no reflection. This happens at 3.26 MHz for the ordinary-wave of the E layer (f_oE) in Figure 5.5. For frequencies just above- f_oE, the time delay decreases with frequency since the signals at these frequencies find it increasingly easy to penetrate the E layer. However, as the critical frequency for the F1 layer is reached, the signals start to slow down again as they approach penetration. In Figure 5.5, f_oF_1 is at 4.37 MHz for the ordinary-wave and f_xF_1 is at approximately 4.8 MHz. The same decrease followed by an increase in delay time happens for the F2 layer. When the operating frequency exceeds the critical frequency for the F2 layer, f_oF_2, (7.23 MHz in Figure 5.5) ordinary-wave signals penetrate the total ionosphere and continue into space. The extraordinary-wave continues to be reflected up to a frequency of 7.65 MHz (f_xF_2).

When a pulse of HF radio wave energy is vertically transmitted, it is reflected from the ionosphere and returned to the receiver some time T later. The group height or virtual height can be calculated by

$$h' = \frac{cT}{2}, \tag{5.3}$$

where c is the speed of light in free space (Davies, 1990, p. 94).

The ionosphere is however not free space and the velocity of a signal travelling through it is related to the velocity of light by

$$V = \frac{c}{\mu'}, \tag{5.4}$$

where μ' is the group refractive index (Davies, 1990, p. 118).

Along the ionospheric propagation path μ' (and V) change in proportion to the electron density. By working in small segments and integrating over the whole path it is possible to calculate the true height versus frequency (McNamara, 1991, p. 53). This is automatically done in modern ionosondes and displayed as part of the ionogram. In Figure 5.5 there are two black lines. The broken black line just below the red ordinary layer echoes is used for curve fitting calculations and the solid black line starting at the minimum frequency and at a height of just more than 90 km and finally reaching a height of 580 km is the true electron density profile as a function of height.

There are in general two traces for each layer of the ionosphere due to the earth's magnetic field giving rise to the ordinary (O) and extraordinary (X) -waves (McNamara, 1991, p. 54). In Figure 5.5 the O-wave is depicted in red and the X-wave in green. When a plane polarised radio wave hits the ionosphere, it splits into two characteristic waves (ordinary and extraordinary) that propagate independently through the ionosphere. The earth's magnetic field, or geomagnetic field, has important effects on both the ionosphere and HF propagation. There is a relationship between the strength of the geomagnetic field and the electron gyro-frequency (McNamara, 1991, p. 31). Charged particles such as electrons cannot move across a magnetic field line but are forced to spiral or rotate around them. The rate at which they rotate is called the gyro-frequency and depends on how heavy they are, their electric charge

and the strength of the magnetic field. For electrons in the geomagnetic field, the gyro-frequency is typically less than 2 MHz and varies with latitude and longitude over the surface of the earth. The vertical asymptotes (virtual heights) for f_oF_2 and f_xF_2 are separated by approximately half the gyro-frequency, f_b (McNamara, 1991, p. 54). For Grahamstown, South Africa this is approximately 0.38 MHz according to Figure 5.5.

5.5 HF SKYWAVE PROPAGATION

In Figure 5.6, a simplified geometrical model is used to describe the aspects related to ionospheric propagation. For illustrative purposes, use is made of a flat earth and a flat ionosphere.

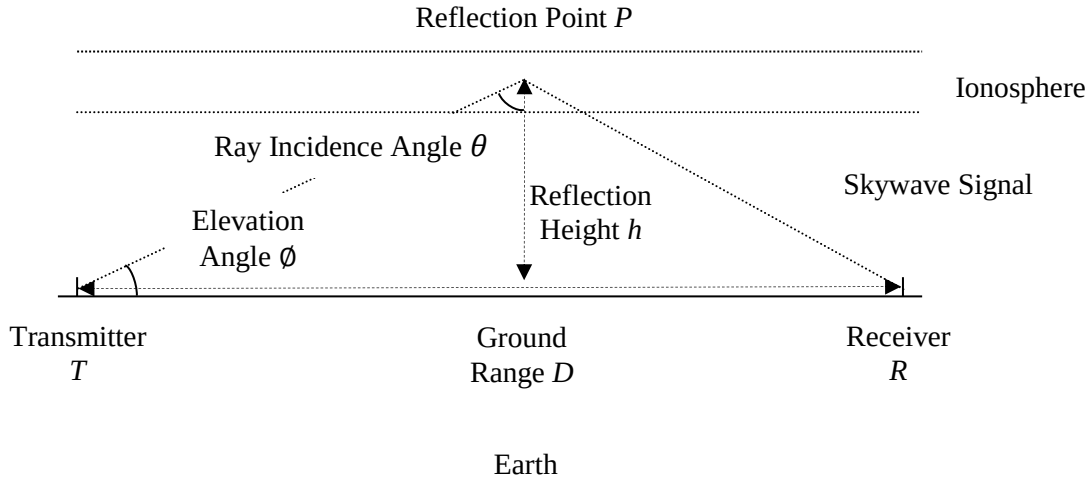

Figure 5.6. Simplified geometrical propagation model.

Conceptually, the radio waves in Figure 5.6 are emitted by the transmitter *T* at an elevation angle ϕ, travel a distance *D/2* before being reflected back to earth by the ionosphere at point *P* and finally arrive at the receiver *R*. In reality, the ray is not reflected at *P*, but is continuously refracted or bent towards the ground as it passes through the ionosphere (Devoldere, 2010, pp. 1, 2; McNamara, 1991, p. 39). The ionosphere at the conceptual point

of reflection *P* is at a height *h* above the midpoint of the circuit. The distance along the ground between the transmitter *T* and the receiver *R* is called the ground range *D*.

The maximum frequency that will be reflected by the ionosphere for a given circuit is the MUF. It is one of the most important and widely published quantities in HF communications (McNamara, 1991, p. 42; Goodman, 1992, p. 153). The basic MUF is a median representation (statistical value) and not an individual value. The MUF depends on just two parameters, the critical frequency, f_c, of the ionosphere at the reflection point *P* and the geometry of the circuit. The MUF is given by the formula

$$MUF = f_c \, sec(\theta), \tag{5.5}$$

where θ is the ray incidence angle as depicted in Figure 5.6. (5.5) is also known as the secant law (Martyn *et al.*, 1935).

For radio propagation purposes it is more convenient to work with the elevation angle ϕ, giving

$$MUF = \frac{f_c}{sin(\phi)}. \tag{5.6}$$

Since $sin(\phi)$ can vary from 0 to 1, (5.6) indicates that the MUF is equal to the critical frequency of the ionosphere for vertical incidence as ϕ = 90° gives $sin(\phi)$ = 1. It also indicates that the MUF and ground range *D* are much higher for low elevation angles. In practice the world is round and the curvature of the surface prevents the elevation angle from getting too close to 0°, causing the MUF (and ground range) to reach a finite upper limit for a given ionosphere.

(5.6) may be used to calculate the MUF for reflection at a given altitude in the F layer, provided the critical frequency f_c (f_oF_2) is replaced by the plasma frequency at the reflection height, $f_n(h)$.

$$MUF(h) = \frac{f_n(h)}{sin[\phi(h)]}, \tag{5.7}$$

where *h* indicates what is happening if the reflection occurs at the height *h*. In general, the higher the frequency, the higher the signals must penetrate into the ionosphere to find a plasma frequency high enough to reflect them.

For propagation to be possible on a given circuit, the operating frequency, f_o, must be less than or equal to the MUF for the circuit. At higher frequencies the signals would simply penetrate the ionosphere. For communication purposes the MUF is calculated as a median frequency, defined as the highest frequency at which skywave communication are possible 50% of the days in a month (McNamara, 1991, p. 49). Half the time, the actual MUF observed on any day will be higher than the median and half the time it will be lower. The Highest Possible Frequency (HPF) is taken as 115% of the MUF and should support propagation 10% of the time (Devoldere, 2010, pp. 1–6). The LUF is the frequency at which communication with a required minimum SNR for a specified time period is possible 90% of the undisturbed days of the month and is normally determined by the amount of D-layer absorption and the atmospheric noise level (Goodman, 1992, p. 227).

It is possible to use the MUF to determine an Optimum Working Frequency (OWF) or Frequence Optimum de Travail (FOT) (Hagn, 1992). The FOT is the frequency that is equal to the lower decile value of the thirty or thirty-one individual MUFs for the month. The OWF or FOT is the internationally agreed standard for the best or optimum frequency to use at a given hour on a given circuit. Its use will result in successful communications (at least as far as the correct choice of frequency is concerned) 90% of the time (27 days of the month) (McNamara, 1991, p. 49). It is possible to get an estimated value of the FOT (EFOT) by taking 85% of the median MUF (Goodman, 1992, p. 226; Davies, 1990, p. 180). This is a convenient definition to calculate the FOT for a given circuit.

Under certain conditions, a skip zone or dead zone may exist up to a certain distance from the transmitter. If the operating frequency is higher than the critical frequency (f_oF_2), reflection will only occur if the elevation angle is low enough to comply with (5.6). It will not be possible to communicate with stations within the skip zone unless the operating frequency is reduced to be less than or equal to the MUF for the required distance (backscatter modes were not considered for this study). The skip zone for a given transmitter will depend on the operating frequency (getting larger as the frequency increases) and the critical frequency of the reflecting layer. The skip zone can be put to good effect if secure communications are required.

The propagation of HF signals through the ionosphere can be graphically illustrated by plotting the ground range for all elevation angles (0 to 90°) for a specific frequency, transmitter position, time of day, date, operating frequency and ionosphere.

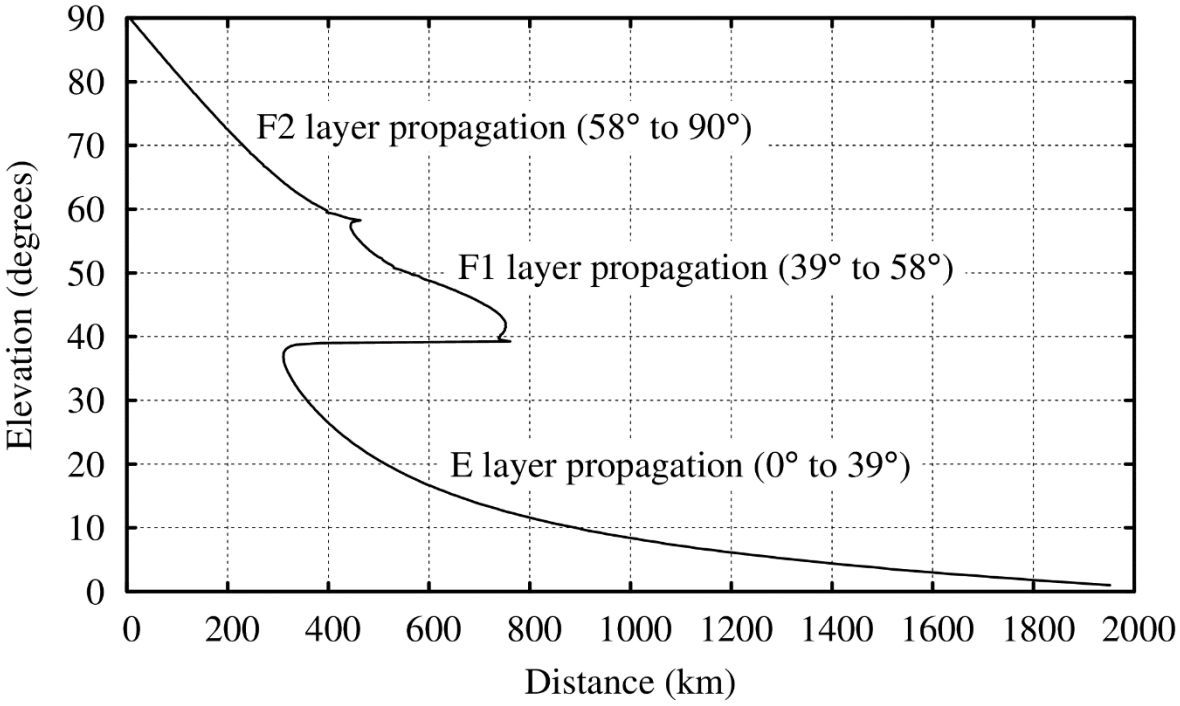

Figure 5.7. Calculated propagation of a 5 MHz signal through the 2012 International Reference Ionosphere model.

The 2012 version of the IRI (Bilitza, 2001) ionospheric model was used to generate the ionospheric data required to calculate the ground range for all elevation angles as depicted in Figure 5.7. The time of the day was taken as noon UTC, which is 14h00 in South Africa. The season was towards the end of summer and the position was taken as Pretoria, located at 25°44'41.48" S and 28°16'16.29" E. The solar activity was very low with a smoothed sunspot number of 16.3. A frequency of 5 MHz was chosen as it can be seen to support successful communications for both very short distances (NVIS) and longer distances up to a few hundred kilometres under the above conditions.

Ray-tracing techniques (McKinnell, 2002; Coleman, 2011) were used to model the ray path through the ionosphere. Possible propagation via three ionospheric layers can be identified: E layer propagation for elevation angles between 0° and approximately 39° and F layer for higher elevation angles (Goodman, 1992, p. 245). The critical frequency of the E layer (f_oE) of the ionosphere used to generate Figure 5.7 is 3.21 MHz. As the operating frequency (5 MHz) is considerably higher than the critical frequency of the E layer, f_oE, only low-angle signals will be reflected by the E layer. The situation is quite different for the F2 layer as f_oF_2 is 8.69 MHz with the result that all high-angle signals are reflected back to earth by the F2 layer. No skip or dead zone exists for 5 MHz under the conditions used to generate Figure 5.7 and skywave communications from very close to the transmitter up to a distance of nearly 1 900 km are possible dependent on the radiation angles of the antennas used.

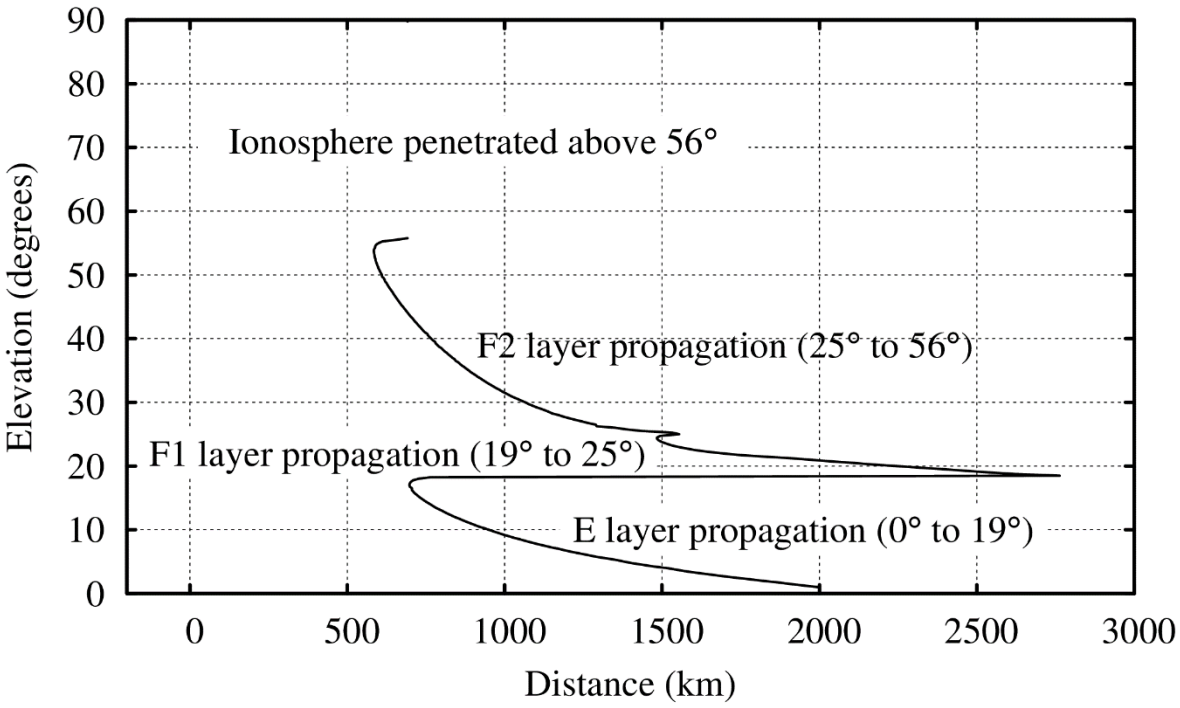

Figure 5.8. Calculated propagation of an 11.5 MHz signal through the 2012 International Reference Ionosphere.

Figure 5.8 uses the same parameters as Figure 5.7, but the operating frequency is now 11.5 MHz, considerably higher than the critical frequency of any of the ionospheric layers. The E layer will support propagation for signals with elevation angles between 0° and approximately 19°. Above 19°, the F1 and F2 layers take over up to approximately 56°. For elevation angles higher than 56°, the 11.5 MHz signal cannot be refracted back to earth by the ionosphere. Due to the fact that propagation is not possible for elevation angles higher than 56°, a skip zone of approximately 600 km exists. Communications over distances of between zero and 600 km are thus not possible using skywave propagation under the conditions depicted in Figure 5.8. It should be noted that short-range, ground wave propagation and line-of-sight propagation exist, but have been ignored in the above discussion. Also note that for distances between 750 and 2 000 km, propagation via both the E and F layers is possible (multipath propagation). If the antenna radiates most of the energy between 0 and 42°, signal fading or inter-symbol interference may be experienced due to the different path lengths. Multipath propagation should be avoided for reliable SSL

results (ITU-R Handbook on Spectrum Monitoring, 2011, pp. 293–294), unless super-resolution techniques are incorporated in the direction finder.

A direction finder that makes use of super-resolution techniques (MUSIC) will provide multiple wave angle (azimuths and elevations) results for the operational frequency. Each wave angle (azimuth and elevation) will represent a unique path that the ray travelled through the ionosphere. Using the elevation angles as inputs to the ray-tracing algorithm should result in (more-or-less) the same distance result, depending on the accuracy of the ionospheric model and ray-tracing algorithm implemented. A non-super-resolution DF tends to provide an average value for the various elevation results due to the histogram used to determine the most probable answer. This result will obviously be of very little use.

For oblique propagation at frequencies below the MUF for the circuit, at least two ray paths become possible (McNamara, 1991, p. 39; Goodman, 1992, pp. 237–245; Davies, 1990, pp.159–164).

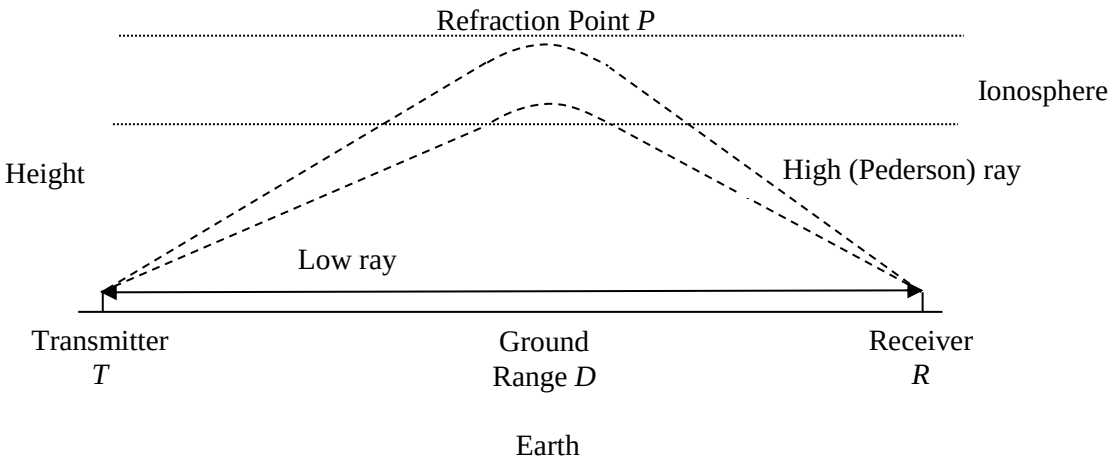

Figure 5.9. A greatly simplified, but still useful view of "low ray" and "high ray" (Pederson) ionospheric propagation over a fixed distance.

The “low ray” corresponds to propagation via the lower virtual height and the “high-ray” or Pederson ray close to the MUF for the specific layer (Goodman, 1992, p. 238).

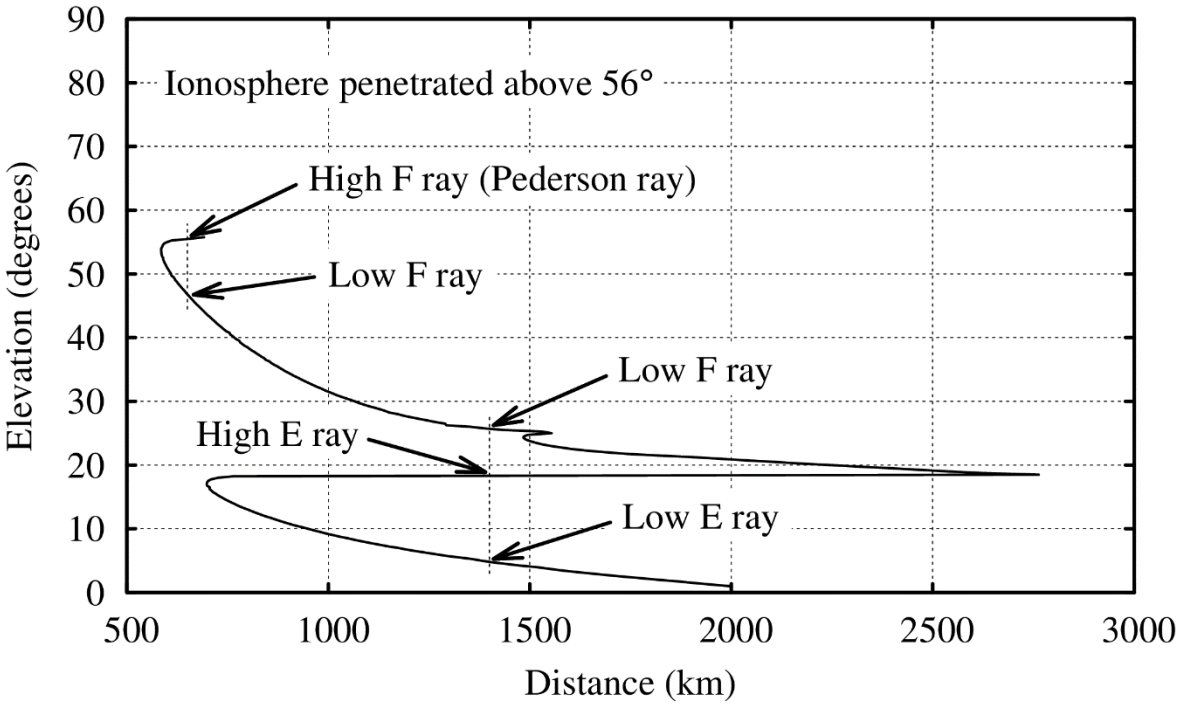

Figure 5.10. Calculated propagation (ray-tracing result) of an 11.5 MHz signal through the 2012 IRI illustrating the “low ray” and high angle (Pederson) ray resulting in the same ground range.

Referring to Figure 5.10 it can be seen that for a distance of for example 1 400 km, propagation is possible at an elevation angle of about 5°, the so-called "low E ray". But propagation over a 1 500 km distance is also possible via the E layer at an elevation angle of about 18°, the so-called "high E ray". A third propagation path over the 1 400 km path also exists at an elevation angle of 26°, the so-called "low F ray". Signal fading or inter symbol interference (on data signals) may be experienced due to the multiple propagation paths.

Under certain ionospheric and operational conditions, a focussing effect may be experienced (Goodman, 1992, pp. 244–246). The ray-tracing result for a frequency of 13 MHz is shown in Figure 5.11. If a vertical transmitting antenna over mediocre ground is utilised, very little radiation will occur at elevation angles below approximately 6° (Braun, 1982, p. 313). A vertical antenna also has an overhead null (at elevation angles greater than approximately 60°) in its radiation pattern (Braun, 1982, p. 305). The majority of the energy will be radiated

at elevation angles supporting propagation via the F2 layer in Figure 5.11. The energy is thus focussed over distances of between approximately 600 and 1 100 km in the example. The focussing gain may be as much as 6 to 9 dB (Goodman, 1992, p. 246). Focussing gain can thus be realized if the antenna radiates the majority of the signal at elevation angles associated with the FOT and the MUF of the circuit. For NVIS applications this implies that the antenna must radiate the majority of its energy at very high radiation angles.

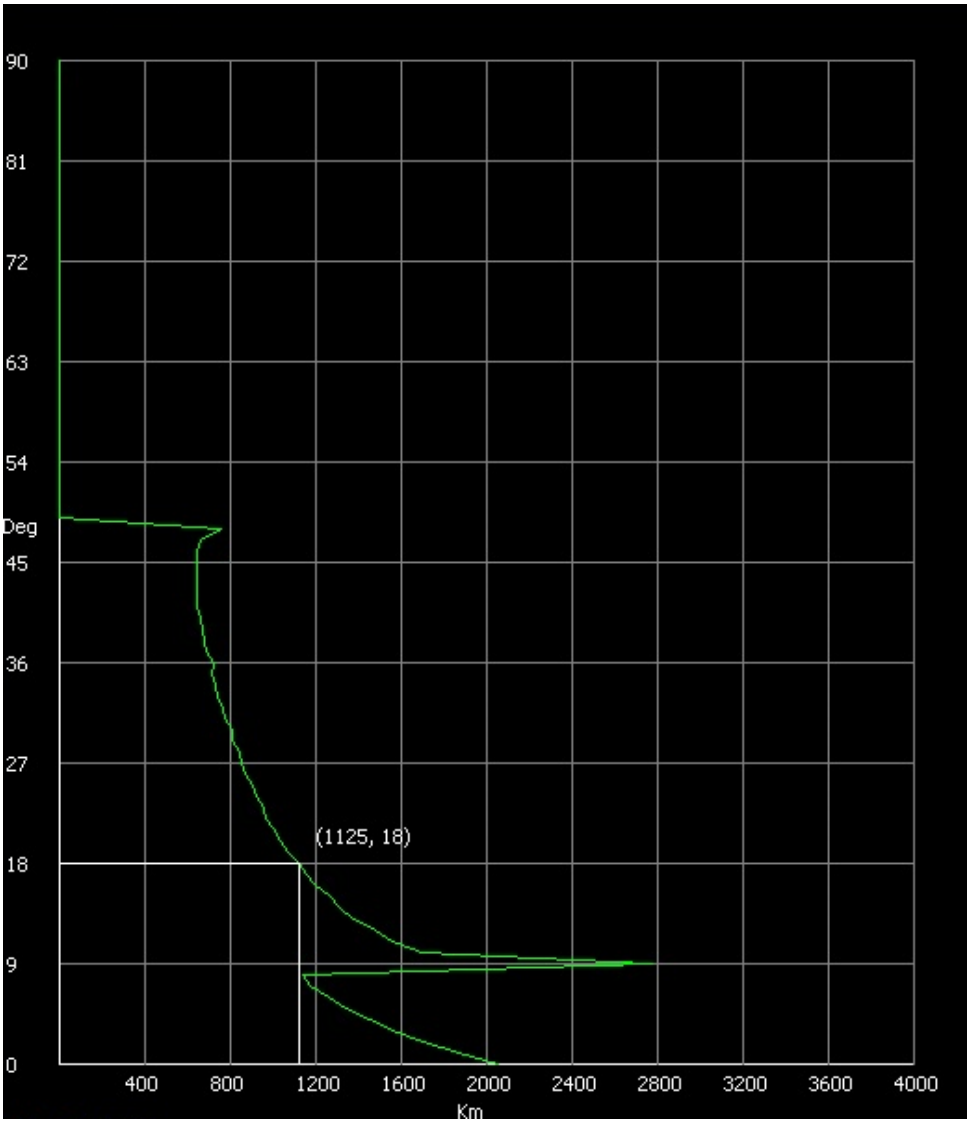

Figure 5.11. Calculated propagation (ray-tracing result) of a 13 MHz signal through the 2007 IRI illustrating the possibility of focussing gain over distances of 600 to approximately 1 100 km if an antenna radiates the majority of the energy at elevation angles of 18 to 50°.

5.6 SUMMARY

The composition of the ionosphere and ionosondes used to characterise it, in terms of radio propagation, were discussed. Ionograms and the electron density profile as a function of height were introduced. The relationship between the electron density profile as a function of height and the layer critical frequencies was presented for both the ordinary-wave as well as the extraordinary-wave. Ray-tracing through an ionospheric model was presented as a tool to analyse reigning propagation conditions for a specific frequency. The ray-tracing results in the form of graphs of elevation angle versus ground range was introduced as a powerful tool to illustrate the most commonly used HF propagation terminology including the MUF, FOT, skip zone, F region propagation, E layer propagation, low ray, high or Pederson ray, etc. The ray-tracing graphs illustrated the importance of the antenna's vertical radiation angle and the correct choice of operational frequency to prevent the occurrence of multipath propagation or the occurrence of no propagation at all due to the wave penetrating the ionosphere and getting lost in space.

In short: ionospheric propagation is not "black magic" or a "black art," but rather a well-defined and accurate science. It would have been even more utilised and better understood by the general public if it was not for the extremely dynamic nature of the ionosphere that so often plays havoc with the best frequency prediction efforts.

CHAPTER 6 SINGLE SITE LOCATION PERFORMANCE

6.1 INTRODUCTION

Reliable HF skywave communications are highly dependent on utilizing the correct frequency for the applicable distance and on the reigning ionospheric conditions. It is also important that the antenna radiates adequate energy at the required wave angle (azimuth and elevation angles).

SSL is based on skywave propagation, which suggests that SSL performance can be estimated from conventional skywave propagation metrics.

A technique to estimate the performance of SSL based on HF interferometric DF for reigning ionospheric propagation conditions is described in this chapter. This technique is based on classic propagation information (MUF, FOT, OWF, HPF, LPF, etc.) which can be deduced by ray-tracing through an ionospheric model such as the IRI. The correlation between the elevation angle measured by an interferometric direction finder and the angles corresponding to the propagation conditions are used to assign a quality factor to the calculated SSL ground range result (Coetzee *et al.*, 2016).

6.2 BACKGROUND

In 1887, H. Hertz developed the first radio transmitter. His companion receiver made use of a loop antenna. With this simple equipment, he was able to determine the basic transmission

properties of radio waves. The loop receiver, with its directional properties, enabled him to determine the direction to the transmitter. Basic direction finding is thus as old as the art of radio itself (Goodman, 1992, p. 5).

Angle of arrival (AoA) measurements were also used by Appleton, Breit and Tuve and a number of other researchers in the 1920's during their studies of ionospheric propagation (Goodman, 1992, p. 7).

Traditional HF DF relies on azimuth observations from multiple DF sites and uses the triangulation method to determine the geographical position of the transmitter. Until the end of World War 2, DF systems mostly operated on line-of-bearing principles. The most common were the crossed loop or Adcock type. In many instances, "shielded loops" were used to reduce "polarization" errors due to simultaneous propagation via ground wave and skywave (McNamara, 1991, p. 149). With Adcock systems, little consideration is given to the medium supporting the propagation, i.e. the ionosphere. Neglecting the influence of the ionosphere has a negative impact on the accuracy that can be obtained with DF systems.

In the late 1950's R. F. Treharne, Z. R. Jeffrey and C. G. McCue developed an operational system for determining the location of an HF transmitter that **relied** on the signal being reflected by the ionosphere (McNamara, 1991, p. 3). This technique, known as single site location (SSL) demands an even greater knowledge of the ionosphere than does HF communications. In 1989 relevant ray-tracing techniques were discussed by Baker and Lambert where use is made of multiple, quasi-parabolic (MQP) segments to generate an electron density as a function of height profile (Baker, *et al.*, 1989).

Ray-tracing through an electron density profile as a function of height generated by an ionospheric model promises enhanced accuracy for DF systems. Examples include the Segmented Method for Analytic Ray Tracing (SMART) (Norman, *et al.*, 1999) that makes use of the Parameterized Ionospheric Model (PIM) (Daniell, *et al.*, 1995), McKinnel that

developed an ionospheric model based on Neural Network principles (McKinnel, 2002) that can be used for ray-tracing based on Snell's law and Proplab-Pro (Solar Terrestrial Dispatch, Alberta, USA, 2018) that uses advanced two-dimensional and three-dimensional ray-tracing algorithms in conjunction with the 2007 IRI model. Coleman also developed curved earth ray-tracing algorithms that can be used with various ionospheric models (Coleman, 2011).

The interferometric direction finder used in this thesis uses the ray-tracing algorithm developed by McKinnel in conjunction with the 2016 IRI (Bilitza, *et al.*, 2017) model for the ground range calculations. The IRI ionospheric model is updated on a regular basis to ensure the highest degree of DF accuracy on skywave signals.

6.3 SINGLE SITE LOCATION PRINCIPLES

SSL (also known as Single Station Location) direction finding (simply referred to as SSL) is a technique to determine the origin (position) of a long-distance HF signal with the aid of a single, interferometric direction finder (ITU-R Handbook on Spectrum Monitoring, 2011, pp. 293–294). The elevation angle of the intercepted signal is used to calculate a ground range by modelling the path that the signal travelled through the ionosphere. The best results are obtained with the aid of ray-tracing (sometimes referred to as ray-retracing) techniques. With the measured direction (azimuth angle) and the calculated ground range, it is possible to determine the origin of the HF transmission with useful accuracy. Position is usually determined by triangulating the azimuth results of multiple direction finders, so the requirement for only a single direction finder is a significant benefit of SSL.

Simply being able to intercept (monitor) a signal and determining the wave angle with the aid of an interferometric direction finder does not guarantee the quality of the calculated SSL ground range. The reigning propagation conditions for the communications circuit must also be taken into consideration for optimum results. However, computing the performance of an SSL system is a complex problem that requires accurate modelling of the ionospheric conditions and complex ray-tracing techniques. To overcome this difficulty, a quality factor,

which only depends on the standard parameters for HF communication links, is proposed. Measured results are presented to demonstrate that this quality factor is a useful indicator of SSL performance.

6.4 ASSIGNING A QUALITY FACTOR TO THE CALCULATED SSL DISTANCES

The most reliable skywave HF communications are obtained if use is made of the FOT for the given circuit and reigning ionosphere. Operating on a higher frequency will result in a better SNR but communications reliability will suffer. Starting at the FOT and progressively reducing the operating frequency will result in a deteriorating SNR, to the point where the SNR required to ensure reliable communications cannot be maintained for 90% of the time anymore. Under these circumstances the LUF or lowest useable frequency for the circuit is reached.

The elevation angle of the received signal as measured by an interferometric direction finder can be related back to the MUF, FOT, HPF, etc. for the reigning ionospheric conditions when ray-tracing techniques are applied to the ionospheric data. The relevant ionospheric data may be provided by an ionosonde or obtained from an ionospheric model such as the IRI as shown in Figure 6.1.

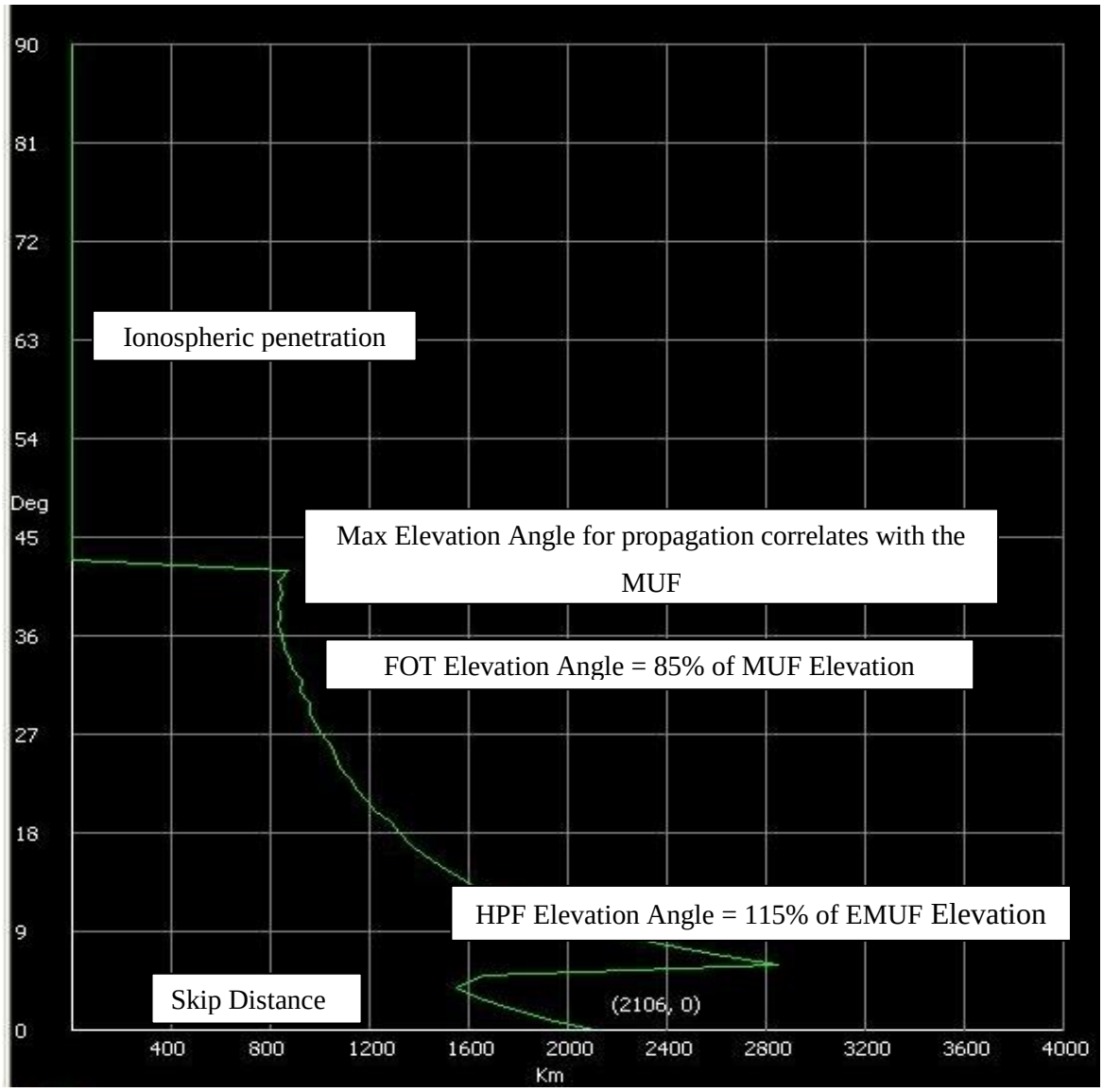

Figure 6.1. Relating elevation angle to propagation conditions using ray-tracing techniques.

When a SSL is performed on an operating frequency above the FOT, the reliability of the result will suffer along with the reliability of the communications. In Figure 6.1, an intercepted elevation angle of approximately 36° (0.85 × 42°) corresponds to the FOT for the F2 layer. Although it is statistically possible that a frequency above the MUF (ϕ > 42° in Figure 6.1) may propagate (HPF = 115% MUF), it will not be possible to calculate a SSL distance under the circumstances used to plot Figure 6.1.

The FOT is defined as having a reliability of 90% for a given circuit. If a SSL is performed under these near ideal conditions, a quality factor of 0.9 (or 90%) can be assigned to the result. For stable ionospheric conditions an SSL accuracy of 90% can thus also be assumed, or conversely a minimum distance (ground range) error of ±10% (McNamara, 1991, p. 49; Lai, 2008).

When SSL is performed on a progressively lower elevation angle (corresponding to an operational frequency lower than the FOT), two factors influence the quality of the SSL result and thus ultimately the accuracy of the calculated distance to the transmitting station. Firstly, while operating in the stable or linear region of the applicable layer, the reduction in SNR will reduce the accuracy of the calculated SSL ground range (ITU-R Handbook on Spectrum Monitoring, 2011, p. 279). Secondly, when the elevation angle gets so low that the transition region between the F and E ionospheric layers is approached (elevation angle approximately 8° in Figure 6.1), the HPF of the E layer will start to dominate the accuracy of the SSL result. Once this transition region is reached the SSL result will for all practical purposes become useless. A quality factor of 0.1 was used here as the statistical nature of the parameters used to compute the relevant angle mean that useful results may still be possible under exceptional circumstances.

A non-linear interpolation between the 90% reliability (quality factor of 0.9) result of a SSL calculation at the elevation angle corresponding to the FOT for a layer (e.g. the F2 layer) and the 0.1 quality factor for the HPF for the next lower layer (e.g. the E layer) is proposed to provide an indication of the quality of SSL DF results. Based on observations a quality factor of 0.7 is proposed if the elevation angle corresponds to 50% of the angle for the FOT. A quadratic polynomial function of the form

$$y = ax^2 + bx + c, \tag{6.1}$$

was fitted to the three sets of data points corresponding to the ratios of the elevation angles relative to the elevation angle for the FOT as defined above (variable x). The coefficients were calculated as $a = -1.2222$, $b = 2.2333$ and $c = -1.2222$.

This result makes it possible to calculate a quality factor for any elevation angle where propagation is possible. This quality factor has the benefit that it can easily be computed from readily available ionospheric parameters (the MUF and HPF), while still providing valuable information about SSL accuracy as shown by the measurements in Section 6.4.

6.5 VALIDATION

The majority of South Africa's maritime HF traffic is handled by a station at Goedverwacht, just outside Cape Town. The location of this transmitter is 33°47'20.00" S and 18°41'40.71" E. This station makes use of high-power transmitters operating on multiple frequencies. A wideband interferometric direction finder manufactured by GEW Technologies (Pretoria, South Africa) was deployed at Pretoria to measure the wave angles of the various transmissions over the 1 300 km path. Measurements were performed at various frequencies and times that corresponded to both the FOT for the circuit as well as to non-ideal (not near the FOT) combinations of frequencies and times. Figure 6.2 is a summary of the range error versus the calculated quality factor for all the measured SSL results.

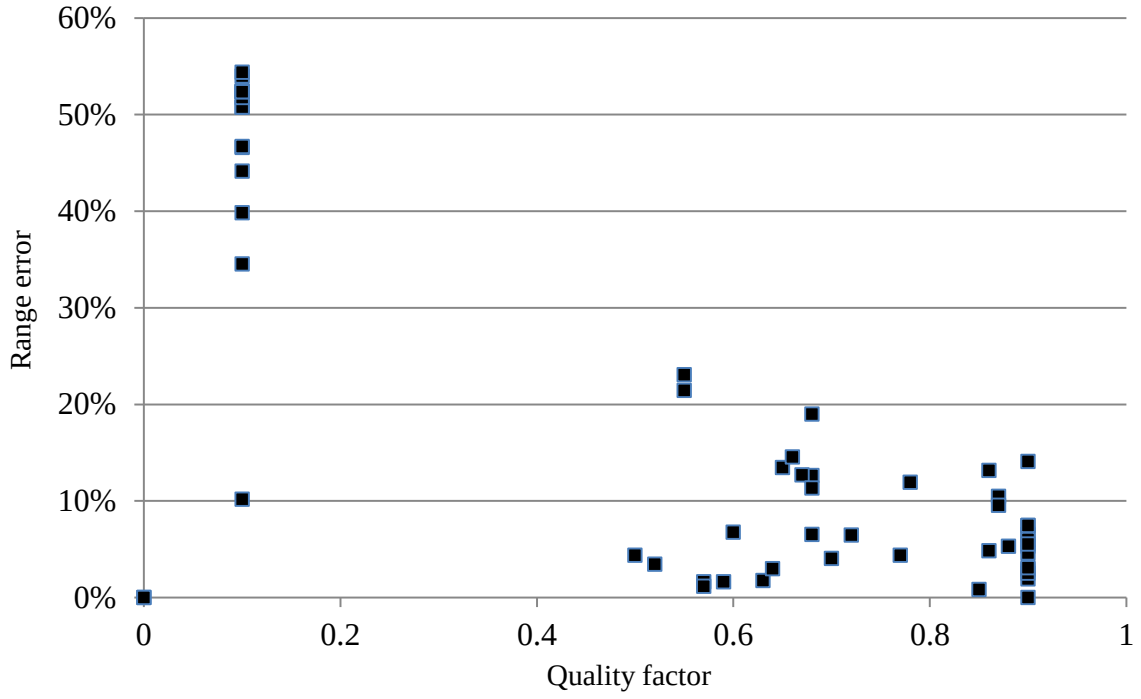

Figure 6.2. The calculated quality factor and the range error summarized for all the SSL measurements.

The direction finder's Graphical User Interface (GUI) is presented in Figure 6.3, demonstrating how the necessary information can be presented to a user in a real-world system. Figures 6.4 and 6.5 illustrate some of the SSL results obtained.

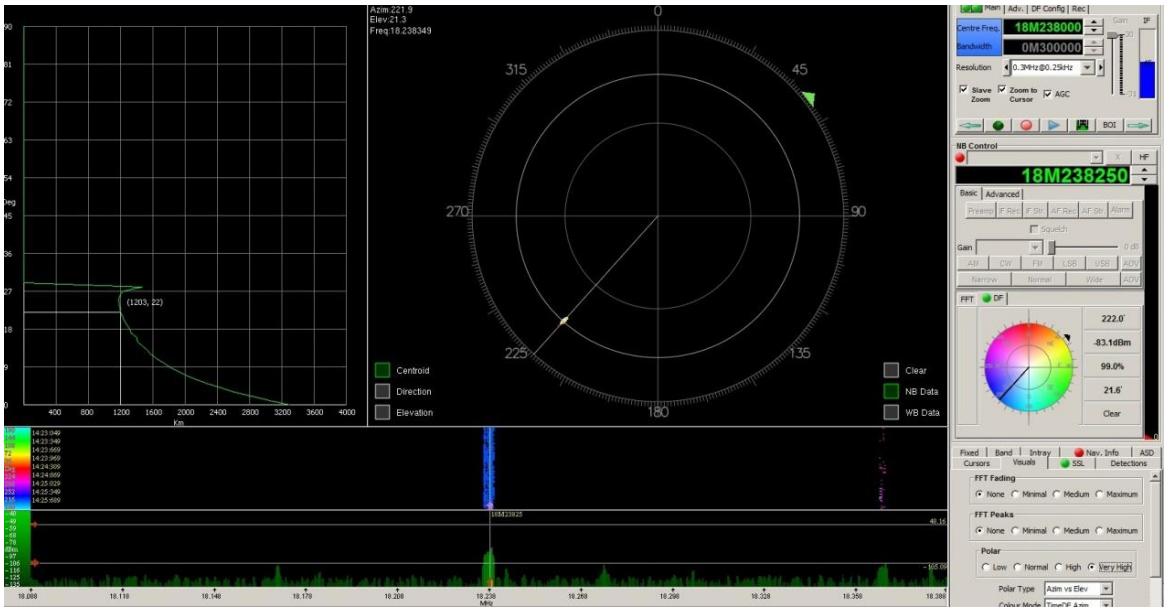

Figure 6.3. GEW Technologies wideband HF interferometric direction finder's graphical user interface.

The calculated propagation of an 18.238 MHz signal is displayed in the top left hand graph of Figure 6.3. It can be seen that the signal will not propagate at elevation angles above approximately 30° and that there is a skip zone of slightly less than 1 200 km. When this measurement was performed, single-hop propagation was not possible over distances of more than approximately 3 200 km, corresponding to an elevation angle of approximately 0°. The intercepted transmission arrived at an elevation angle of 22°, corresponding to a ground range of 1 203 km as indicated by the white lines and the white numerals. This ray-traced elevation angle versus range graph is simply referred to as the SSL Graph.

The graph to the right of the SSL Graph is the Polar Display. The Polar Display provides a line-of-bearing (LoB) as well as indicating the elevation angle of the received signal. Signals arriving at low elevation angles are plotted towards the outside of the Polar Display while NVIS signals are displayed closer to the centre. A signal arriving from directly overhead (90° elevation angle) will be displayed in the centre of the Polar Display. A persistence function implemented in software ensures that a visual histogram is formed allowing the operator to judge the quality of the DF result. A stable DF result forms a small grouping

while unstable ionospheric conditions or multi-hop propagation cause the results to be more spread out leading to greater uncertainty regarding the correct wave angle of the target signal.

The direction finder's centre frequency, bandwidth, resolution and other RF functions are set in the right hand side panel. The DF result is displayed in the coloured rosette near the bottom. In Figure 6.3, the measured bearing is 222° and the signal level is –83.1 dBm. The noise floor is at approximately -125 dBm, giving a received SNR of 41.9 dB. The DF requires a SNR of at least 20 dB to achieve an azimuth RMS error of ≤1°.

The bottom graph of Figure 6.3 is a spectrum display showing amplitude over the selected 300 kHz bandwidth or span. The resolution bandwidth (bin size) is 250 Hz. A direction result is calculated for each bin, thus 1 200 in total. The 18.238 MHz target frequency in the centre of the display is also the strongest signal.

The graph above the spectrum display is a sonogram or history of the received energy that exceeds the selectable threshold level. Colour is used to identify the direction of arrival of the signal, aiding an operator in immediately determining whether a signal originates from a specific target area. The dark blue of the 18.238 MHz signal corresponds to the DF result displayed on the small rosette to the right. A signal originating from the north will be displayed in red for example. The homogenous colour result of the target frequency indicates stable propagation as required by the ITU with no scatter modes present (ITU-R Handbook on Spectrum Monitoring, 2011, pp. 293–294).

The measured elevation angle of 22° corresponds well with a calculated FOT angle of 25.5° (0.85 of the MUF angle of 30°). Using (6.1) a quality factor of 0.9 was calculated. The SSL distance estimate is 1 203 km resulting in a range error of 7.5% over the 1 300 km path.

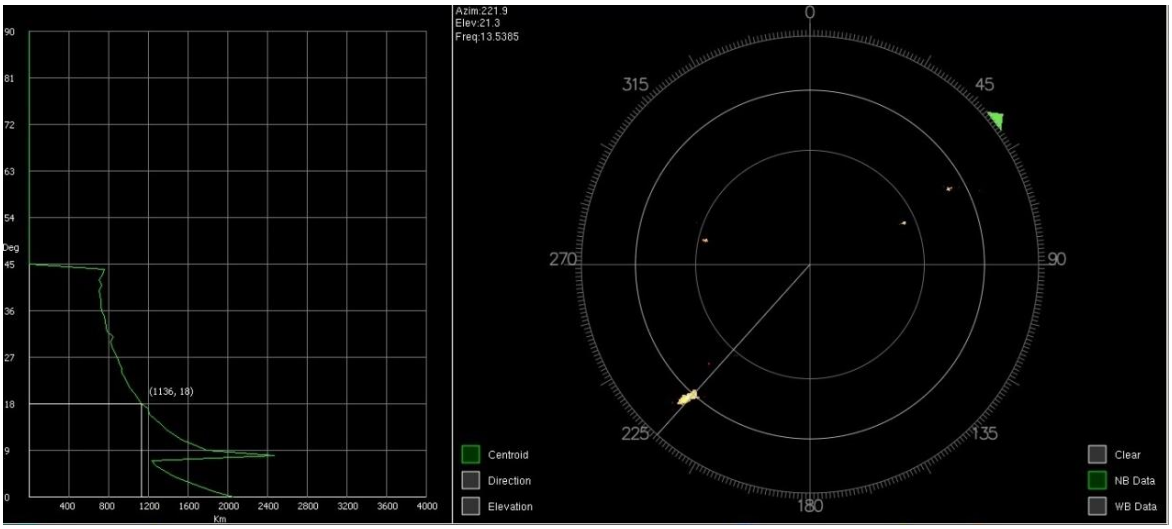

Figure 6.4. SSL result of a signal considerably below the FOT for the circuit.

The measured elevation angle of Figure 6.4 indicates that the 13.538 MHz transmission is 47% of the angle associated with the FOT (18° versus 38°) for the circuit at that moment in time. A quality factor of 0.67 is calculated for the SSL distance estimate of 1 136 km (range error of 14%). Stable propagation conditions (indicated by a small grouping on the rosette) contribute to the operational usefulness of the result of Figure 6.4.

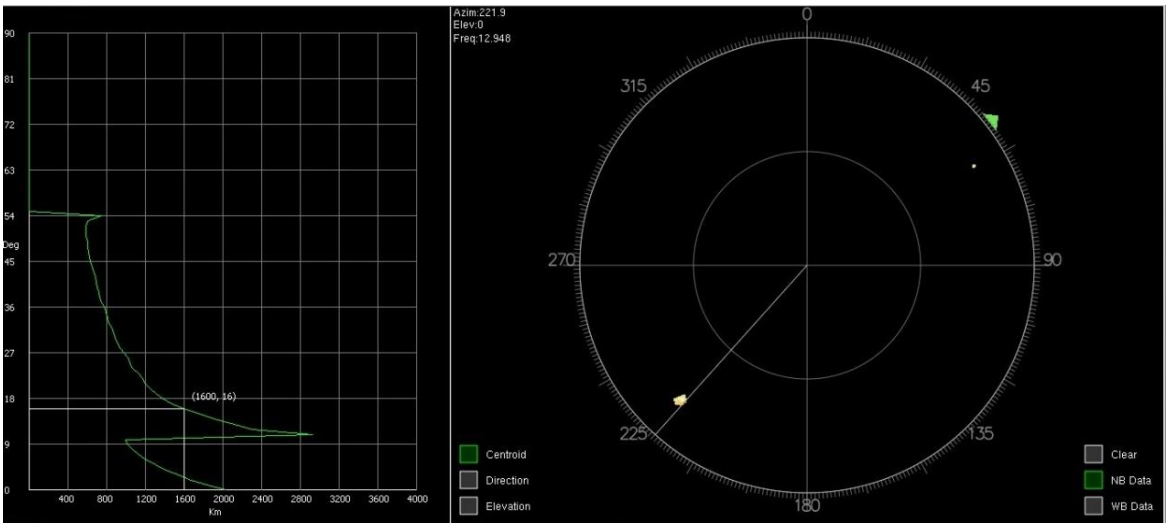

Figure 6.5. SSL result of a signal approaching the transition between ionospheric layers.

The 12.948 MHz signal of Figure 6.5 is well received with the correct bearing indicated, but the SSL performance is less spectacular (1 600 km versus a true range of 1 300 km resulting

in a range error of 23%). The signal is propagating too close to the transition of the E- and F2 layers (approaching the HPF of the E layer) with the expected non-ideal result (calculated quality factor is 0.55).

The measurements of Figures 6.3 to 6.5 were performed during stable geo-magnetic conditions to ensure that the results are applicable to the described technique (ITU-R Handbook on Spectrum Monitoring, 2011, p. 295).

More examples of various propagation conditions as studied with an interferometric DF are provided in the Addendum. From the ray-tracing graphs in the Addendum, it is clear that single hop propagation via the F layer is not possible under certain conditions as depicted in Figures A.4, A.5 and A.6. When a too low operational frequency is chosen for the 1 300 km circuit, double hop F layer propagation tend to be the preferred propagation mechanism. The data from the SSL campaign was adapted to reflect these conditions when double hop, F layer propagation occurred. When this occurred the single hop distances were used in Figure 6.6. The updated ground range error percentage versus the elevation angle as a percentage of the elevation angle associated with that of the FOT is summarised in Figure 6.6.

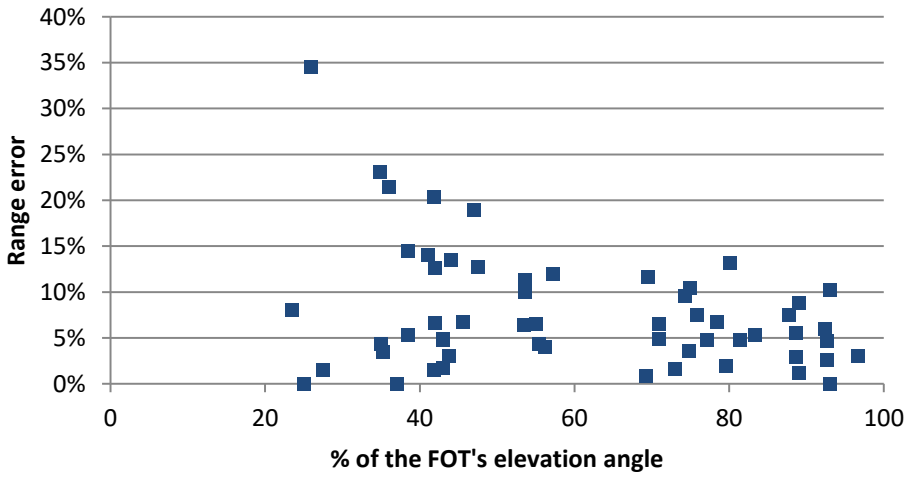

Figure 6.6. Ground range error versus the correlation of the measured elevation angle with that of the FOT's elevation angle.

In Figure 6.6, it appears that the range error mostly stays below 15% until the measured elevation angle decreases to approximately 50% of that associated with the FOT. At elevation angles less than 50%, the range error tends to increase. From this, it may be concluded that the stable region of the F layer of the ionosphere, in terms of propagation, extends from the elevation angle associated with that of the FOT for the circuit down to approximately 50% of that of the FOT.

In terms of HF frequency planning, it implies that stable propagation cannot only be expected at the FOT, but also over a frequency range less than the FOT. The lower boundary for stable propagation over a defined circuit can be determined by first determining the elevation angle associated with the FOT by means of ray-tracing. The operational frequency is then reduced to the point where the calculated elevation angle for the circuit is approximately 50% of that for the FOT.

In general, the SSL results were better (more stable and accurate) during the morning than the afternoons. From the test results, it seems that the ionosphere is especially unstable in the afternoons, adding another dimension of uncertainty to the SSL results. To compensate for the instability of the ionosphere multiple measurements over a longer time had to be taken, as recommended by the ITU (ITU-R Handbook on Spectrum Monitoring, 2011, p. 280).

6.6 POSSIBLE FUTURE WORK

Another deduction can be made from the results of the SSL campaign, as presented in Figure 6.2. When the quality factor is less than 50%, the range error increases rapidly, or conversely, the range error seems to remain stable between elevation angles associated with the FOT down to a value of approximately 50% of the elevation angle associated with the FOT. This indicates that the stable portion of the ionospheric layer extends from the elevation angle associated with the FOT to as low as 50% of the angle associated with the FOT as indicated in Figure 6.7.

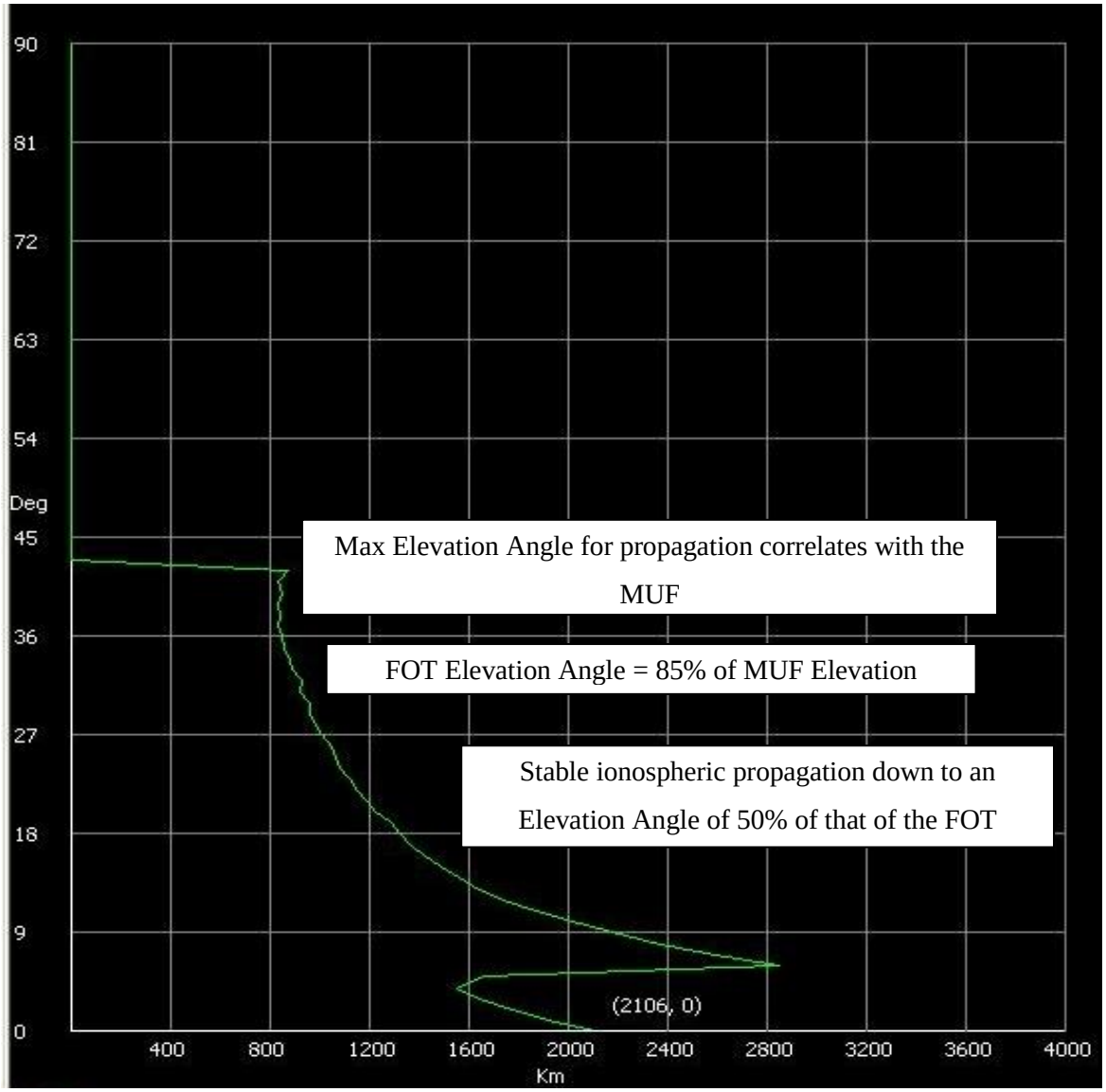

Figure 6.7. The stable region of the F layer extends as low as 50% of the angle associated with the FOT.

A future campaign utilising test transmissions over various distances, an interferometric DF and a suitable ray-tracing algorithm can be utilised to further study the stable propagation region of the ionosphere. The aim of such as study will be to determine if the stable propagation region of the ionosphere extends down to an angle of 50% of that associated with the FOT, or if not, to quantify the lowest percentage of the angle associated with the FOT that will still support stable ionospheric propagation.

6.7 DISCUSSION AND SUMMARY

The performance of SSL HF direction finding can be estimated by determining the correlation of the measured elevation angle with the angles associated with the FOT and the MUF of the circuit using ray-tracing techniques.

When the measured elevation angle corresponds to the angle associated with the FOT, the SSL distance estimate is expected to be accurate. The expected distance accuracy will deteriorate as the measured elevation angle approaches the angle associated with the HPF of the next lower layer (typically the E layer). However, if the measured elevation angle falls in the transition region of the E– and F layers, the SSL distance is in principle undefined and the SSL result basically useless (very low quality).

Based on these observations, a quality factor for SSL range estimates was proposed based on widely-available ionospheric propagation parameters (the MUF, FOT and HPF). This quality factor was shown to be useful by comparing estimated performance to measurements. Both the measurements and the quality factor show that useful SSL results can be obtained at elevation angles as low as 50% of that associated with the reigning FOT. It came as a bit of a surprise that stable ionospheric propagation extends down to such a low percentage of the elevation angle associated with the FOT. This implies that the implemented quadratic curve fit used to determine the quality factor of the SSL result may not be optimal and it may be worth investigating other curve fit options as well.

The best SSL results can only be expected if the target transmitter is at an optimum distance (corresponding to an optimum measured elevation angle and an operating frequency close to the FOT) from the DF for the reigning ionospheric conditions. From this, it can be deduced that multiple DF sites throughout a country will be required to ensure the most reliable SSL position determination of a target signal.

CHAPTER 7 CONCLUSION

HF radio propagation (both skywave and ground wave) has been in use for more than a century but is still actively studied, as some answers remain elusive. In some instances, the advent of modern, cost effective computers and especially DSP techniques and hardware have opened new opportunities to study classic phenomena such as the tilt of a HF ground wave signal and the propagation of a skywave signal. Methods were described to perform this in real time by measuring the received elevation angle with the aid of a state-of-the-art interferometric DF.

The proposed TDR-soil moisture technique offers significant advantages in terms of simplicity, speed and cost when compared to current techniques to determine the electromagnetic constants of ground at HF. The results obtained by this method compare favourably with those obtained by using the technique based on the impedance of a low horizontal dipole. The received signal strength of a ground wave HF transmission also compares favourably with that predicted by GRWAVE when using ground constants calculated by the TDR-soil moisture technique in conjunction with the previously published universal RC network soil model.

An interferometric DF offers significant advantages in terms of simplicity, speed and cost in determining the wave tilt of an HF ground wave signal when compared to current manual techniques. Although only the forward tilt is measured, sufficient information is obtained to determine the electromagnetic properties of the soil in close proximity to the antenna field with useful accuracy. This is done in conjunction with the previously published universal RC network soil model and the soil moisture technique.

With the correct electromagnetic ground constants for the applicable frequency determined, it is now possible to more accurately model ground wave propagation, transmitter area coverage, ground penetration of a RF signal, radiation patterns and impedances of HF antennas as well as ground reflections at reflective antenna test ranges such as Paardefontein, South Africa.

The performance of SSL HF direction finding that uses an interferometric DF can be estimated by determining the correlation of the measured elevation angle with the angles associated with the FOT and the MUF of the circuit as determined with ray-tracing techniques. Based on these observations, a quality factor for SSL range estimates was proposed based on widely available skywave metrics (the MUF, FOT and HPF). This quality factor was shown to be useful by comparing estimated performance to measurements.

In conclusion, it has been shown that it is possible to achieve much more with a modern interferometric DF than just determining the azimuth and elevation angles of a HF signal. Evidence of this is shown in this dissertation by the ability to determine the electromagnetic ground constants from the measured wave tilt angle of a ground wave signal. An interferometric DF is also an ideal instrument to monitor and analyse the reigning skywave propagation conditions in conjunction with an advanced ray-tracing algorithm. It is now possible to distinguish between single and multi-hop and -layer propagation and also to determine the skip or dead zone. In short, an interferometric DF is facilitating our understanding of HF skywave propagation in a way not previously possible. Unfortunately, it has not gained wide spread acceptance yet, probably due to the complexity and cost involved as well as researchers' lack of access to such an instrument.

REFERENCES

Adams, J. E., Carrol, J. C., Costa, E. A., Ebaugh, D. R. Jr, Godwin, J. R., Haakinson, E. J., Layton, D. H. and Smith, D. (1984). Measurements and predictions of HF ground wave radio propagation over irregular, inhomogeneous terrain, *NTIA Report 84–151, Boulder, Colorado, USA.*

Alipio, R. and Visacro, S. (2014).Impulse Efficiency of Grounding Electrodes: Effect of Frequency-Dependent Soil Parameters, *IEEE Transactions on Power Delivery* **29**(2): 716–723.

Appleton, E. V. and Builder, G. (1933). The Ionosphere as a Double Refracting Medium, *Proc. Phys. Soc.* **8**(22): 2557–2571.

Armscor Defence Institutes (Pty) Ltd (2013). The South African National Antenna Test Range. www.paardefontein.co.za. Last accessed on 21 May 2017.

Baker, D. C. and Burden, J. J. (1992). Effect of F1-layer L condition on ranging accuracy for SSL HFDF systems, *Electronic Letters* **28**(21): 1956–1958.

Baker, D. C. and Lambert, S. (1989). Range Estimation for SSL HFDF by Means of Multiquasiparabolic Ionospheric Model, *IEEE Proc.* **136**(2): 120–125.

Baker-Jarvis, J. and Kim, S. (2012). The Interaction of Radio-Frequency Fields with Dielectric Materials at Macroscopic to Mesoscopic Scales, *J Res Natl Inst Stand Technol,* **117**: 1–60.

Bilitza, D. (2001). International Reference Ionosphere 2000, *Radio Science* **36**(2): 261–275.

Bilitza, D., Altadill, D., Truhlik, V., Shubin, V., Galkin, I., Reinisch, B. and Huang, X. (2017). International Reference Ionosphere 2016: From ionospheric climate to real-time weather predictions, *Space Weather* **15**(2): 418-429.

Beziuk, G. and Mydlikowski, R. (2007). Determination of near-surface apparent resistivity by means of high frequency mutual impedance measurements, *Acta Geodyn. Geomater*. **4**(148): 89–95.

Blomquist, Å. (1975). Seasonal effects on ground-wave propagation in cold regions, *Journal of Glaciology* **15**(73): 285–303.

Braun, G. (1982). *Planning and Engineering of Shortwave Links*, Siemens Aktiengesellschaft, Heyden & Son Ltd., London, UK.

Burke, G. J., Miller, E. K and Poggio, A. I. (2004). The Numerical Electromagnetics Code (NEC) – A Brief History, *IEEE APS*, Monterey, CA, USA.

Cavanagh, J. F. (1985). GRWAVE Release 2, *Naval Surface Warfare Centre*.

Cavka, D., Mora, N. and Rachidi, F. (2014). A Comparison of Frequency-Dependent Soil Models: Applications to the Analysis of Grounding Systems, *IEEE Transactions on Electromagnetic Compatibility* **56**(1): 177–187.

CCIR Report 714–2. (1990). *Groundwave propagation in an exponential atmosphere*, International Telecommunication Union, Geneva, Switzerland.

Coetzee, P. J. (2004). Applications of the IRI (International Reference Ionosphere) in Southern Africa, *Advances in Space Research* **34**(4): 2075–2079.

Coetzee, P. J. (2014). A technique to determine the electromagnetic properties of soil using moisture content, *South African Journal of Science* **110**(5/6): 85–88.

Coetzee, P. J. and du Plessis, W. P. (2016). Definition of a quality factor for single site location estimates, *Radio Science* **51**(6): 555–562.

Coleman, C. J., (2011). Point-to-point ionospheric ray tracing by a direct variational method, *Radio Science* **46**(5): RS5016.

Daniell, R. E., Brown, L. D., Anderson, D. N., Fox, M. W., Doherty, P. H., Decker, D. T., Sojka, J. J. and Schunk, R. W. (1995). Parameterized Ionospheric Model: A Global Ionospheric Parameterization Based on First Principle Models, *Radio Science* **30**(5): 1499–1510.

Davies, K. (1990). *Ionospheric Radio*, Peter Peregrinus Ltd., London, United Kingdom.

Davila, C.V. (1993). Thesis: Comparison of HF groundwave propagation models, *Naval Postgraduate School*, Monterey, California.

Debye, P. (1929). *Polar molecules*, Dover, Mineola, NY.

DeMinco, N. (1999), Medium frequency propagation prediction techniques and antenna modelling for intelligent transportation systems (ITS) broadcast applications, *NTIA Report 99–368*.

Devoldere, J. (2010). *ON4UN's Low-Band DXing*, 5th edition, The American Radio Relay League, Inc., Newington, CT, USA.

Eaton, J. L. (1976). The wave-tilt method of measuring electrical ground constants in the L.F. and M.F. bands, *BBC Research Department Technical Report*, BBC–RD–1976/15.

Eliassen, K. E. (1957). A survey of ground conductivity and dielectric constant in Norway within the frequency range 0.2–10 Mc/s, *Geofysiske Publikasjoner*, **19**(11): 5–30.

Fieldscout TDR 300. Spectrum Technologies, IL, USA. www.specmeters.com. Last accessed on 4 January 2018.

Frissell, N. A., Miller, E. S., Kaeppler, S. R., Ceglia, F., Pascoe, D., Sinanis, N. Smith, P., Williams, R. and Shovkoplyas, A. (2014) Ionospheric Sounding Using Real-Time Amateur Radio Reporting Networks, *Space Weather*, **12**: 651–656.

Giesbrecht, J. E., Clarke, R. and Abbott, D. (2004). Improved techniques for monitoring the HF spectrum, *Proceedings of SPIE*, SPIE, Bellingham, WA, USA, Vol. 5274.

Goodman, J. M. (1992). *HF Communications Science and Technology*, Van Nostrand Reinhold, New York.

Hagn, G. H. (1992). MUFs and MOFs and LUFs and LOFs, Stand on Standards, *IEEE Antennas and Propagation Magazine*, **34**(6): 68–73.

Hill, D. A. (1982). HF Ground Wave Propagation over Forested and Built-up Terrain, *U.S. Department of Commerce*, NTIA Report 82–114.

Hill, D. A. and Wait, J. R. (1980). Ground wave attenuation function for a spherical earth with arbitrary surface impedance, *Radio Science*, **15**(3): 637–643.

IEEE Std 356–2010. (2011). *IEEE Guide for Measurements of Electromagnetic Properties of Earth Media*, The Institute of Electrical and Electronics Engineers, Inc. 3 Park Avenue, New York, NY 10016-5997, USA.

ITU-R Recommendation P.832–4. (2015). *World atlas of ground conductivities*, ITU-R Recommendations, P Series, Radiowave Propagation. International Telecommunication Union, Radiocommunication Sector, Geneva, Switzerland.

ITU-R Recommendation P.527–3. (1992). *Electrical characteristics of the surface of the Earth*, ITU-R Recommendations, P Series, Radiowave Propagation. International Telecommunication Union, Radiocommunication Sector, Geneva, Switzerland.

ITU-R Recommendation P.527–4. (2017). *Electrical characteristics of the surface of the Earth*, ITU-R Recommendations, P Series, Radiowave Propagation. International Telecommunication Union, Radiocommunication Sector, Geneva, Switzerland.

ITU-R Report P.879–1. (1986). *Methods for estimating effective electrical characteristics of the surface of the Earth*, ITU-R Reports, P Series, Radiowave Propagation. International Telecommunication Union, Radiocommunication Sector, Geneva, Switzerland.

ITU-R Study Group 3. (2018). GRWAVE, https://www.itu.int/en/ITU-R/study-groups/rsg3/Pages/iono-tropo-spheric.aspx. Last accessed on 21 January 2018.

ITU-R (2011). *Handbook on Spectrum Monitoring*, International Telecommunication Union, Radiocommunication Sector, Geneva, Switzerland.

King, R. J. (1976). Wave-tilt measurements, *IEEE Transactions on Antennas and Propagation*, **24**(1): 115–119.

King, R. J. (1969). Electromagnetic wave propagation over a constant impedance plane, *Radio Science* **4**(3): 225–268.

King, R. W. P. and Smith, G. S. (1981), *Antennas in Matter.* Cambridge, MA, MIT Press.

Kirby, S. S., Berkner, L. V. and Stuart, D. M. (1934). Studies of the ionosphere and their application to radio transmission, *Research Paper RP632*, *Bureau of Standards Journal of Research* **12**, pp. 15–51.

Kissick, W. A., Haakinson, E. J. and Stonehocker, G. H. (1978). Measurements of LF and MF Radio Propagation over irregular, inhomogeneous terrain, *NTIA-Report*, 78–12.

Lai, K. (2008). A Real-Time HF Single-Station Location System Development, *IEEE International Conference on Radar, 2-5 September 2008*, pp. 307–310.

Lewallen, R. W. (2013). EZNEC+ v. 5.0.62, www.eznec.com. Last accessed on 21 May 2017.

Longmire, G. L. and Longley, H. J. (1973). Time domain treatment of media with frequency-dependent electrical parameters, *Theoretical Notes*, Note 113, 25 September 1973, Contract No. DASA 01–71–C–0105, Mission Research Corporation, Santa Barbara, CA.

Longmire, G. L. and Smith, K. S. (1975). A universal impedance for soils, *Topical Report for period 1 July 1975 to 30 September 1975*, Report No. MRG–N–214, Contract DNA 001–75–6–0094, Mission Research Corporation, Santa Barbara, CA.

Lytle, J. R. (1973). Measurement of earth medium electrical characteristics: techniques, results and applications, *Lawrence Livermore Laboratory,* TID–4500, UC–34, Physics, General.

Makki, S. V. A., Ershadi, T. Z. and Abrishamian, M. S. (2008). Determining the specific ground conductivity aided by the horizontal electric dipole antenna near the ground surface, *Progress in Electromagnetics Research B,* **1**: 43–65.

Martyn, D. F., Cherry, R. O. and Green, A. L. (1935). Long Distance Observations of Radio Waves of Medium Frequencies, *Proc. Phys. Soc.*, **47**(2): 340–351.

McKinnell, L. A. (2002). *A Neural Network based Ionospheric model for the bottomside electron density profile over Grahamstown South Africa*, Ph.D. thesis of Rhodes University, Grahamstown, South Africa.

McKinnell, L. A., Ssessanga, N., Coetzee, H. and Okoh, D. (2011). The South African ionosonde network: Past and Present, *General Assembly and Scientific Symposium, 2011 XXXth URSI*.

McNamara, L. F. (1991). *The Ionosphere: Communications, Surveillance, and Direction Finding*, Krieger Publishing Company, Malabar, Florida.

Mewes, H. (1997). Long term azimuth and elevation measurements in the HF band, *HF Radio Systems and Techniques*, 7-10 July 1997, IEE Conference Publication **411**: 344–348.

Mokhtari, M., Abdul-Malek, Z. and Wooi, C. L. (2016). Integration of Frequency Dependent Soil Electrical Properties in Grounding Electrode Circuit Model, *International Journal of Electrical and Computer Engineering (IJECE),* **6**(2): 792–799.

Nichol, C., Beckie, R. and Smith, L. (2002). Evaluation of Uncoated and Coated Time Domain Reflectometry Probes for High Electrical Conductivity Systems, *Soil Sci. Soc. Am. J.*, **66**: 1454–1465.

Nicol, J. L. (1980). The input impedance of horizontal antennas above an imperfect earth, *Radio Science*, **15**(3): 471–477.

Norman, R. J. and Cannon, P. S. (1997). An evaluation of a new 2-D analytic ionospheric ray tracing technique – SMART, *Radio Science*, **32**(2): 489 – 499.

Norton, K. A. (1935). Propagation of radio waves over a plane earth, *Nature*, **135**: 954-955.

Oswald, B., Benedickter, H. R., Bächtold, W. and Flühler, H. (2004). A Single-Rod Probe for Time Domain Reflectometry Measurements of the Water Content, *Vadose Zone Journal*, **3**: 1152–1159.

Ott, R. H. (1971a). An alternative integral equation for propagation over irregular terrain, 2, *Radio Science*, **5**: 767–771.

Ott, R. H. (1971b). A new method for predicting HF ground wave attenuation over inhomogeneous, irregular terrain, *U.S. Dept. of Commerce*, Office of Telecommunications, TRER 7, (NTIS Accession No. AD721179).

Ott, R. H., Vogler, L. E. and Hufford, G. A. (1979). Ground wave propagation over irregular, inhomogeneous terrain: comparison of calculations and measurements, *NTIA Report 79-20*, May (NTIS Accession No. PB 298668/AS).

Pearce, D. C., Hulse, W. H. and Walker, J. W. (1973). The Application of the Theory of Heterogeneous Dielectrics to Low Surface Area Soil Systems, *IEEE Transactions, Geoscience, Electron*, **11**: 167.

Pedrosa, A. G., Alipio, R. S., Schroeder, M. A. O. and Afonso, M. M. (2010). Simulation of behavior electrical grounding-comparative analysis for the performance in frequency-domain, in *Proc. Int. Workshop Appl. Model Simul.*

Portela, C. M. (1999). Measurement and modelling of soil electromagnetic behavior, in *Proc. IEEE Int. Symp. Electromagn. Compat.* **2**: 1004–1009.

Robinson, D. A., Jones, S. B., Wraith, J. M., Or, D. and Friedman, S. P. (2003). A Review of Advances in Dielectric and Electrical Conductivity Measurement in Soils Using Time Domain Reflectometry, *Vadose Zone Journal*, **2**: 444–475.

Robinson, D. A., Jones, S. B., Blonquist Jr, J. M. and Friedman, S. P. (2005). A Physically Derived Water Content/Permittivity Calibration Model for Coarse-Textured, Layered Soils, *Soil Sci. Soc. Am. J.*, **69**: 1372–1378.

Rohde & Schwarz GmbH & Co. KG[DE], Munich, Germany. www.rohde-schwarz.com. Last accessed on 4 January 2018.

Roth, K., Schulin, R., Flühler, H. and Attinger, W. (1990). Calibration of Time Domain Reflectometry for Water Content Measurement Using a Composite Dielectric Approach, *Water Resources Research*, **26**(10): 2267–2273.

Rotheram, S. (1981). Ground wave propagation I: Theory for short distances, *IEE Proceedings, Part F*, **128**: 275–284.

Santos, T., Johansson, A. J. and Tufvesson, F. (2009). Dielectric Characterization of Soil Samples by Microwave Measurements, *Series of Technical Reports*, **10**, ISSN 1402–8840, Dept. of Electrical and Information Technology, Lund University.

Scott, J. H. (1971). Electrical and Magnetic Properties of Rock and Soils, *Note 18, Electromagnetic Pulse Theoretical Notes*, AFWL EMP 2–1.

Shovkoplyas, A. DX Atlas and HamCap. www.dxatlas.com. Last accessed on 22 April 2018.

Sommerfeld, A. N. (1909). Über die Ausbreitung der Wellen in der Drahtlosen Telegraphie (In English: The propagation of waves in wireless telegraphy), *Annale Physik*, (Leipzig) **4**(28): 665–736.

Solar Terrestrial Dispatch. (2018). *Proplab-Pro Version 3*, www.spacew.com/www/proplab.html. Last accessed on 18 February 2018.

Tascione, T. F., Kroehl, K. W. and Hausman, B. A. (1987). A technical description of the ionospheric conductivity and electron density profile model (ICED, version 196–II), *Syst. Doc Vol. VII, Air Weather Serv.*, U.S. Air Force, Scott Air Force Base, Ill.

Terman, F. E. (1955). *Electronic and Radio Engineering*, New York, McGraw-Hill Book Co.: 803–808.

Tesche, F. M. (2002). On the Modeling and Representation of a Lossy Earth for Transient Electromagnetic Field Calculations, *Theoretical Notes*, Note 367, Swiss NEMP Laboratory, Contract 151–186.

Teters, L. R., Lloyd, J. L., Haydon, G. W. and Lucas, D. L. (1983). Estimating the Performance of Telecommunication Systems Using the Ionospheric Transmission Channel, *Institute for Telecommunication Sciences* NTIA Report 83–127.

Topp, G. C., Davis, J. L. and Annan, A. P. (1980). Electromagnetic determination of soil water content; measurements in coaxial transmission lines, *Water Resources Research*, **16**: 574–582.

Topp, G. C., Davis, J. L. and Annan, A. P. (2003). The Early Development of TDR for Soil Measurements, *Vadose Zone Journal*, **2**: 492–499.

Ulaby, F. T. (2007). *Fundamentals of Applied Electromagnetics,* Fifth Edition, The University of Michigan, Pearson Prentice Hall, Pearson Education, Inc., Upper Saddle River, NJ 07458, ISBN 0–13–241326–4.

Underhill, M. J. (2012). Anomalous groundwave tilt measured over wet ground, *12th IET International Conference on Ionospheric Radio Systems and Techniques (IRST 2012). 15–17 May 2012.*

Viggiano, A. A. (2006). Reexamination of ionospheric chemistry: high temperature kinetics, internal energy dependences, unusual isomers, and corrections, *Physical Chemistry Chemical Physics*, **8**(22): 2557–2571.

Visacro, S. and Alipio, R. (2012). Frequency Dependance of Soil Parameters: Experimental Results, Predicting Formula and Influence on the Lightning Response of Grounding Electrodes. *IEEE Transactions on Power Delivery,* **27**(2): 927–935.

Wagner, L. S. (1977). Communications Media Analysis – HF, *NRL Memo Rpt. 3428*, Naval Research Laboratory, Washington DC 20375–5000.

Wait, J. R. (1998). The ancient and modern history of EM ground-wave propagation, *IEEE Antennas and Propagation Magazine*, **40**(5): 7–24.

Wait, J. R. and Nabulsi, K. A. (1996). Wave tilt of radio waves propagating over a layered ground, *Geophysics,* **61**(6): 1647–1652.

Witvliet, B. A. (2015). *Near Vertical Incidence Skywave Interaction of Antenna and Propagation Mechanism*, Ph.D. thesis of the University of Twente, Enschede, The Netherlands.

Witvliet, B. A., van Maanen, E., Petersen, G. J., Westenberg, A. J., Bentum, M. J., Slump, C. H. and Schiphorst, R. (2015). Measuring the Isolation of the Circularly Polarized Characteristic Waves in NVIS Propagation [Measurements Corner], in *IEEE Antennas and Propagation Magazine*, **57**(3): 120–145.

Witvliet, B. A., van Maanen, E., Petersen, G. J., Westenberg, A. J., Bentum, M. J., Slump, C. H. and Schiphorst, R. (2015). Near Vertical Incidence Skywave propagation: Elevation angles and optimum antenna height for horizontal dipole antennas, in *IEEE Antennas and Propagation Magazine*, **57**(1): 129–146.

Zenneck, J. (1907). Über die Fortpflanzung Ebener Electromagnetischer Wellen einer Ebener Leiterflache und ihre Beziehung zur Drahtlosen Telegraphie, *Ann. Phys.* Leipzig **23**: 846.

ADDENDUM A SSL RESULTS FOR TWO CIRCUITS

This dataset includes SSL results for the South African circuits of Cape Town to Pretoria and Durban to Pretoria. The data was captured at various times of the day as well as at various frequencies. Some of the results correlate well with the elevation angle associated with the FOT for the circuit at that moment in time whiles others do not comply with the criteria at all, leading to less than spectacular SSL results. Some of the presented results were selected to highlight specific propagation conditions such as multi-hop and multi-layer.

The expected distance for the Cape Town to Pretoria circuit is approximately 1 300 km. For the Durban to Pretoria circuit, it is approximately 520 km.

The results are analysed as case studies in terms of the reigning ionospheric conditions as well as the propagation stability.

The results are summarised in Table A.1.

Table A.1. Summary of the SSL results for the Cape Town to Pretoria and Durban to Pretoria circuits.

Range (km)	Range Error (%)	% of the FOT's elevation angle	Quality Figure
1 203	7.5	86	0.9
1 136	14	47	0.67
1 600	23	23	0.55
1 237	4.8	71	0.86
1 203	7.5	86	0.9
467	10.2	93	0.9
619	52.4	43	0.1
618	52.5	43	0.1
1 125	13.5	44	0.65
1 136	12.6	42	0.68
851	34.5	26	0.1
486	6.5	55	0.68
1 053	19	47	0.68
1 384	6.5	53.5	0.72
1 129	13.2	80.1	0.86
1 203	7.5	75.8	0.9
1 323	1.8	43	0.6
726	55.8	69.5	0.1

Case A.1

The polar display of Figure A.1 indicates stable, single layer propagation. The Cape Town signal is received at a slightly lower angle than the elevation angle associated with the FOT for the circuit. The estimated distance of 1 237 km corresponds well with the 1 300 km expected distance, resulting in a range error of 4.8%. This is a SSL result with a high quality factor of 0.86.

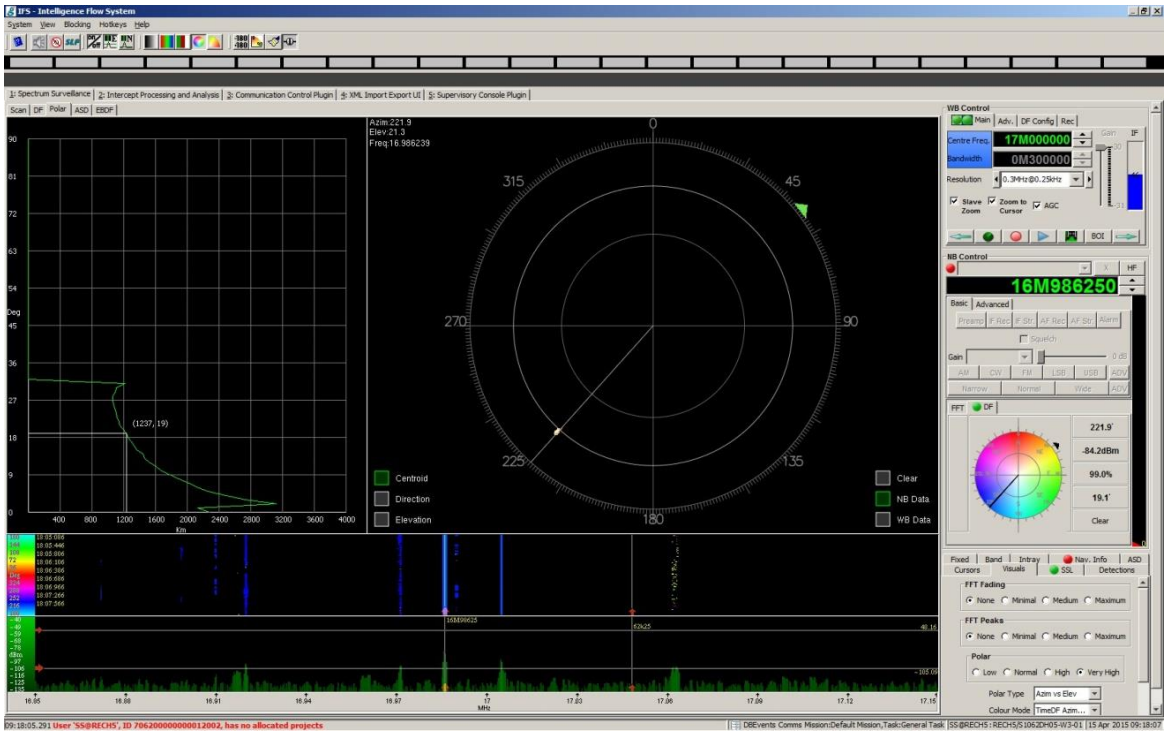

Figure A.1. The measured elevation angle is slightly lower than the elevation angle associated with the angle for the FOT resulting in a SSL quality estimate of 0.86. The range error is 4.8%.

Case A.2

The polar display of Figure A.2 indicates stable, single layer propagation. The Cape Town signal is received at close to the elevation angle associated with the FOT for the circuit. The estimated distance of 1 203 km corresponds well with the 1 300 km expected distance, resulting in a range error of 7.5%. This is a SSL result with a high quality factor (0.9).

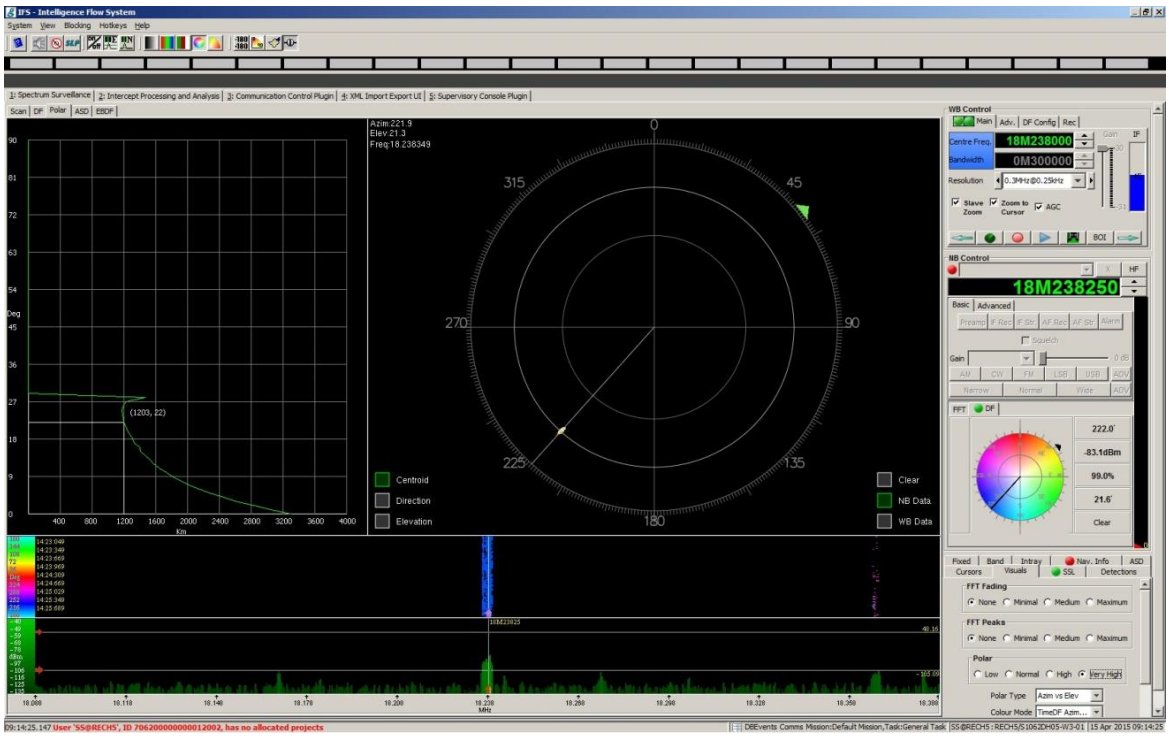

Figure A.2. The measured elevation angle corresponds well with the elevation angle associated with the angle for the FOT resulting in a SSL quality estimate of 0.9. The range error is 7.5%.

Case A.3

The rosette of Figure A.3 indicates multi-layer propagation (multiple results on the polar display). The Durban signal is received at an elevation angle associated with the transition between the E and F layers. This is in contradiction with the requirements of the ITU (ITU-R Handbook on Spectrum Monitoring, 2011, pp. 293-294). Despite this, the estimated distance of 467 km corresponds reasonably well with the 520 km expected distance, resulting in a range error of 10.2%. This is a SSL result with a low quality factor.

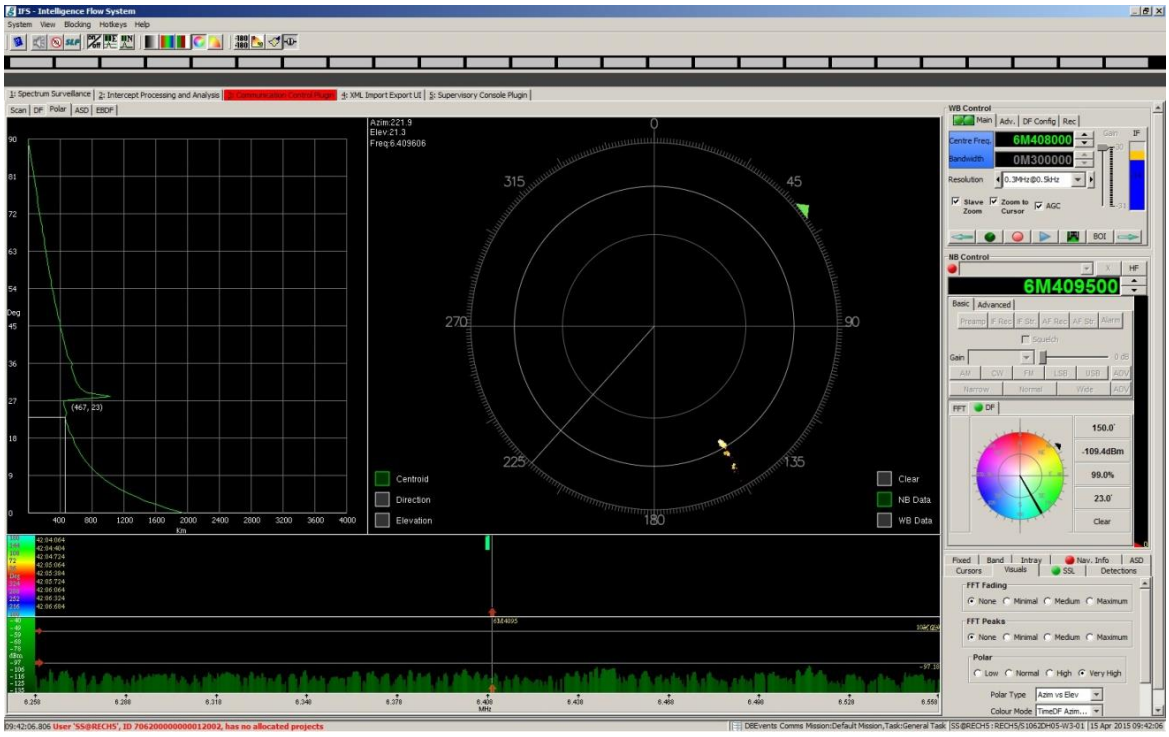

Figure A.3. Multi-layer propagation of a signal from Durban resulting in a poor quality factor SSL estimate. The range error is 10%.

Case A.4

The polar display of Figure A.4 indicates stable, single layer propagation (results are closely grouped on the polar display). The Cape Town signal is received well below the elevation angle associated with the FOT for the circuit. The estimated distance of 619 km indicates double-hop propagation (approximately half of the 1 300 km expected distance). The range error is 52.4% but reduces to 4.8% if double-hop propagation is taken into consideration. According to the SSL graph, single-hop propagation over a distance of 1 300 km is only possible via the E layer at an elevation angle of less than 4°. This is a SSL result with a low quality factor.

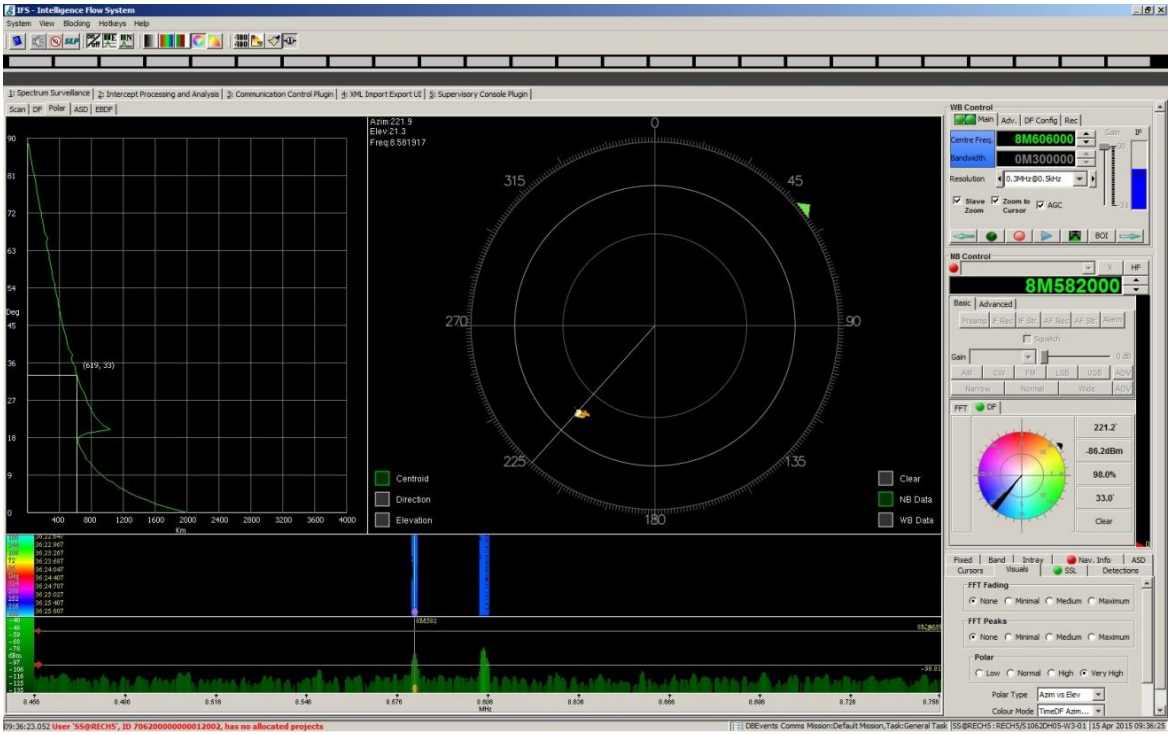

Figure A.4. Double-hop propagation results in a SSL estimate with a very poor quality factor. The range error is 52.4% but reduces to 4.8% if double-hop propagation is taken into consideration.

Case A.5

The polar display of Figure A.5 indicates unstable, single layer propagation (results are not closely grouped on the polar display). The Cape Town signal is received well below the elevation angle associated with the FOT for the circuit. The estimated distance of 618 km indicates double-hop propagation (approximately half of the 1 300 km expected distance). The range error is 52.5% but reduces to 4.9% if double-hop propagation is taken into consideration. This is a SSL result with a low quality factor.

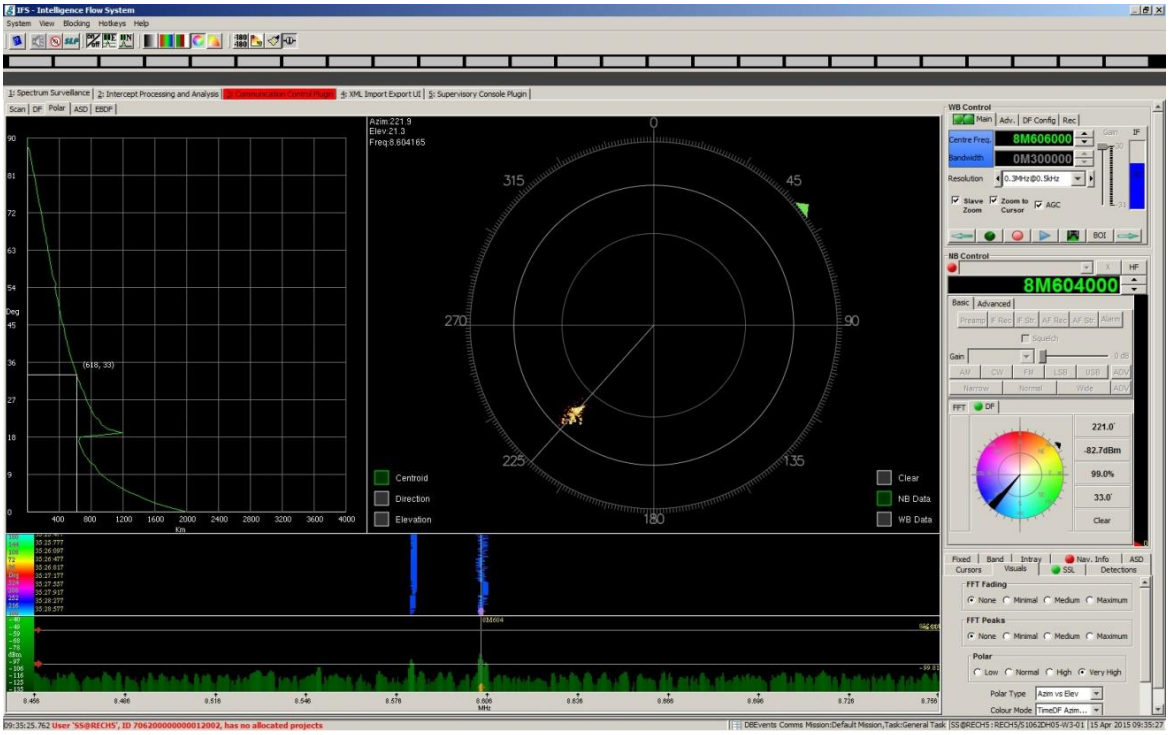

Figure A.5. Double-hop, unstable propagation results in a SSL estimate with a very poor quality factor. The range error is 52.5% but reduces to 4.9% if double-hop propagation is taken into consideration.

Case A.6

The polar display of Figure A.6 indicates stable, single layer propagation. The Cape Town signal is received at an elevation angle of less than 50% of the elevation angle associated with the FOT for the circuit. The estimated distance of 1 125 km results in a range error of 13.5%. This is a SSL result with a lower quality factor (0.65).

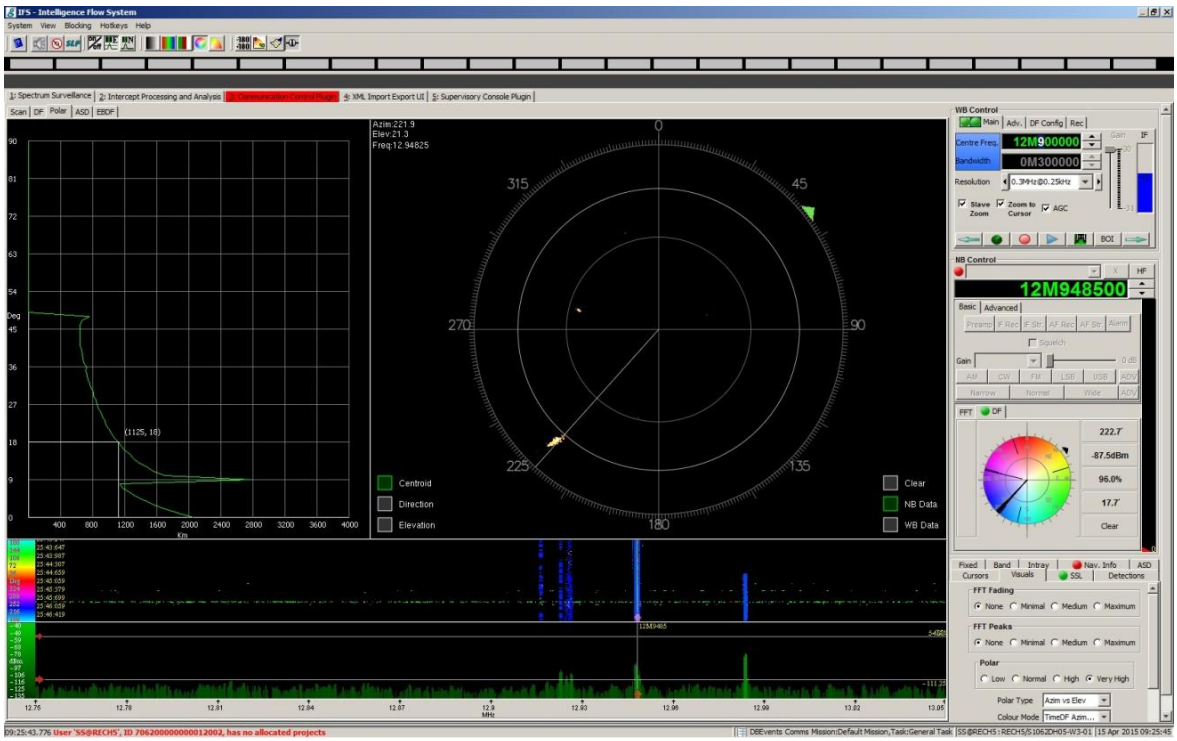

Figure A.6. The measured elevation angle is less than 50% of the elevation angle associated with the angle for the FOT, resulting in a SSL estimate with a quality factor of 0.65. The range error is 13.5%.

Case A.7

The polar display of Figure A.7 indicates stable, single layer propagation. The Cape Town signal is received at an elevation angle of less than 50% of the elevation angle associated with the FOT for the circuit. The estimated distance of 1 136 km results in a range error of 12.6%. This is a SSL result with a lower quality factor (0.68).

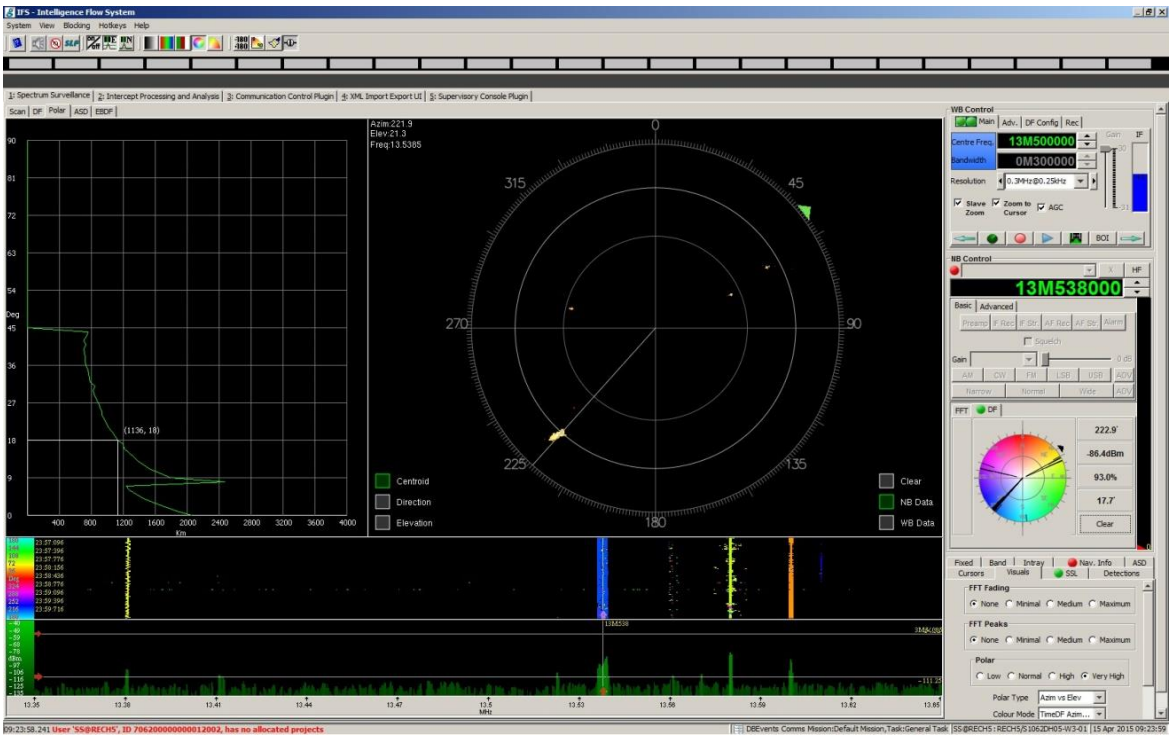

Figure A.7. The measured elevation angle is less than 50% of the elevation angle associated with the angle for the FOT, resulting in a SSL estimate with a quality factor of 0.68. The range error is 12.6%.

Case A.8

The polar display of Figure A.8 indicates unstable propagation (results not closely grouped on the polar display). According to the SSL graph, the Cape Town signal is received at an elevation angle associated with the transition between the E and F layers. This is in contradiction with the requirements of the ITU for quality SSL results (ITU-R Handbook on Spectrum Monitoring, 2011, pp. 293-294). The estimated distance of 851 km results in a range error of 34.5% and does not correspond at all with the 1 300 km expected distance. This is a SSL result with a very low quality factor

.

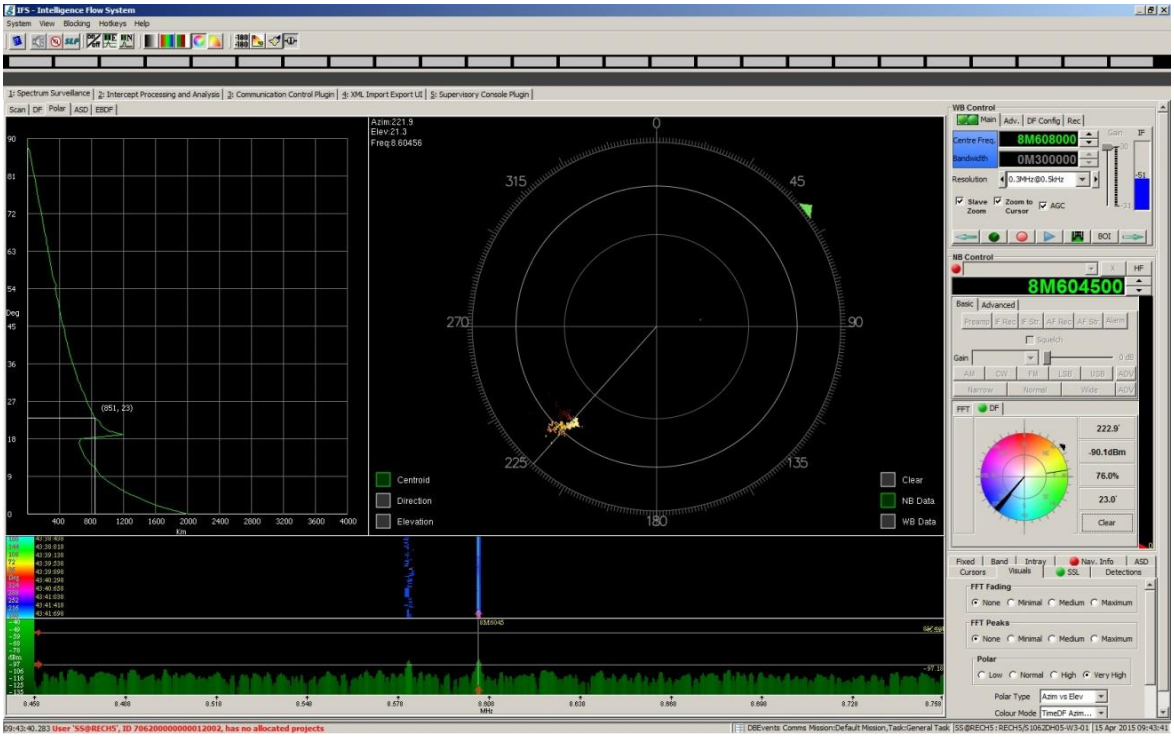

Figure A.8. Unstable propagation close to the transition between the E and F layers resulting in a SSL estimate with a low quality factor. The range error is 34.5%.

Case A.9

The polar display of Figure A.9 indicates stable, single layer propagation. The Durban signal is received at an elevation angle of slightly less than 50% of the elevation angle associated with the FOT for the circuit. The estimated distance of 486 km results in a range error of 6.5% over the 520 km path. Ideally, a higher operating frequency should be utilised for this circuit. This is a SSL result with a lower quality factor (<0.7).

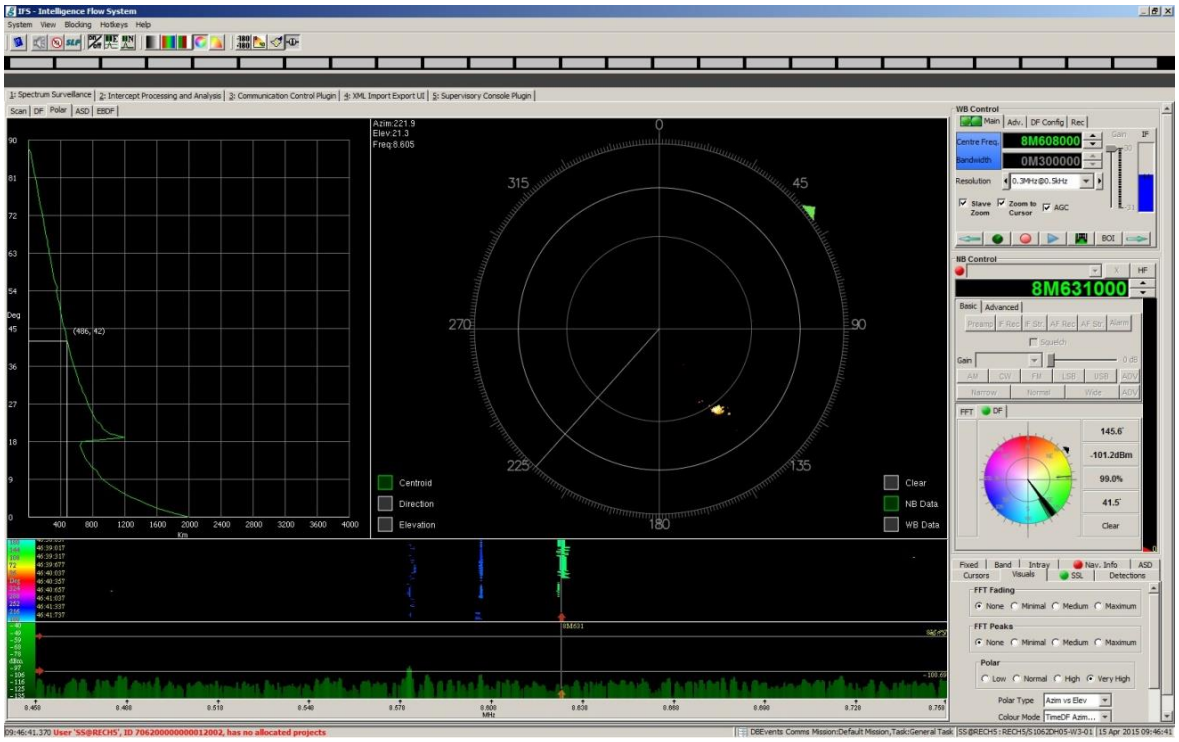

Figure A.9. The measured elevation angle is less than 50% of the elevation angle associated with the angle for the FOT, resulting in a SSL estimate with a quality factor of <0.7. The range error is 6.5%.

Case A.10

The polar display of Figure A.10 indicates unstable (results not closely grouped on the polar display), single layer propagation. The Cape Town signal is received at an elevation angle of less than 50% of the elevation angle associated with the FOT for the circuit. The estimated distance of 1 053 km results in a range error of 19% over the 1 300 km path. This is a SSL result with a lower quality factor (<0.7).

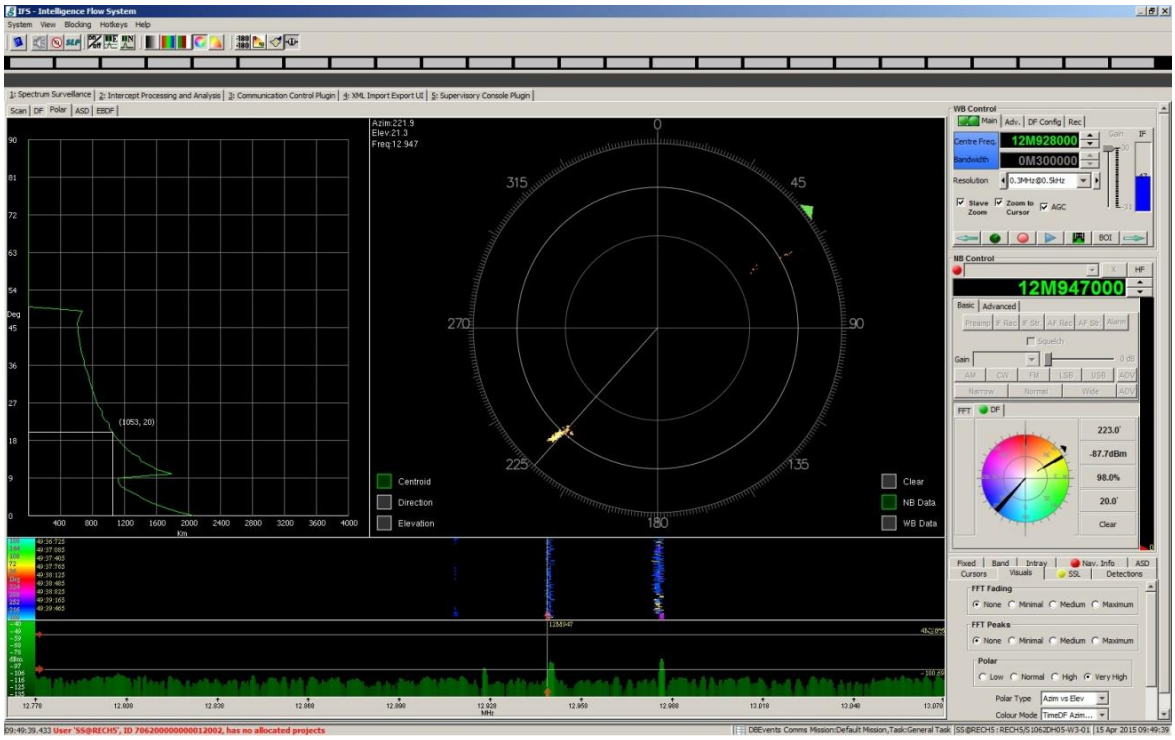

Figure A.10. The measured elevation angle is less than 50% of the elevation angle associated with the angle for the FOT, resulting in a SSL estimate with a quality factor of <0.7. The range error is 19%.

Case A.11

The polar display of Figure A.11 indicates stable, single layer propagation. The Cape Town signal is received at an elevation angle of slightly more than 50% of the elevation angle associated with the FOT for the circuit. The estimated distance of 1 384 km corresponds well with the 1 300 km expected distance, resulting in a range error of 6.5%. This is a SSL result with a better quality factor (>0.7).

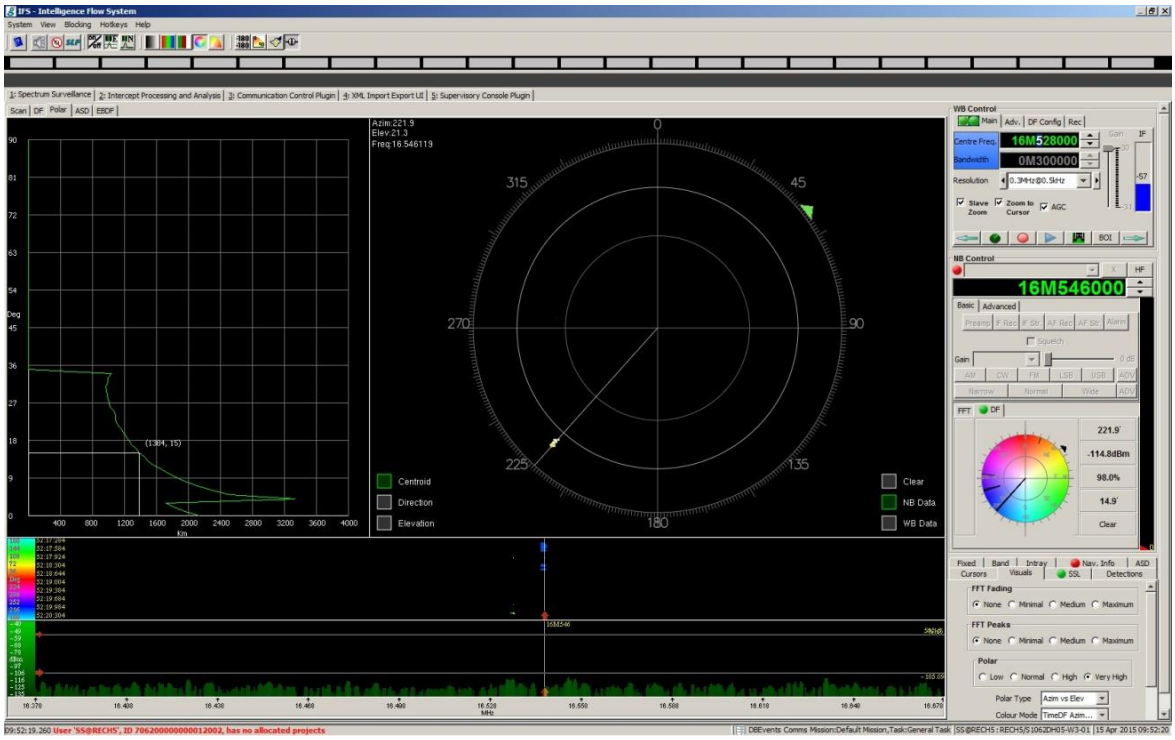

Figure A.11. The measured elevation angle is slightly more than 50% of the elevation angle associated with the angle for the FOT, resulting in a SSL estimate with a quality factor of >0.7. The range error is 6.5%.

Case A.12

The polar display of Figure A.12 indicates stable, single layer propagation. The Cape Town signal is received at an elevation angle of slightly less than the elevation angle associated with the FOT for the circuit. The estimated distance of 1 129 km corresponds fairly well with the 1 300 km expected distance, resulting in a range error of 13.2%. This is a SSL result with a quality factor of 0.86

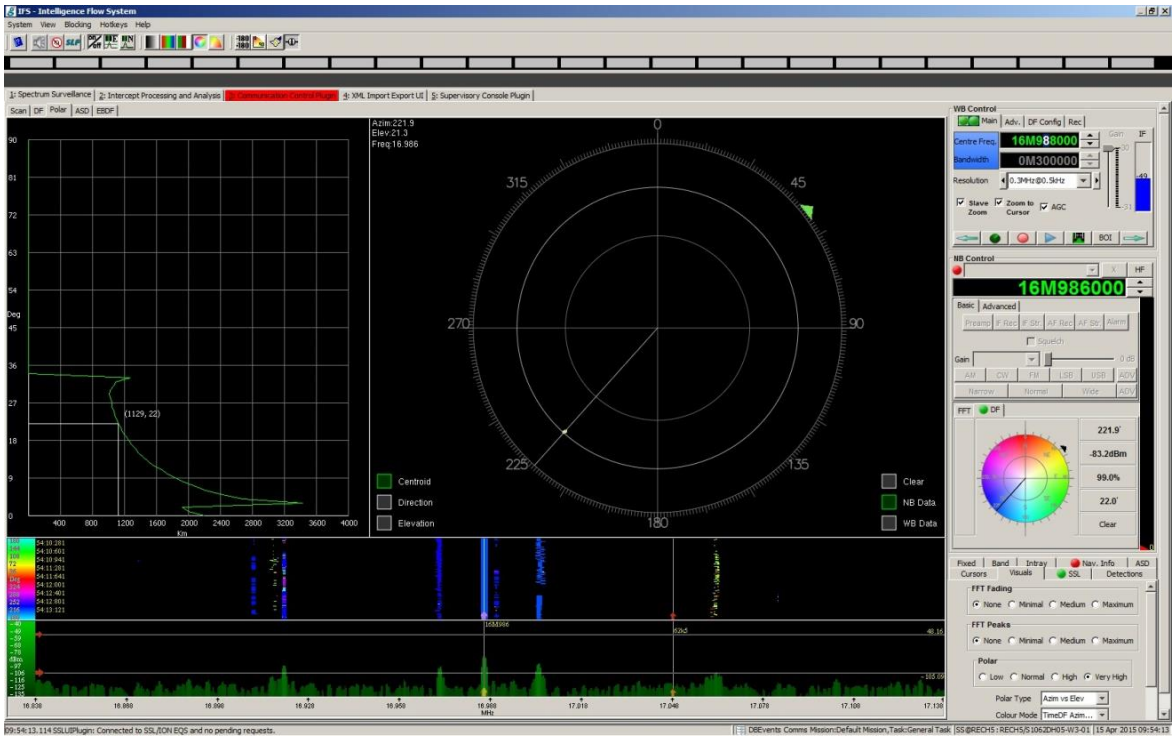

Figure A.12. The measured elevation angle corresponds well with the elevation angle associated with the angle for the FOT, resulting in a high quality SSL estimate. The range error is 13.2%.

Case A.13

The polar display of Figure A.13 indicates stable, single layer propagation. The Cape Town signal is received at close to the elevation angle associated with the FOT for the circuit. The estimated distance of 1 203 km corresponds well with the 1 300 km expected distance, resulting in a range error of 7.5%. This is a SSL result with a high quality factor (0.9).

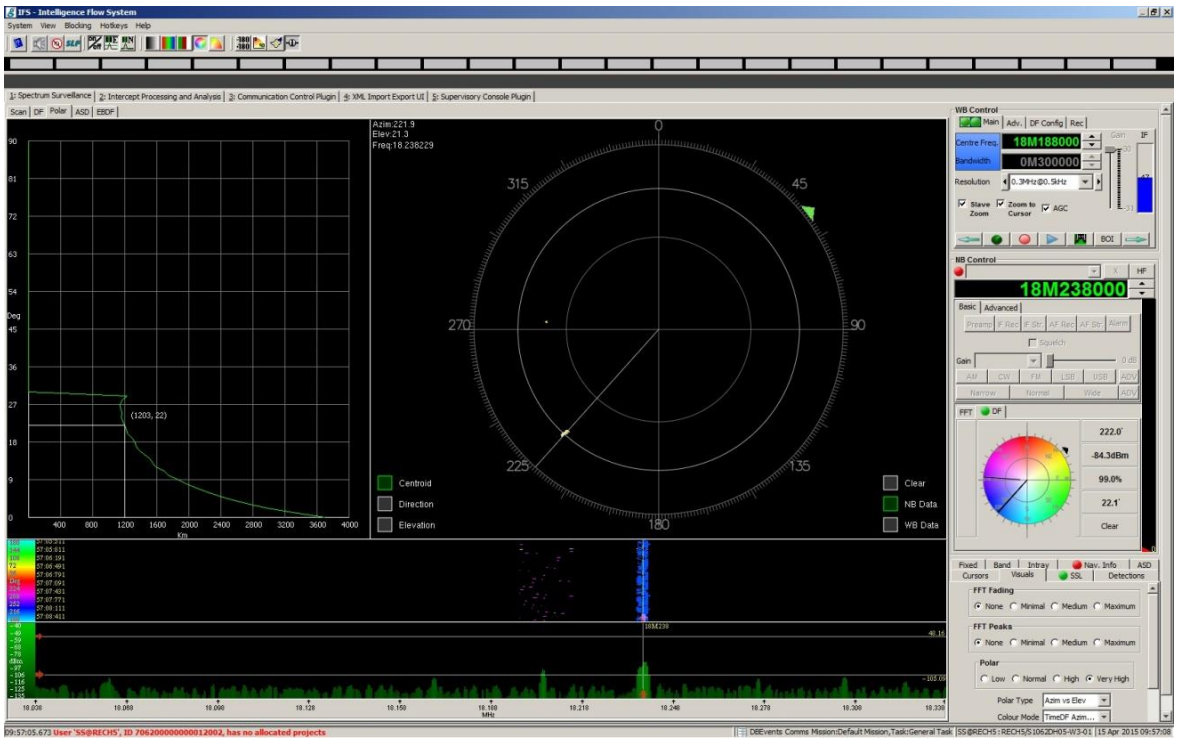

Figure A.13. The measured elevation angle corresponds well with the elevation angle associated with the angle for the FOT, resulting in a high quality SSL estimate. The range error is 7.5%.

Case A.14

The polar display of Figure A.14 indicates stable, single layer propagation. The Cape Town signal is received at an elevation angle of less than 50% of the elevation angle associated with the FOT for the circuit. The estimated distance of 1 323 km results in a range error of 1.8% over the 1 300 km distance. This SSL result with a lower quality factor (<0.7) confirms the ITU's recommendation of taking multiple measurements over a period of time to improve the confidence in the result (ITU-R Handbook on Spectrum Monitoring, 2011, p. 280).

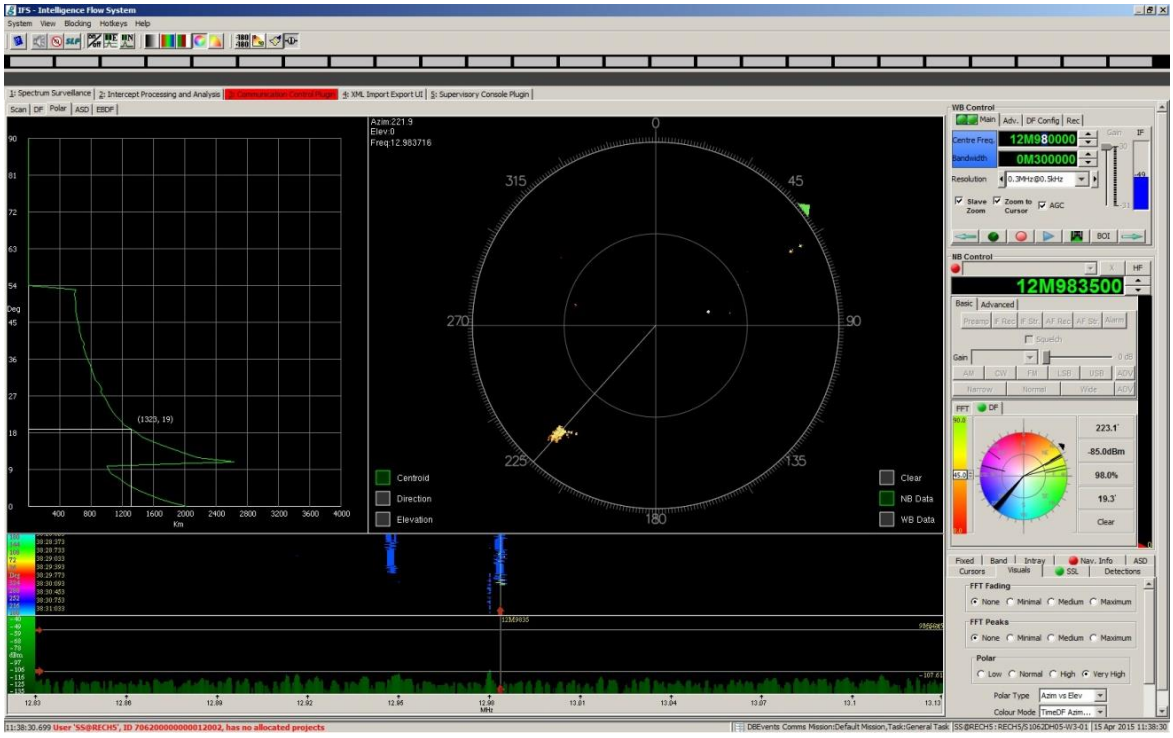

Figure A.14. The measured elevation angle is less than 50% of the elevation angle associated with the angle for the FOT, resulting in a SSL estimate with a quality factor of <0.7. The range error is 1.8%.

Case A.15

The polar display of Figure A.15 indicates multi-layer propagation (multiple results on the polar display). Judging from the SSL graph multi-hop propagation will also exist over the 1 300 km path, as the elevation angle required for single hop propagation via the E layer is very low, below 4°. This multi-layer propagation is in contradiction with the requirements of the ITU (ITU-R Handbook on Spectrum Monitoring, 2011, pp. 293-294). The estimated distance of 726 km results in a range error of 55.8% over the 1 300 km path. If double-hop propagation is taken into consideration, the range error is 11.7%. This is a SSL result with a very low quality factor.

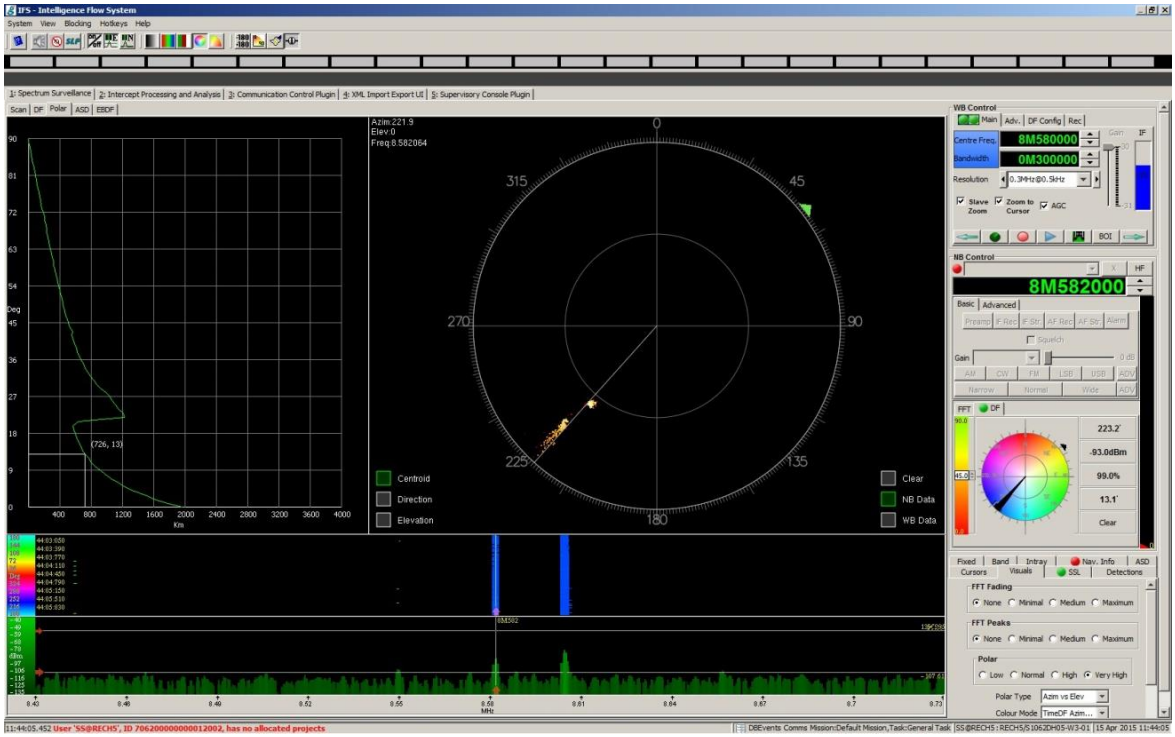

Figure A.15. Multi-layer, multi-hop propagation of a signal from Cape Town resulting in a SSL estimate with a very low quality factor. The range error is 55.8% but reduces to 11.7% if double-hop propagation is taken into consideration.